Examining Structure-Morphology-Property Relationships of Novel Styrenic-Based Macromolecules for Emerging Applications

Chainika Jangu

Dissertation submitted to the faculty of the Virginia Polytechnic Institute and State University in partial fulfillment of the requirements for the degree of

Doctor of Philosophy
In
Macromolecular Science & Engineering

Timothy E. Long, Chair
Robert B. Moore
Judy S. Riffle
Kevin J. Edgar
Richey M. Davis

June 5, 2015
Blacksburg, VA

Keywords: imidazole; triblock copolymers; reversible addition-fragmentation polymerization; ion conductivity

Examining Structure-Morphology-Property Relationships of Novel Styrenic-Based Macromolecules for Emerging Applications

Chainika Jangu

ABSTRACT

For the first time, triblock copolymers of novel styrenic-based macromolecules were investigated in detail and examined for structure-morphology-performance relationships. We were able to design novel imidazolium- and phosphonium-containing styrenic macromolecules using controlled radical polymerization and conventional free radical polymerization strategies, for a variety of potential applications including electromechanical devices, ionic liquids, adhesives, and lithium-ion batteries. Block copolymers have a unique architecture providing physical crosslinking to behave as thermoplastic elastomers. We preferred ABA triblock copolymers as compared to random and diblock copolymers for improved mechanical performance. ABA triblock copolymers synthesized using nitroxide-mediated polymerization (NMP) of polystyrene external blocks and a charged imidazolium-containing central block, exhibited sufficient modulus and ionic conductivity for electromechanical transducers. We successfully reported the actuation behavior of triblock copolymers in the presence of added ionic liquid for the first time. We proposed that diluting the ion concentration of the ion-rich phase with neutral polymer comonomers that reduces T_g, increases ion dissociation, and potentially maximizes ionic conductivity.

Tendency of ethylene-oxide units to coordinate cations, forming stable crown ether-like, multi-nuclear coordination complexes, promotes solvation and dissociation of ionic aggregates. *In situ* Fourier transform infrared spectroscopy (FTIR) was used to monitor the thermal polymerization in various acrylate and methacrylate monomers. It was found that acrylates have lower activation energy than methacrylates. The copolymerizations of poly(ethylene

glycol)methyl ether acrylate (EG_9MEA) and imidazole-containing monomer (VBIm) resulted in controlled polymerization kinetics with narrow molecular weight distributions. The control behavior of the copolymerizations is likely attributed to the observed decrease in calculated apparent rate constants for the copolymerizations with addition of VBIm as comonomer. Reversible addition fragmentation transfer (RAFT) successfully synthesized well-defined A-BC-A triblock copolymers containing a synergy of pendant ether and imidazolium sites. We demonstrated that electromechanical transducers derived from these triblock copolymer membranes with added ionic liquid showed superior actuation performance compared to a benchmark Nafion® membrane, suggesting potential for ionic polymer device applications. This was attributed to optimum modulus, improved ionic conductivity, and microphase-separated morphology of triblock copolymers.

Conventional free radical polymerization and anion metathesis of 4-(diphenylphosphino)styrene (DPPS) successfully generated high molecular weight triaryl phosphine-containing copolymers. These macromolecules have no $-CH_2$ group at the benzylic position increasing the thermal stability of the DPPS-containing polymers. Counterion exchange to fluorinated, bulkier anions broadened the library of polyelectrolytes, led to improved thermal stabilities, lower glass transition temperatures, and tunable wetting behavior. We also reported the synthesis of salt-responsive copolymers using conventional free radical polymerization. Adhesive performance measurements such as peel tests and probe tack enforced the application of these polymers as pressure sensitive adhesives.

We also demonstrated the synthesis and subsequent neutralization of novel, well-defined A-BC-A triblock copolymers containing a soft central “BC” block consisting of Sty-Tf_2N and DEGMEMA with polystyrene external blocks. Sty-Tf_2N monomer enables an important

delocalization of the negative charge. Li^+ has weak interactions with this anionic structure, consequently enabling a high dissociation level. Li^+ ions are associated to the polymer chain to produce high transport numbers. Furthermore, incorporating DEGMEMA lowers the T_g of the charged block copolymers, thereby increasing the segmental mobility and thus ionic conductivity. Finally, the structure-property-morphology study of these triblock copolymers will be helpful for their use in potential applications such as ion-containing membranes, lithium-ion batteries.

Acknowledgements

There are many people to thank for their assistance and support during my career as a graduate student. First, I would like to thank Prof. Tim Long. The skill sets developed under his direction and creative approach to polymer science will continue throughout my professional life. The opportunities that he provided during my graduate career have truly enhanced my education experience at Virginia Tech. and I was privileged to participate in various on-campus and off campus short courses as well as various national meetings. He always encouraged excellent communication skills and technical writing, which will help in my future endeavors. I would like to thank my committee members: Prof. Bob Moore, Prof. Judy Riffle, Prof. Kevin Edgar and, Prof. Rick Davis for their helpful suggestions and insightful comments. Prof. Riffle helped editing a research paper in the writing class and I was able to learn technical writing during the semester. There were many helpful discussions with Prof. Moore regarding my research are valuable to me. I would also like to thank Prof. Louis Madsen, whom I enjoyed interacting with in my last semester in graduate school. He was able to serve as a committee member for my defense.

One of the funding source during my graduate career was the Ionic Liquids in ElectroActive Devices (ILEAD) Multi-University Interdisciplinary research initiative (MURI). During this project I was privileged to collaborate with Dr. Dong Wang and Prof. Randy Heflin at Virginia Tech.; Greg Fahs and Prof. Moore at Virginia Tech.; Sharon Wang and Prof. Karen Winey at University of Pennsylvania; Helen Wang; Prof. Ralph Colby at Pennsylvania State

University; Zhiyang Zhang and Prof Louis Madsen. The opportunity to work with such diverse and interdisciplinary team enhanced my graduate learning experience.

It is impossible for a graduate student to survive without the help from administrative staff, who constantly help schedule meetings, complete paper work, and so many other things. I would sincerely like to thank Tammy Jo Hiner, Brent Bowden, Teresa Dickerson, Laurie Good, Cyndy Graham, Owens Valerie, and Naya.

I was fortunate to work in a diverse group with so many talented people in the Long group. Everyday was a learning experience and will take many memories with me as I move forward. I would love to thank Matthew Green, Mike Allen, Shijing Cheng, Tianyu Wu, Steve June, Renlong Gao, Mana Tamami, Dan Buckwalter, David Inglefield, Evan Margaretta, Keren Zhang, John Herlihy, Joe Dennis, Justin Sirrine, Ryan Mondschein, Ming Tao, Allison Pekkanen, Makito Yokoe, Asem Abdulahad, and Zhiyang Zhang. I would like to thank Alie Schultz for her friendship throughout these years at Virginia Tech. Her constant laughter, fun-loving personality, and long conversations with her helped brighten my time during most difficult phase in graduate school. I would specially like to thank two undergraduates whom I mentored, Michael Robertson and Cole Gage. I would also like to thank Dr. Sachin Bobade, whom I collaborated with in my last semester on an industrially funded project. He is a very skilled scientist and I was very fortunate to work with him.

I would not have survived graduate school without loving, caring and understanding roommates who made me feel home away from home. I would like to thank several of my roommates as well as friends: Meenal Chhabra, Shradha Parab, Nivisha Shah, Nidhi Parikh, and Padmapriya Muralidharan, who supported and helped me in various ways during my stay at Virginia Tech.

Finally and most importantly, I profusely thank my family for their love, support and trust in me during all these years. I would specially like to thank my parents who believed in me, supported my decisions, and always encouraged me to give my best. I would like to thank my brother, Ankit Singh Jangu who has always helped me look at the bright side of any situation and be happy. Certainly not the least, I must thank my best friend and my life partner, Dr. Shantanu Ranade. He has always encouraged and inspired me to think out of the box and have vision. With him my graduate school journey was enjoyable and learning with fun. I am forever thankful for all you have done and I can only hope that you know how much grateful I am.

Attributions

Prof. Timothy Long- is the primary advisor to the author and contributed to the direction of the research and extensively edited the chapters.

Jin-Han Helen Wang- is from Department of Chemical Engineering at The Pennsylvania State University. She performed dielectric relaxation spectroscopy (DRS) to measure ion transport properties for all the imidazole-containing triblock copolymers discussed in chapters 2 and 3.

Prof. Ralph H. Colby-advised Jin-Han Helen Wang and provided helpful discussions to understand ion transport trends and mechanisms in all imidazole-containing triblock copolymers discussed in chapters 2 and 3.

Sharon Sharick- is a graduate student in Department of Materials Science and Engineering at University of Pennsylvania. She performed small angle X-ray scattering experiment for imidazole-containing triblock copolymers discussed in chapter 2.

Prof. Karen Winey- advised Sharon Wang and provided helpful discussion on understanding structure-morphology relationships of imidazole-containing ABA triblock copolymers

Dong Wang- was a graduate student in Department of Physics at Virginia Tech. He fabricated and tested triblock copolymers for applications in electromechanical actuators discussed in chapters 2 and 3.

Prof. James R. Heflin- advised Dong Wang and provided helpful suggestions on design of imidazole-triblock copolymers as electromechanical transducers.

Gregory Fahs- was a graduate student in Department of Chemistry at Virginia Tech. and performed small angle X-ray scattering experiments discussed in chapter 3.

Prof. Robert Moore- advised Gregory Fahs and provided helpful discussions on morphology of triblock copolymers discussed in chapter 3.

Candace Wall- performed contact angle experiments on DPPS-containing copolymers in chapter 6.

Alan Esker-advised Candace Wall and provided helpful discussions on wetting behavior of DPPS-containing copolymers in chapter 6.

Shantanu R. Ranade-was a graduate student in MACRO at Virginia Tech. and he performed probe tack experiments for switchable pressure sensitive adhesives and also provided helpful discussions regarding adhesives in chapter 7.

Prof. David A. Dillard-advised Shantanu R. Ranade and provided helpful discussions on adhesives in chapter 7.

Alice M. Savage- performed X-ray scattering and microscopy experiments at U.S Army Research Laboratory in chapter 9.

Frederick L. Beyer-advised Alice M. Savage and provided helpful discussions on scattering and microscopy experiments in chapter 8.

Zhiyang Zhang- postdoc in Department of Chemistry at Virginia Tech. and performed NMR experiments in chapter 8 for diffusion measurements of sulfonamide-based triblock copolymers.

Table of Contents

List of Figures

List of Tables

List of Schemes

Chapter 1: **Introduction**

1.1 *Dissertation Overview*

The overall focus of this dissertation revolves around structure-morphology-performance relationships of novel styrenic-based macromolecules. We were able to design novel imidazolium- and phosphonium-containing styrenic macromolecules for a variety of potential applications including electromechanical devices, ionic liquids, adhesives, and lithium-ion batteries.

ABA triblock copolymers have a critical architecture for thermoplastic elastomers. We preferred ABA triblock copolymers as compared to random and diblock copolymers for improved mechanical performance. Chapter 2 details the synthesis of a well-defined phase-separated ABA triblock copolymers using nitroxide-mediated polymerization (NMP) of polystyrene external blocks and a charged imidazolium-containing central block. These triblock copolymers exhibited sufficient modulus and ionic conductivity for electromechanical transducers with long-range order of microphase separation as observed in small-angle X-ray scattering (SAXS). For the first time, we reported the actuation behavior of triblock copolymers in the presence of added ionic liquid. To further improve the ion transport properties of triblock copolymers, we proposed diluting the ion concentration of the ion-rich phase with a choice of neutral polar comonomers that have high dielectric constant, reduces T_g, increases ion dissociation, and potentially maximizes ionic conductivity. Tendency of ethylene-oxide units to coordinate cations, forming stable crown ether-like, multi-nuclear coordination complexes, promotes solvation and dissociation of ionic aggregates.

Chapter 3 reports the investigation of the thermal polymerization behavior of acrylate and methacrylate monomers. *In situ* Fourier transform infrared spectroscopy (FTIR) monitored the thermal polymerization behavior and acrylates have lower observed activation energy as compared to their methacrylate analogs, suggesting relatively less control in the polymerizations. NMP copolymerizations of EG_9MA with VBIm as comonomer exhibited controlled polymerization behavior confirmed by kinetic plots coupled with narrow molecular weight distributions observed from SEC chromatograms. The control behavior of the copolymerization is likely attributed to the observed decrease in calculated apparent rate constants for the copolymerizations with addition of VBIm as comonomer.

Chapter 4 demonstrated the role of morphology with block copolymer nanoscale structures providing superior ionic conductivity and mechanical performance compared to random copolymers. Reversible addition fragmentation transfer (RAFT) enabled the synthesis of well-defined A-BC-A triblock copolymers containing a synergy of pendant ether and imidazolium sites. Under a 4 V direct current (DC) applied voltage, electromechanical transducers derived from these triblock copolymer membranes with added ionic liquid showed superior actuation performance compared to a benchmark Nafion® membrane, suggesting potential for ionic polymer device applications. This was attributed to optimum modulus, improved ionic conductivity, and microphase-separated morphology of triblock copolymers.

Chapter 5 describes the literature review on phosphonium cation-based ionic liquids (ILs), with a focus on structure-property relationships of ammonium- and phosphonium-containing polyelectrolytes and ionic liquids. Phosphonium-containing macromolecules display a broad range of improved properties compared to ammonium macromolecules described well in Chapter 5.

Chapter 6 focuses on another new commercially available styrenic monomer, 4-(diphenylphosphino)styrene (DPPS), which has no -CH_2 group at the benzylic position increasing the thermal stability of the DPPS-containing polymers. Conventional free radical polymerization and anion metathesis of DPPS successfully generated high-molecular-weight triaryl phosphine-containing copolymers. Counterion exchange to fluorinated, bulkier anions broadened the library of polyelectrolytes, leading to improved thermal stabilities, lower glass transition temperatures, and tunable wetting behavior. Phosphonium-containing macromolecules are widely studied for many emerging technologies because of their enhanced thermal stability, potential biocompatibility, and improved conductivity.

Chapter 7 reports the synthesis of salt-responsive copolymers using conventional free radical polymerization. Adhesive performance measurements such as peel tests and probe tack enforced the application of these polymers as pressure-sensitive-adhesives. Ultimately, the designed copolymers displayed tunable salt-response with potential applications as adhesives.

Chapter 8 demonstrates the synthesis and subsequent neutralization of novel, well-defined A-BC-A triblock copolymers containing a soft central "BC" block consisting of Sty-Tf_2N and DEGMEMA with polystyrene external blocks. In the central block, Sty-Tf_2N monomer enables an important delocalization of the negative charge. Li^+ ions are not strongly associated to the polymer chain, thus enabling fast transport and high ion conductivity. Furthermore, incorporating DEGMEMA lowers the T_g of the charged block copolymers, thereby increasing the segmental mobility. The chapter discusses the relationships among chemical composition, morphology, ionic conductivity, and mechanical properties of triblock copolymers.

Finally, Chapters 9 and 10 provide overall conclusions of the dissertation and suggested future work to continue the research efforts, respectively.

Chapter 2: **Well-Defined Imidazolium ABA Triblock Copolymers as Ionic-Liquid-Containing Electroactive Membranes**

(Published in *Macromolecular Chemistry and Physics* **2014**, *215* (13), 1319-1331)

Chainika Jangu[1], Jing-Han Helen Wang[2], Dong Wang[3], Sharon Sharick[4], James R. Heflin[3], Karen I. Winey[4], Ralph H. Colby[2], and Timothy E. Long[1*]

[1]*Department of Chemistry, Macromolecules and Interfaces Institute, Virginia Tech., Blacksburg, VA 24061*
[2]*Department of Chemical Engineering, The Pennsylvania State University, University Park, Pennsylvania 16802*
[3]*Department of Physics, Virginia Tech., Blacksburg, VA 24061*
[4]*Department of Materials Science and Engineering, University of Pennsylvania, Philadelphia, Pennsylvania 19104*

[*]To whom correspondence should be addressed E-mail: telong@vt.edu. TEL: (540)231-2480 FAX: (540)231-8517

Keywords: Nitroxide-mediated polymerization, block copolymers, actuators

2.1 *Abstract*

Nitroxide-mediated polymerization (NMP) afforded the synthesis of well-defined ABA triblock copolymers with polystyrene external blocks and a charged poly(1-methyl-3-(4-vinylbenzyl)imidazolium bis(trifluoromethane sulfonyl)imide central block. Aqueous SEC and ^{1}H NMR spectroscopic studies confirmed the control of the composition and block lengths for both central and external blocks. Dynamic mechanical analysis (DMA) revealed a room temperature modulus suitable for fabricating these triblock copolymers into electroactive devices in the presence of added ionic liquid. Dielectric relaxation spectroscopy (DRS) elucidated the ion-transport properties of the ABA triblock copolymers with varied compositions. Ionic conductivity in these single-ion conductors exhibited Vogel-Fulcher-Tammann (VFT) and

Arrhenius temperature dependence, and electrode polarization (EP) analysis determined the number density of simultaneously conducting ions and their mobility. The actuators derived from these triblock copolymer membranes experienced similar actuation speeds at an applied voltage of 4V DC as compared to benchmark Nafion® membranes. These tailorable ABA block copolymers are promising candidates for ionic-polymer device applications.

2.2 *Introduction*

Electroactive polymers (EAP) have attracted significant attention in the last decade.[1-5] EAPs potentially enable large strains (>1%) at low applied voltages (<10 V)[1], and involve multiple physical processes such as electrostatic interaction between charged electrodes, generated stress upon the application of an electric field, and ion-transport and charge accumulation to facilitate electromechanical coupling.[1,6,7] Ion-containing polymeric membranes form a class of devices classified as ionic-polymer transducers, and these electromechanical transducers enable potential applications including sensors and actuators, energy-harvesting devices, and biomimetic materials.[8,9] For example, an electromechanical actuator typically consists of an ionic polymeric membrane with conductive network composite (CNC) layers and external electrodes coated on both sides. The CNC is often fabricated through layer-by-layer self-assembly using positively charged poly(allylamine) hydrochloride and anionic gold nanoparticles.[10-12] The CNC layers serve to increase the interfacial surface area and porosity of the electrode, which improves ion-transport and ion accumulation, leading to improved performance of actuation.[1,9,13,14]

The most widely studied ionic polymer for transducer membranes is Nafion®, serving as a benchmark for optimized properties and response required for the preparation of

electromechanical transducers.[15,16] A microphase-separated morphology contributes to superior performance as a transducer, i.e. the semi-crystalline perfluorinated backbone provides mechanical stability, and perfluorinated polyether side chains terminated with sulfonic acid groups enable ion (proton) conduction. This multiphase morphology provides an ion-cluster morphology and ion channels upon hydration.[17,18] The synthesis of ABA triblock copolymer architectures is an attractive strategy to mimic the morphology of Nafion®, where the external blocks provide mechanical reinforcement and an ion-rich central block facilitates ion migration.[19] The previous literature describes the tuning of thermomechanical properties, morphology, and ionic conductivity for electroactive membrane applications.[12,20] However, a detailed study of charged ABA triblock copolymers with intentionally added ionic liquid remains unprecedented. The charged ABA triblock copolymer serves to localize the ionic liquid electrolyte at the nanometer dimension.

Tuning ABA triblock composition enables tailored charge content, mechanical properties, and morphology.[21,22] The interplay between glass transition temperature (T_g) and ionic conductivity is firmly described in the literature, and recent studies focused on the influence of diblock copolymer morphology on ionic conductivity.[22-24] The triblock copolymers provided suitable mechanical properties for device fabrication; however, fundamental studies of the influence of composition on morphology and ion-transport remain deficient. A significant disadvantage of commercially available polymers for electromechanical transducers is the lack of rational synthetic design of many parameters such as thermomechanical properties, morphology, molecular weight, and composition.

The self-assembled, nanostructured morphologies of block copolymers enable their use as solid-state polyelectrolytes, specifically tuning morphology to benefit ion-transport. A recent

report on charged block copolymers demonstrated that morphology is dependent on both composition and film processing conditions, and these differences in morphology had significant impact on ionic conductivity. Elabd *et al.* demonstrated a two-order increase in ionic conductivity from random copolymers to block copolymers.[25] Our group has also reported the synthesis of high molecular weight ABA triblock copolymers using RAFT methods, and triblock copolymers with added ionic liquid showed electro-responsiveness under the application of a low voltage (2-4 V).[11]

Our research group has described ABA triblock copolymers using nitroxide-mediated polymerization of polystyrene external blocks and a charged imidazolium-containing central block.[12] These triblock copolymers exhibited sufficient modulus and ionic conductivity for electromechanical transducers, however, the synthetic consequence of homopolymer central block and diblock copolymer contamination limited long-range order of microphase separation and prevented precise formation as observed in small-angle X-ray scattering.[12] Also, earlier efforts did not report actuation behavior in the presence of added ionic liquid.

This manuscript will investigate cationic imidazole-containing ABA triblock copolymers that mimic the combined mechanical properties and ion conductivity of commercially available Nafion® with comparable actuation performance. Nitroxide-mediated polymerization was successfully used to obtain targeted molecular weight and tunable compositions. The manuscript will describe novel ABA triblock copolymers with optimized conditions for quaternization and anion exchange reactions as compared to earlier reported results to obtain well-defined triblock copolymers with narrow PDIs. Thermomechanical properties displayed microphase-separation and a modulus suitable for device fabrication. Dielectric relaxation spectroscopy (DRS) determined ion-transport properties of these charged ABA triblock copolymers with different

compositions. The electrode polarization (EP) model provided ionic mobility, dielectric constant, and mobile ion concentration for these triblock copolymer systems. Furthermore, these triblock copolymers with suitable morphology and modulus were cast into ductile films with ionic liquid and fabricated into electromechanical actuators. These ABA triblock copolymers show actuation behavior in the presence of ionic liquid for the first time in the literature.

2.3 *Experimental*

2.3.1 Materials

4-Vinylbenzyl chloride (VBCl, Sigma, 90%) and imidazole (Sigma, 99%), 1-bromoethane (Sigma 98%), sodium bicarbonate (Sigma >99.5%), sodium acetate (Sigma >99%), sodium hydroxide (Sigma >98%), glacial acetic acid (Sigma >99%), hydrochloride acid (Sigma, 37%), 1-ethyl-3-methylimidazolium trifluoromethane sulfonate (EMIm-TfO, IoLiTec Inc., 99%) and lithium bis(trifluoromethane sulfonyl)imide (Tf_2N) ($LiTf_2N$, Aldrich, 99%) were used as received. Styrene (Sigma, 99%) was passed over silica to remove inhibitor prior to use. Acetone (Fisher Scientific, HPLC grade), ethyl acetate (Fisher Scientific, HPLC grade), diethyl ether (Fisher Scientific, ACS grade), methanol (Fisher Scientific, HPLC grade), hexanes (Fisher Scientific, HPLC grade), and *N, N*-dimethylformamide (DMF, Fisher Scientific) were used as received. DEPN and $DEPN_2$ were synthesized according to previous literature procedures.

2.3.2 Analytical Methods

^1H NMR spectroscopy was performed using a 400 MHz Varian Unity at 25 °C. Thermogravimetric analysis (TGA) was performed using a TA Instruments TGA 2950 at a 10 °C/min heating ramp. Differential scanning calorimetry (DSC) was performed using a TA

Instruments Q1000. Scans were obtained under N_2 with heating at 10 °C/min and cooling at 100 °C/min; T_g's were recorded on the second heating cycle. Dynamic mechanical analysis (DMA) was performed with a TA Instruments Q800 at a 3 °C/min heating ramp in film tension mode, and a single frequency of 1 Hz. Aqueous size exclusion chromatography (SEC) in a ternary mixture of water, methanol, and acetic acid (54:23:23 v/v/v%) with 0.1 M sodium acetate at 35 °C, and a flow rate of 0.8 mL/min, determined the absolute weight-average molecular weights (M_w) using the refractive index detector and a multi-angle laser light scattering (MALLS) detector. Poly(1-(4-vinylbenzyl)imidazole) neutral as well as charged homopolymers (1.0 mg/mL) were dissolved in the ternary mixture and injected into the dRI detector with a syringe pump. Refractive index increment (dn/dc) measurements were performed using a Wyatt Optilab T-rEX equipped with a 690 nm laser at 35 °C. The dn/dc values were determined with the Astra V software from Wyatt for the determination of absolute M_w from SEC.

Samples for dielectric relaxation spectroscopy (DRS) measurements were solvent-cast films from mixtures of 80:20 $CHCl_3$:CH_3OH and vacuum annealed for 5 d at 120 °C. Samples were then placed on a freshly polished brass electrode and dried in a vacuo at 353 K for 48 h and finally a second brass electrode was placed on top of the sample. A Novocontrol GmbH Concept 40 broadband dielectric spectrometer measured the dielectric permittivity. Frequency sweeps were performed isothermally from 10 MHz to 0.01 Hz, in the temperature range from 233 to 453 K under dry nitrogen. The samples were initially held at a temperature above 393 K for at least 30 min to minimize the amount of water and avoid a change in water content during the experiment. The measurements were performed during subsequent cooling under a flow of dry N_2, and the sample was subsequently heated to the starting temperature, revealing that data are perfectly reproducible during the second heating to the highest temperature.

Small-angle X-ray scattering (SAXS) was performed on a multi-angle X-ray scattering system, which generates Cu-Kα X-rays, λ = 0.154 nm, from a Nonius FR 591 rotating anode operated at 40 kV and 85 mA. The bright, highly collimated beam was obtained via Osmic Max-Flux optics and pinhole collimation in an integral vacuum system. The scattering data were collected using a Bruker Hi-Star two-dimensional detector with a sample-to-detector distance of 150 cm. Room-temperature data were collected along the through-plane direction for 1 h. Data were analyzed using Datasqueeze software.[26] The intensities were first corrected for primary beam intensity and background scattering was subsequently subtracted. The isotropic 2-D scattering patterns were then azimuthally integrated to yield 1-D intensity versus scattering vector (q) profiles. The intensities were reported in arbitrary units (a.u.).

The layer-by-layer (LbL) fabrication process is identical to our previous publications,[12,27] where negatively charged gold nanoparticles (3 nm diameter, 20 ppm, Purest Colloids) are deposited layer-by-layer with positively charged inert long chain polyelectrolyte (10 mM poly(allylamine hydrochloride), PAH, Sigma-Aldrich). The highly conductive and porous CNC layers within the actuator provided extra volume for ion accumulation and thus enhance the bending performance of the actuator. After hot-pressing (80 °C, 500 lbs) with 50 nm thick gold foil on both sides as electrodes to the power supply, the membrane was cut into 1 mm × 1 cm strips for testing. 4V DC step input was applied to the actuator and a high definition camera recorded bending. As a reference, Nafion® based actuators were fabricated by coating 30 BLs CNC on both sides of the membrane and soaking in EMI-TfO IL to 35 wt.% uptake. The same gold foil was hot-pressed under 90 °C, 700 psi. The membrane was cut into strips and tested under identical conditions.

2.3.3 Synthesis of Poly(VBIm)

As an example, VBIm (20.6966 g, 112.3 mol), $DEPN_2$ (135.6 mg, 0.17 mmol), and DEPN (11.3 mg, 0.03 mmol) were synthesized as our previously published procedure,[9,12,28,29] and dissolved in DMF (25 mL) and degassed using three freeze pump thaw cycles. The flask was back-filled with argon and heated to 125 °C for 2 h. The solution was cooled to 23 °C, diluted with DMF (20 mL), and precipitated into ethyl acetate. The product was redissolved in methanol and precipitated into diethyl ether. Poly(VBIm) was filtered and dried at reduced pressure (0.5 mm Hg) at 40 °C for 18 h. Molecular weight increased linearly with conversion and the PDIs remained narrow (<1.1) throughout the polymerization. SEC chromatographs shifted to lower elution times with increasing polymerization time or conversion.

2.3.4 Quaternization of Poly(VBIm)

Poly(VBIm) and alkyl halide, either 1-bromoethane or methyl iodide, were dissolved in methanol. The solution was purged with argon, and heated to 60 °C with 1-bromoethane and at 23 °C with methyl iodide for 18 h as shown in

Scheme 2.1. The solution was cooled to 23 °C and the product was precipitated into ethyl acetate. Poly(EVBIm-Br) or poly (MVBIm-I) was isolated through filtration and dried under reduced pressure (0.5 mmHg) at 40 °C for 18 h.

Scheme 2.1 Quaternization of poly(VBIm) using 1-bromoethane at 60 °C. (Used with permission of John Wiley and Sons, 2015)

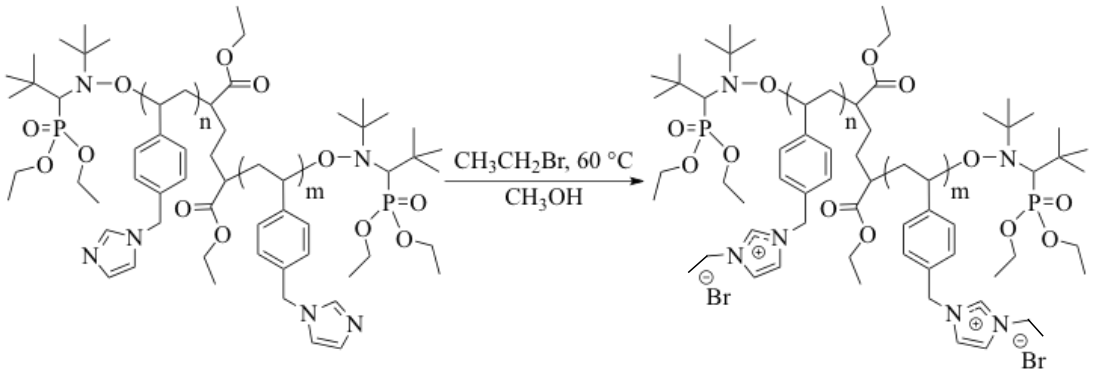

2.3.5 Anion Exchange

Poly(EVBIm-Br) (14.8135 g, 50.5 mmol of repeat unit) or poly (MVBIm-I) and $LiTf_2N$ (72.0395 g, 0.250 mol) were dissolved in separate solutions of water (50 mL each). The solutions were mixed together, immediately forming a white precipitate, and stirred at 23 °C for 24 h as shown in Scheme 2.2. Poly(EVBIm-Tf_2N) or poly(MVBIm-Tf_2N) was dialyzed against methanol for 3 d to ensure removal of ionic impurities from the central block.

Scheme 2.2 Quaternization of poly(VBIm) using methyl iodide at 23 °C and subsequent anion exchange with $LiTf_2N$ (Used with permission of John Wiley and Sons, 2015)

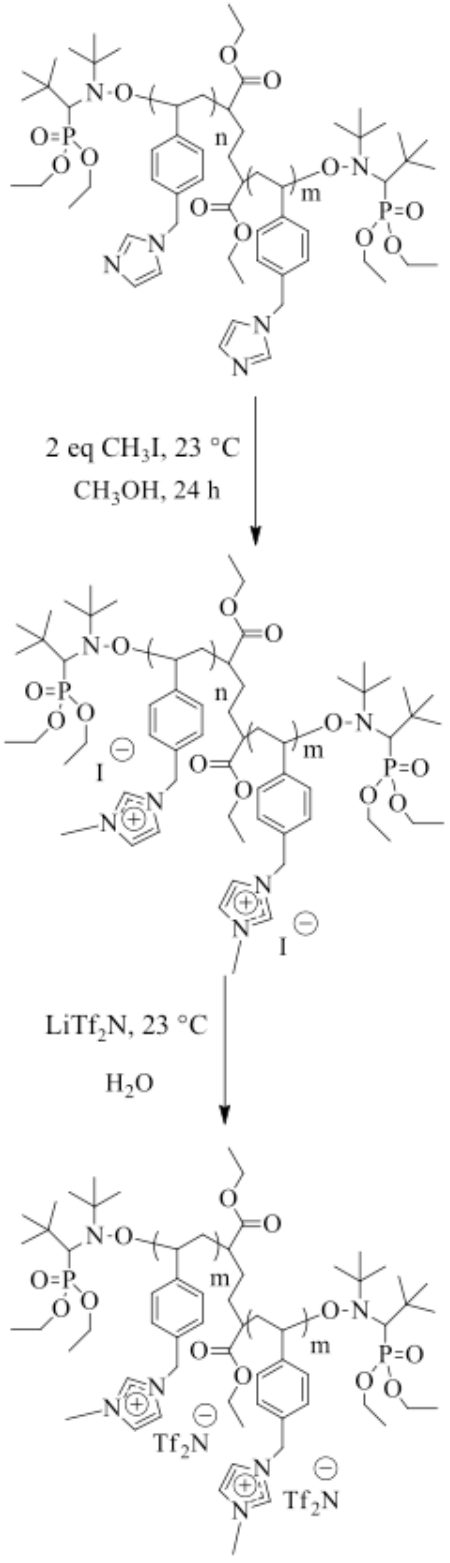

2.3.6 Chain Extension of Poly(EVBIm-Br-20°C)

To confirm controlled polymerization, poly(EVBIm-Tf_2N) (9.2 x 10^{-6} mol), VBIm (10.1415 g, 97.3 mmol), and DEPN (4.0 mg, 0.01 mmol) were dissolved in DMF (17.2 mL). The solution was degassed using three freeze pump thaw cycles and back-filled with argon. The solution was then heated to 125 °C for polymerization shown in Scheme 2.3. The solution was cooled to 23 °C, diluted with acetone (50 mL), and precipitated into hexanes. Polymer was isolated through filtration and dried at reduced pressure (0.5 mm Hg) at 40 °C for 18 h.

Scheme 2.3 Synthesis of ABA triblock copolymer using DEPN at 125 °C with polystyrene external blocks using nitroxide-mediated polymerization. (Used with permission of John Wiley and Sons, 2015)

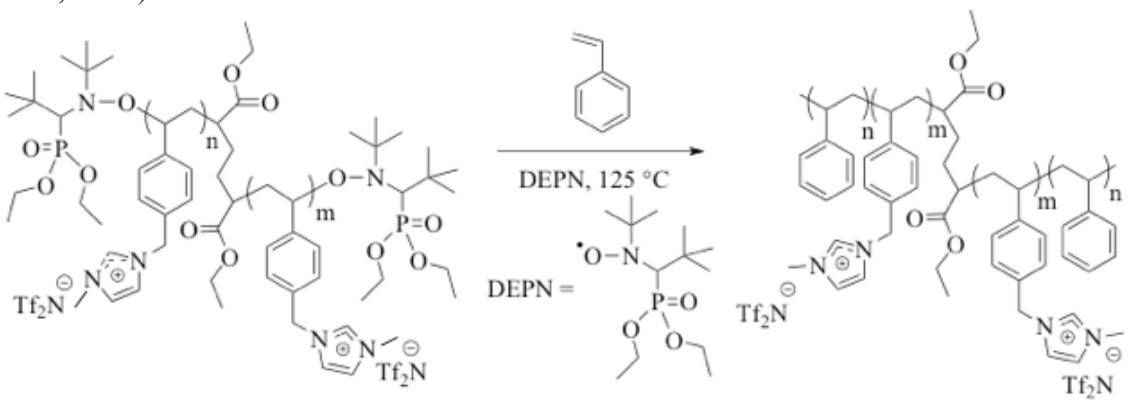

2.4 *Results and Discussions*

For triblock copolymers as efficient electromechanical membranes, ionic conductivity originates from the central block, which is positively charged poly(VBIm) with a mobile anion. The synthesis of poly(VBIm) was successfully reported in the earlier literature.[12,30,31] The molecular weight increased linearly with conversion with narrow PDIs throughout the polymerization of poly(VBIm). Ionic conductivity is a critical property for the application of these triblock copolymers in electromechanical membranes and the charged central block

contributes to the ion transport in these triblock copolymer systems. The procedure for quaternization as reported in the earlier literature at 60 °C shown in

Scheme 2.1 yielded bimodal distributions as observed in aqueous SEC and shown in Figure 2.1. Therefore, quaternization conditions were probed at temperatures of 20, 40 and 60 °C.

As shown in Figure 2.1, although bimodality disappeared at 20 °C, the % quaternization, as calculated from ^{1}H NMR, was low with 1-bromoethane. Thus, a more reactive alkylating agent, methyl iodide (CH_3I), was used for quaternizing poly(VBIm) at 23 °C. Figure 2.1 shows that the PDI remains narrow after quaternization with CH_3I and also after anion exchange with Tf_2N^- (Scheme 2.2). Nitroxide links are prone to cleavage at higher temperatures due to the inherent instability of C-ON bond generating radicals. The observed high molecular weight is contributed to the radical-radical coupling reactions under the reflux conditions at high temperatures (40 and 60 °C). Using a stronger alkylating agent (methyl iodide), it is possible to avoid reflux conditions and still obtain 100 % quaternization. This supports the formation of a central block having narrow PDIs and similar molecular weights. The quantitative anion exchange was confirmed using ^{1}H NMR spectroscopy and X-ray photoelectron spectroscopy (XPS). An increase in molecular weight was observed upon chain extension VBIm, confirming the controlled nature of the polymerization (Figure 2.1).

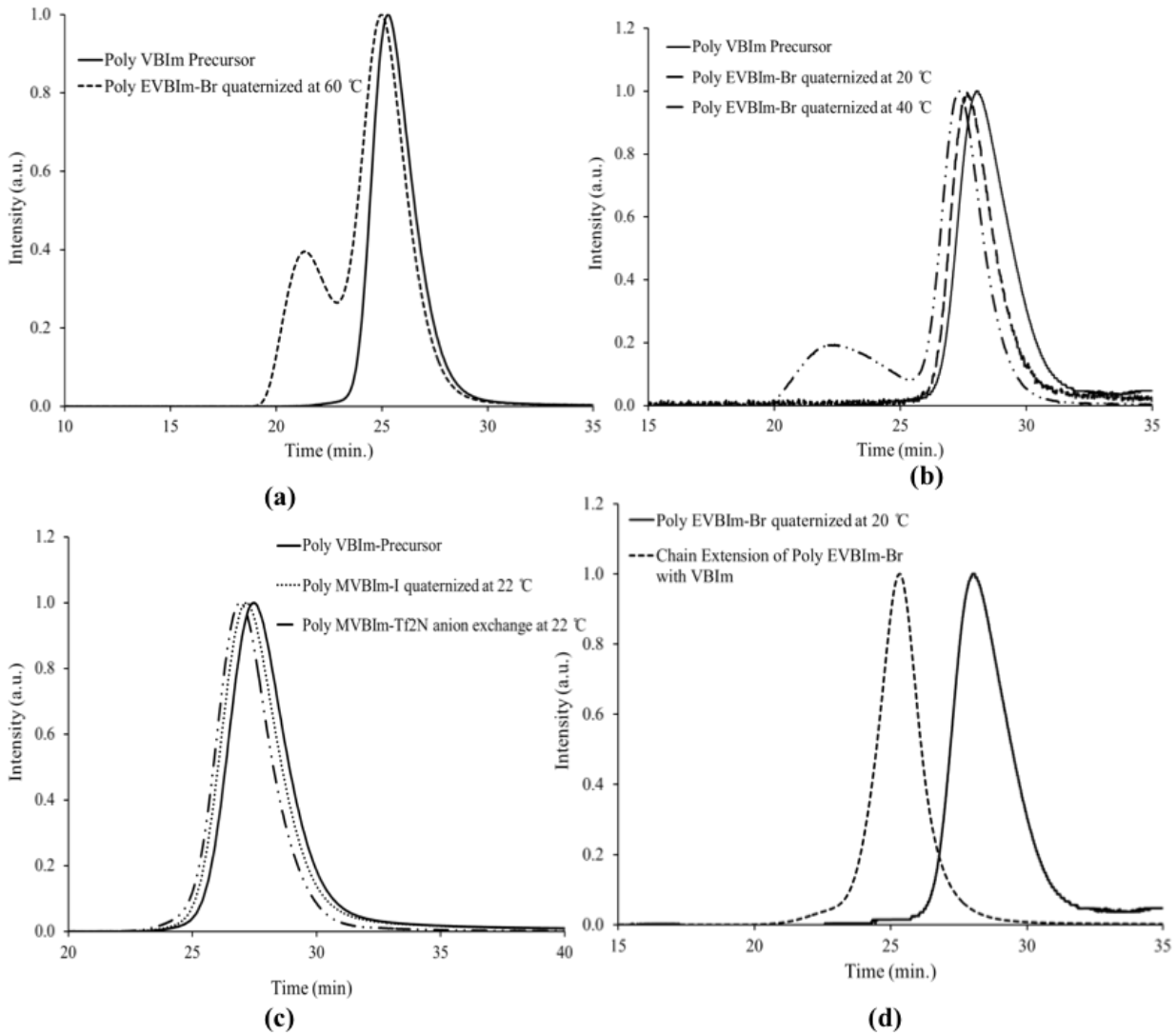

Figure 2.1 (a) Bimodal peak observed in SEC after quaternization of poly(VBIm) using 1-bromoethane at 60 °C. **(b)** SEC traces of poly(VBIm) and poly(EVBIm-Br) obtained from different quaternization temperatures. **(c)** SEC curves showing narrow PDI was maintained after quaternization of poly(VBIm) with methyl iodide and anion exchange with $LiTf_2N$.**(d)** SEC traces of poly (EVBIm-Br-20 °C) precursor and chain extended with VBIm showing increase in molecular weight with conversion and narrow PDI. (Used with permission of John Wiley and Sons, 2015)

The kinetics of poly(MVBIm-Tf_2N) chain extension with styrene (Scheme 2.3) were investigated using ^{1}H NMR spectroscopy to calculate molecular weights. SEC was not used to determine molecular weights due to insolubility issues in the SEC mobile phase. **Figure 2.2**

demonstrate the linear increase in molecular weight with conversion in a controlled fashion to obtain ABA triblock copolymers with polystyrene external blocks and a poly(MVBIm-Tf_2N) central block.

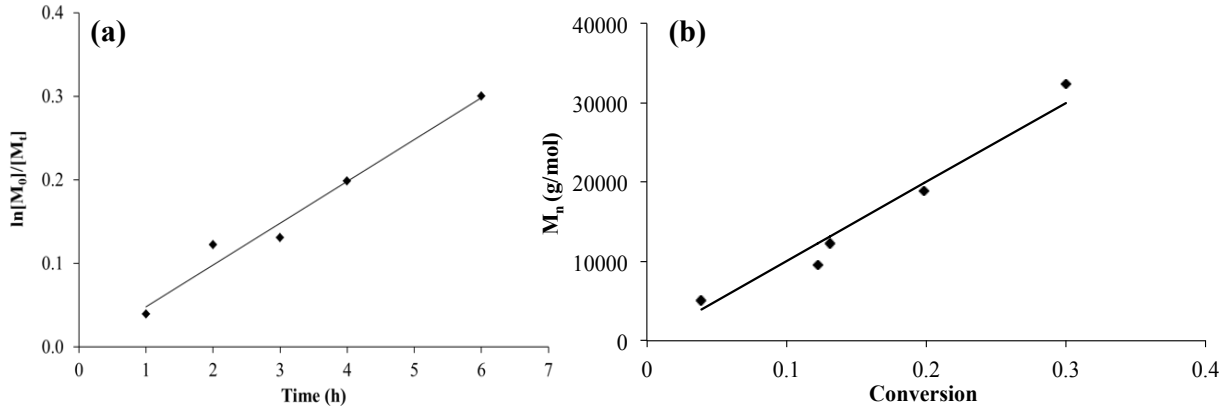

Figure 2.2 (a) Monomer conversion *vs* time plot for chain extension of poly(MVBIm-Tf_2N) with styrene demonstrates pseudo-first order kinetics. Solid line shows the linear increase in monomer conversion with time. **(b)** Plot of number-average molecular weight (M_n) *vs* monomer conversion for chain extension of poly(MVBIm-Tf_2N) with styrene. Solid line represents the ideal molecular weight formation for a controlled radical polymerization. (Used with permission of John Wiley and Sons, 2015)

Thermomechanical properties of these triblock copolymers were ideal for electromechanical actuator applications. The thermal properties depended on the presence of charge and counterion selection. As observed in the literature,[22,31] T_g of the homopolymer poly(VBIm) increased from 105 to 126 °C after quaternization with methyl iodide and decreased to 22 °C after anion exchange to Tf_2N^-. TGA showed that thermal stability decreased after quaternization due to the more basic anion I^- and increased after anion exchange to the less basic couteranion Tf_2N^-. Mahanthappa and coworkers[22] previously determined the degradation mechanism for imidazolium homopolymers with varying counteranion and alkyl substituents. Homopolymers with Tf_2N^- counteranion displayed single-step degradation, which was attributed to the main chain polymer degradation. Table 2.1 shows the PDI remains narrow after

quaternization with CH_3I and anion exchange with $LiTf_2N$. All triblock copolymers exhibited two T_g's, corresponding to the quaternized central block and the second transition arose from the T_g of polystyrene as shown in Table 2.1. All triblock copolymers have high molecular weights and do not exhibit weight loss to 300 °C. ^{1}H NMR spectroscopy determined copolymer compositions, and **Figure 2.2** shows the plot of the molecular weights also calculated using ^{1}H NMR spectroscopy *vs.* monomer conversion.

Table 2.1 Thermal transitions and molecular weights of imidazole-containing polymers. (Used with permission of John Wiley and Sons, 2015)

Polymer	**M_n (g/mol)**	**M_w[a] (g/mol)**	**PDI[a]**	**T_{g1}[c] (°C)**	**T_{g2}[c] (°C)**	**$T_{d,5\%}$[d] (°C)**
Poly(VBIm)	73,000[a]	73,400	1.13	105	-	348
Poly(MVBIm-I)	77,000[a]	94,000	1.16	126	-	251
Poly(MVBIm-Tf_2N)	80,000[a]	99,000	1.17	22	-	339
Poly[Sty_{10}-MVBIm-Tf_2N_{80}-Sty_{10}]	100,000[b]	-	-	22	-	323
Poly[Sty_{35}-MVBIm-Tf_2N_{80}-Sty_{35}]	150,000[b]	-	-	27	106	329
Poly[Sty_{40}-MVBIm-Tf_2N_{35}-Sty_{40}]	200,000[b]	-	-	13	102	334

[a] SEC: 35 °C, 1 mL/min, MALLS detector, 54/23/23 (v/v/v %) H_2O/CH_3OH/AcOH, 0.1 M NaOAc; dn/dc=0.2310 mL/g
[b] ^{1}H NMR spectroscopy: 400 MHz, DMSO-d_6, 25 °C
[c] DSC: 10 °C/min, N_2 atmosphere, second heat
[d] TGA: 10 °C/min, N_2 atmosphere

The morphology of these triblock copolymers was investigated by indexing azimuthally integrated small angle X-ray scattering (SAXS) profiles. In an effort to obtain higher degrees of long-range nanoscale order, samples for SAXS, DRS, and DMA were solvent-cast films from mixtures of 80:20 $CHCl_3$:CH_3OH and vacuum annealed for 5 d at 120 °C. Solvent cast films formed lamellae with long-range order and indicated a microphase-separated morphology. Figure 2.3 shows SAXS data for the triblock copolymer with 47 wt.% styrene. The profile

exhibits reflections at *1q**, *3q** and *5q** with structure factor extinctions of *2q** and *4q** where *1q** is the position of the primary scattering peak, indicating that the solvent cast films contained lamellae morphology with long-range order. The absence of peaks at *2q** and *4q** was due to structure factor extinctions at *2q** and *4q**. This indicates lamellar microstructure with symmetric volume fractions of each block.[32] The domain spacing of the lamellae was ~ 70 nm. This is the first time to observe microphase separation in these triblock copolymers as compared to earlier literature.[12] Wide-angle X-ray scattering (WAXS) shows peaks corresponding to correlation distances between amorphous carbon backbone chains, between phenyl groups and ionic aggregates in these triblock copolymers.

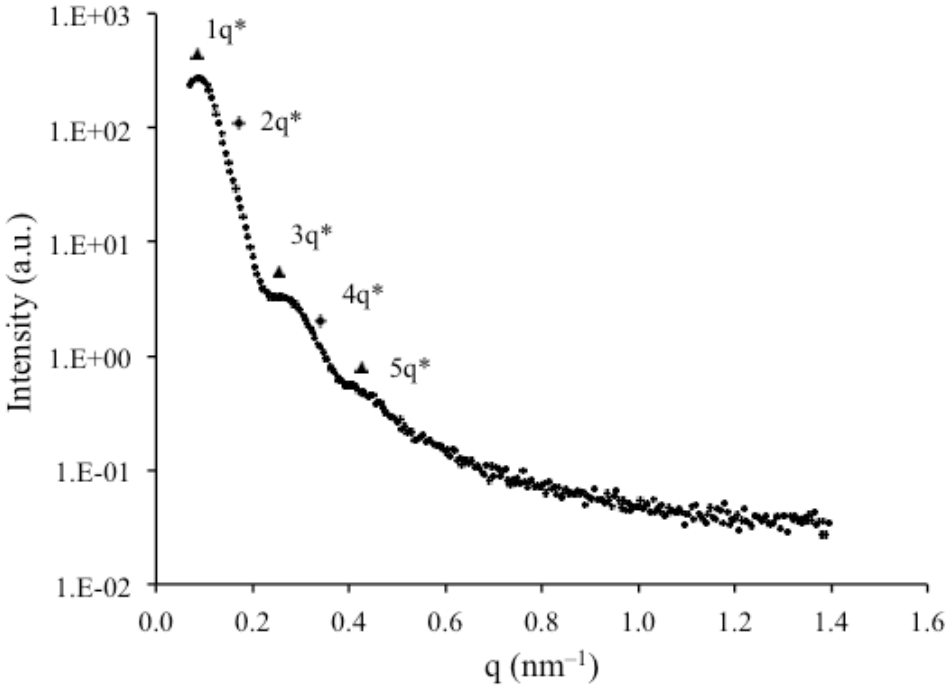

Figure 2.3 Small-angle X-ray scattering (SAXS) profile of charged triblock copolymer having 47 wt. % of styrene. (Used with permission of John Wiley and Sons, 2015).

The interplay of ionic conductivity and membrane modulus is very critical for electromechanical transducer applications. All triblock copolymers displayed mechanical

properties indicative of microphase-separation as shown in Figure 2.4. The DMA T_g's, defined as the temperature where modulus drops 1/2 of the glassy modulus, are 13, 9 and 6 °C for 20, 47 and 60 wt.% styrene. DMA confirmed the presence of two distinct polymer phases with the central block T_g at ~ 10 °C and polystyrene external block T_g at 100 °C. ABA triblock copolymer with 20 wt.% polystyrene external blocks had the highest DMA T_g of the central block without a T_g for the polystyrene external blocks, suggesting polystyrene in the ion-conducting phase. The room temperature modulus of ~100 MPa is ideal for actuator fabrication because this range affords a strong matrix for ion conduction without inhibiting actuation. Moisture content will also significantly influence electromechanical transducers, and chain extension with styrene resulted in an inherently more hydrophobic triblock copolymer. Charged polymers exhibit the ability to absorb moisture, which is quantified using TGA-sorption analysis.[33] These triblock copolymers showed less than 1% weight gain at 25 °C and 10% relative humidity over 10 h.

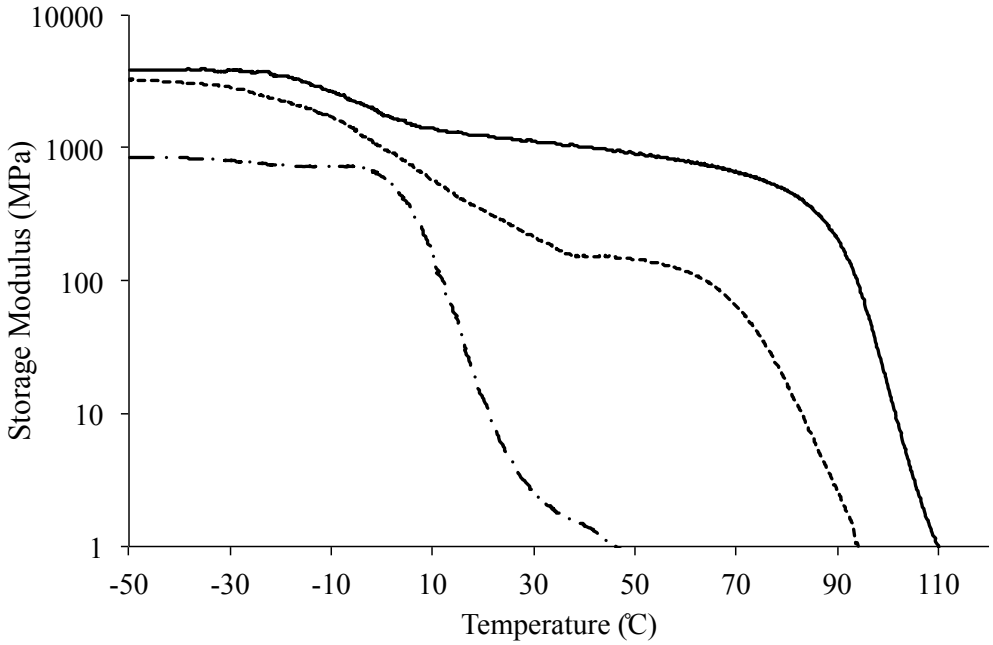

Figure 2.4 Thermomechanical properties of triblock copolymer with (a) 20 (b) 47 and (c) 60 wt. % fractions of polystyrene blocks. (Used with permission of John Wiley and Sons, 2015)

Ionic conductivity in single-ion conductors strongly depends on frequency and temperature.[34] The value of DC conductivity presented in Figure 2.5 is defined as the in-phase component of the conductivity, which is independent of frequency in a roughly 3-decade frequency range. Triblock copolymer which has the lowest weight percent of the ion-conducting blocks, exhibited the highest ionic conductivity and the lowest T_g of the ion conducting block. Ionic conductivity decreased with increasing weight percent of the imidazolium ion-containing block and correlated closely with the T_g of the ion-containing block[15].

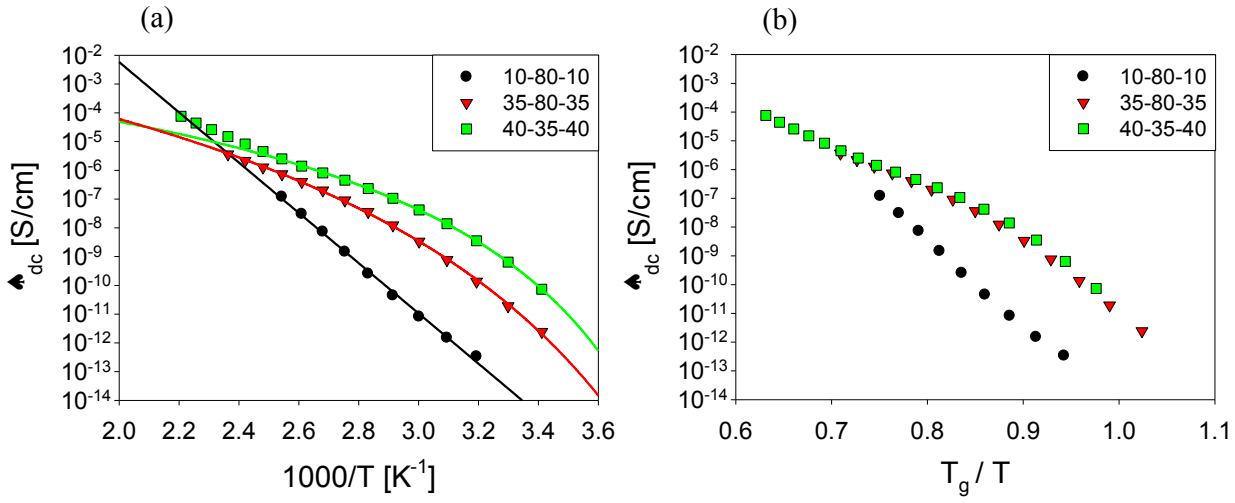

Figure 2.5 (a) Temperature dependence of ionic conductivity for triblock copolymer with different weight percent of the styrene external blocks. Solid curves are equation 8 with parameters in Table 2. **(b)** Ionic conductivity with respect to inverse temperature normalized by T_{g1} in Table 1. (Used with permission of John Wiley and Sons, 2015)

The ionic conductivity (σ) can be simply expressed by

$$\sigma = pe\mu \qquad 1$$

where p, e, and μ are total number density of conducting ions, elementary electric charge, and conducting ion mobility, respectively. It is crucial to determine whether the increase in ionic conductivity has a larger contribution from the number density of simultaneously conducting ions or their mobility in order to understand the anionic counterion conduction. This is assessed with electrode polarization at very low frequencies in dielectric relaxation spectroscopy (DRS).[34]

In DRS, a sinusoidal ac field is applied to a thin-film sample sandwiched between two blocking electrodes. The electrode polarization (EP) occurs at frequencies low enough such that the transporting ions have sufficient time to polarize at the electrodes during each cycle. A physical model of EP,[35-38] which has been applied to a number of single-ion conductors

recently,[2,3,34,39-42] determined the number density of simultaneous conductors and their mobility. The time scale for full polarization at the electrode is

$$\tau_{EP} \equiv \frac{\varepsilon_{EP}\varepsilon_0}{\sigma_{DC}} \qquad 2$$

where ε_{EP} is the effective permittivity after the electrode polarization is complete, ε_0 is the permittivity of vacuum, and σ_{DC} is the DC conductivity. The time scale of conduction or when the ion motion becomes diffusive is

$$\tau_{\sigma} \equiv \frac{\varepsilon_s\varepsilon_0}{\sigma_{DC}} \qquad 3$$

where ε_s is the static dielectric constant. EP is regarded as a simple Debye relaxation in the Macdonald and Coelho model[35-38] with the loss tangent peak expressed as

$$\tan\delta = \frac{\varepsilon''}{\varepsilon'} = \frac{\omega\tau_{EP}}{1+\omega^2\tau_{\sigma}\tau_{EP}} \qquad 4$$

where the peak maximum frequency relates to the geometric mean of the two fitting parameters τ_{EP} and τ_{σ}, demonstrated in Figure 2.6.

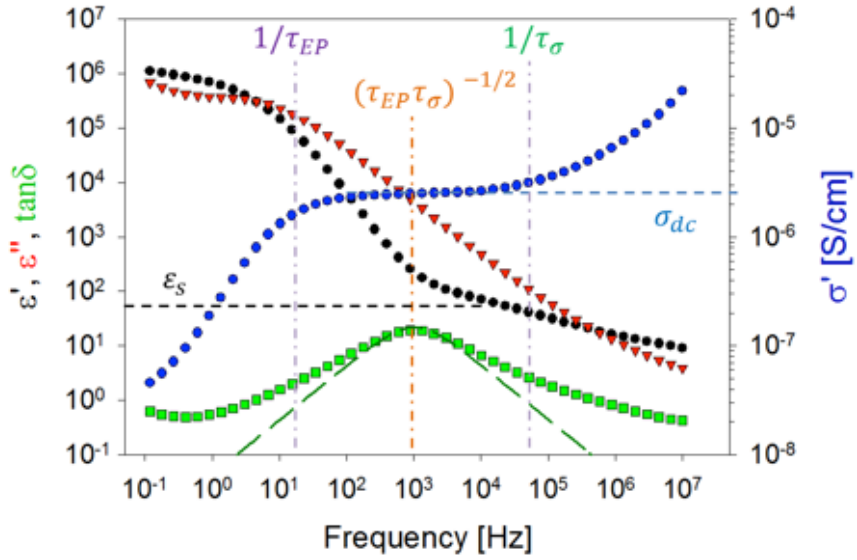

Figure 2.6 Representative dielectric spectra and fitting of the loss tangent peak with Equation 4] at 120 °C. (Used with permission of John Wiley and Sons, 2015).

Since one type of ion is attached to the polymer chain and assumed to be immobilized, the counterion's mobility μ and number density of simultaneous conducting ions p are then determined from the fitting parameters,

$$\mu = \frac{eL^2\tau_\sigma}{4\tau_{EP}{}^2 kT} \qquad 5$$

$$p = \frac{\sigma_{DC}}{e\mu} = \frac{4\sigma_{DC}\tau_{EP}{}^2 kT}{e^2L^2\tau_\sigma} \qquad 6$$

where L is the sample thickness between electrodes, k is Boltzmann's constant, and T is the absolute temperature.

The temperature dependence of the number density of simultaneously conducting ions calculated from Equation 6 is plotted in Figure 2.7 and is well-described using the Arrhenius equation,

$$p = p_\infty \exp(-\frac{E_a}{RT}) \qquad 7$$

where p_∞ is the conducting ion concentration as $T \to \infty$ and E_a is the activation energy for conducting ions listed in Table 2.2. The activation energy is related to the Coulomb energy of a cation-anion pair, and this electrostatic attraction is the main driving force for pair and aggregate formation, mediated by an effective dielectric constant of the ion-conducting block.

Table 2.2 Fitting parameters (Equation 7) for the temperature dependence of the number density of simultaneously conducting ions. (Used with permission of John Wiley and Sons, 2015).

Sample	$\log p_0 (cm^{-3})$	$\log p_\infty (cm^{-3})$	$E_a (kJ/mol)$	p_∞ / p_0
10-80-10	21.23	17.1	6.0	7.4E-5
35-80-35	21.28	18.6	23	0.0021
40-35-40	21.05	21.05	23	1

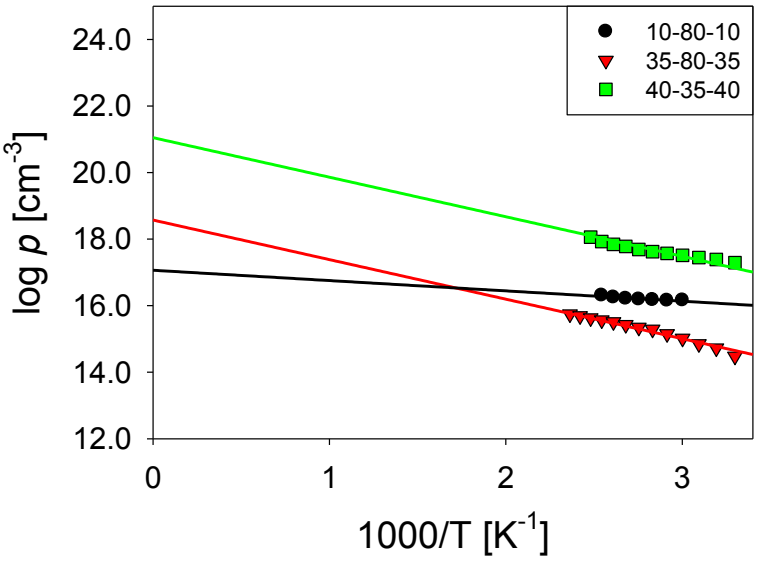

Figure 2.7 Temperature dependence of number density of simultaneously conducting ions for triblock polymer having different weight percent of the styrene external blocks. (Used with permission of John Wiley and Sons, 2015)

The Arrhenius temperature dependence of the conducting ion concentration suggests the conducting ions would be fully dissociated at infinite temperature. Triblock copolymer with 40-35-40 composition has the highest number density of simultaneously conducting ions in the temperature range of DRS measurement, and the intercept of the Arrhenius fit of this sample in Figure 2.7 is fixed to p_0, calculated from a group contribution method with stoichiometry determined from the chemical structure.[43,44] Since all three ionomers have the same cation and mobile anion species, the activation energy (the slope in Figure 2.7), related to the coulomb energy between an ion pair, should be identical. Thus, the conducting ion concentration of polymer with 35-80-35 composition is fitted with the slope fixed to be the same with polymer with 40-35-40 composition and reveals a much smaller ratio of p_∞ / p_0, which represents the fraction of counterions that are participating in conduction. However, the number density of simultaneously conducting ions for polymer with 10-80-10 composition is independent of temperature that corresponds to $p_\infty << p_0$, suggesting the majority of the counterions are trapped and unable to participate in conduction. Since ionic conductivity is obtained over a much wider temperature range than the EP model allows, the activation energies obtained from the Arrhenius fit to the number density of simultaneously conducting ions in Table 2.2 are used polymer with 35-80-35 composition and polymer with 40-35-40 composition to fit the temperature dependence of ionic conductivity with

$$\sigma_{DC} = e\mu_\infty p_\infty \exp(-\frac{DT_0}{T-T_0}) \exp(-\frac{E_a}{RT}) \qquad 8$$

where μ_∞, T_0, and D, listed in Table 2.3, is the highest temperature limit of mobility, Vogel temperature, and the strength parameter that is reciprocally related to fragility, respectively.

Table 2.3 Fitting parameter (Equation 8) for the temperature dependence of ionic conductivity. (Used with permission of John Wiley and Sons, 2015)

Sample	$e\mu_\infty p_\infty (S/cm)$	D	$T_0(K)$	$E_a(kJ/mol)$	$\sigma_{DC}(S/cm)$ at T_g
10-80-10	1.6E+15	0	NA	170	4.3E-15
35-80-35	4.8E-1	9.4	205	23	1.2E-11
40-35-40	2.2E-2	4.5	227	23	1.1E-11

Polymer with 10-80-10 composition shows Arrhenius-like temperature behavior of the ionic conductivity in Figure 2.5 that has also been observed in some polymerized ionic liquid systems,[45,46] suggesting the ion transport does not solely depend on the segmental motion of the ionomer. Thus, the temperature dependence of ionic conductivity for polymer with 10-80-10 composition and was fitted to Equation 8 with D fixed to 0 to reveal a much larger activation energy than the other two triblock copolymers, 96 % comes from mobility. The temperature dependence of the counterion's mobility calculated from Equation 5 is plotted in Figure 2.8. The ion mobility is fitted to the Vogel-Fulcher-Tammann (VFT) equation

$$\mu = \mu_\infty \exp\left(-\frac{DT_0}{T - T_0}\right) \qquad 9$$

with the parameters D and T_0 determined in the fitting of Equation 8. Data for polymer with 10-80-10 composition as the exception is fitted with Arrhenius temperature dependence.

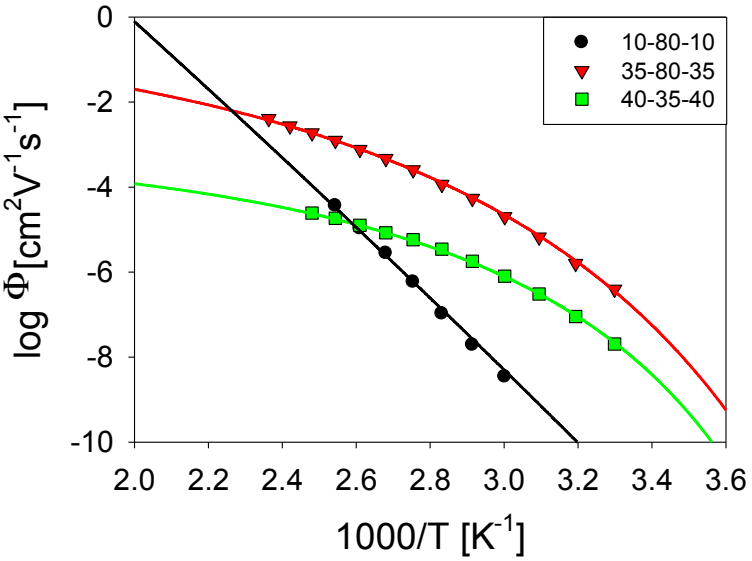

Figure 2.8 Temperature dependence of counterion's mobility for triblock copolymer having different weight percent of the styrene external blocks. (Used with permission of John Wiley and Sons, 2015).

The VFT temperature dependence indicates the coupling of ion transport to segmental motion of the polymer, except for polymer with 10-80-10 composition where both ionic conductivity and ion mobility exhibit Arrhenius temperature dependence. Arrhenius temperature dependence of mobility suggests the polymer with 10-80-10-composition sample has ion motion disconnected from polymer segmental motion, but this sample also shows the lowest conductivity. Polymer with 35-80-35 composition has the highest ion mobility, with mostly contributions from a very small counterion fraction that are not trapped in ionic aggregates. Thus, ionic conductivity remained low because the fraction of ions contributing to conductivity was merely 0.2% if 100% for polymer with 40-35-40 composition The static dielectric constant ε_s shown in Figure 2.9 is calculated from τ_σ in Equation 3 and defined as the low-frequency plateau of the dielectric constant $\varepsilon'(\omega)$ before EP begins.

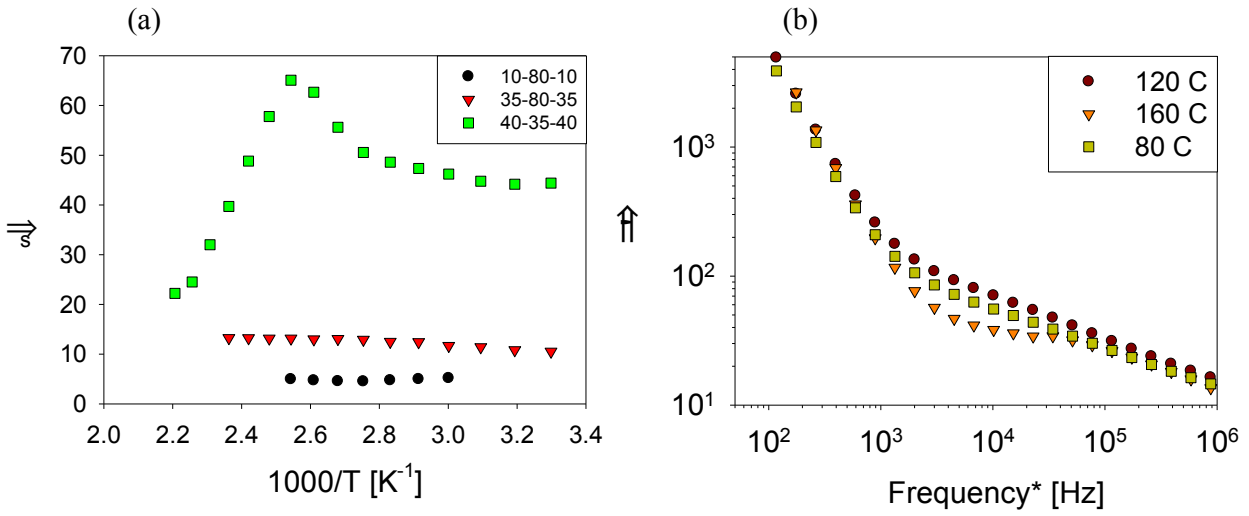

Figure 2.9 (a) Temperature dependence of static dielectric constant for triblock copolymer having different weight percent of the styrene external blocks. (b) Frequency dependence of dielectric permittivity ε' for polymer with 40-35-40 composition at 80 °C, 120 °C, and 160 °C. Data is shifted to align the low frequency EP part for comparison of ε_s, usually defined as the value of ε' before EP starts. (Used with permission of John Wiley and Sons, 2015)

Polymer with 40-35-40 composition has the highest static dielectric constant and is much more polar than the other two triblock copolymers, where the ions are highly aggregated and dipoles cancel. This agrees with the number density of simultaneously conducting ions where polymer with 40-35-40 composition has the largest fraction of ions contributing to conduction and also the highest ionic conductivity. The temperature dependence of static dielectric constant of all three triblock copolymers does not obey the Onsager prediction where thermal randomization of dipoles results in ε_s inversely proportional to temperature and is only applicable to segments with polar groups in the liquid state where their motion is unrestricted by neighbors (far above T_g). The static dielectric constant of polymer with 40-35-40 composition starts to decrease at 120 °C (T_{g2}+20 °C), where cooling toward the T_g of the styrene microphase (T_{g2}) restricts the motion of the neighboring molecules and limits the rotation/alignment of the

dipoles in the ion conducting microphase under an applied field. The decrease of ε_s with decreasing temperature was also observed for poly(alkyl methacrylates) starting near T_g; [47,48]same behavior of ε_s observed in polyacetaldehyde has been associated to an order-disorder transition controlling intermolecular orientation.[49] The very low $\varepsilon_s \cong 5$ for polymer with 10-80-10 composition was consistent with ion motion decoupled from polymer segmental motion as the coulomb interaction between the pendant imidazolium and mobile anion dominate in the low ε_s limit.

The actuation performance of these triblock copolymers *without* ionic liquid was previously reported in the literature and showed ion migration and accumulation at one electrode.[12] In the present study, triblock copolymer polymer with 35-80-35 composition casted with 32 weight percent ionic liquid was fabricated into electromechanical actuators. A cast-with method ensured uniform incorporation of the IL throughout the triblock copolymer.[11] In the evaluation, a 4V DC step input was applied to the actuator at ambient conditions (20 °C and ~ 43% RH) and a high definition camera for further analysis recorded the induced electromechanical actuation. The analysis demonstrated electromechanical actuation upon application of low voltages (Figure 2.10 and Figure 2.11), which is the first time these triblock copolymers have demonstrated actuation. A common feature for electroactive devices containing ionic liquids is a bidirectional bending behavior caused by accumulation of a charged species at one electrode followed by slower accumulation of the opposite charged species at the opposite electrode[27], as is observed in Figure 2.11. The free ions (cations in Nafion® and anions in the reported polymer) did contribute to the bending but their effect is highly limited, due to its much smaller size and amount as compared to the ions of the ionic liquid. Our group has reported the bending

performance of the actuator made of "dry" membrane of another cationic imidazolium-containing polymer, where only one direction bending is observed as a result of the transportation and accumulation of counteranions only. The membranes (both Nafion® and reported polymer) in the current study mainly act as a "container" of ionic liquid, and provide channels for the migration of the ions of ionic liquid. We propose the ions of the ionic liquid are dominating the bending performance of the actuators within this study. These triblock copolymers exhibited electrochemically stability between +4 V and -4 V observed through cyclic voltammetry.

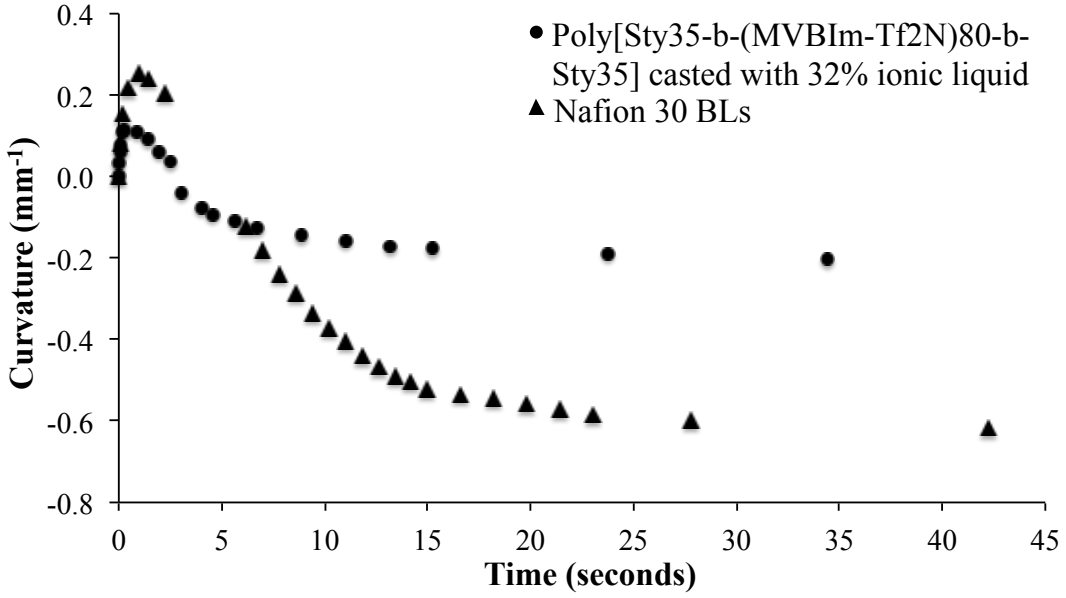

Figure 2.10 Curvature observed under a 4 V applied voltage for electromechanical actuators made from polymer with 35-80-35 composition triblock copolymer casted with 32% of ionic liquid and Nafion® membrane swollen with 34% ionic liquid. (Used with permission of John Wiley and Sons, 2015).

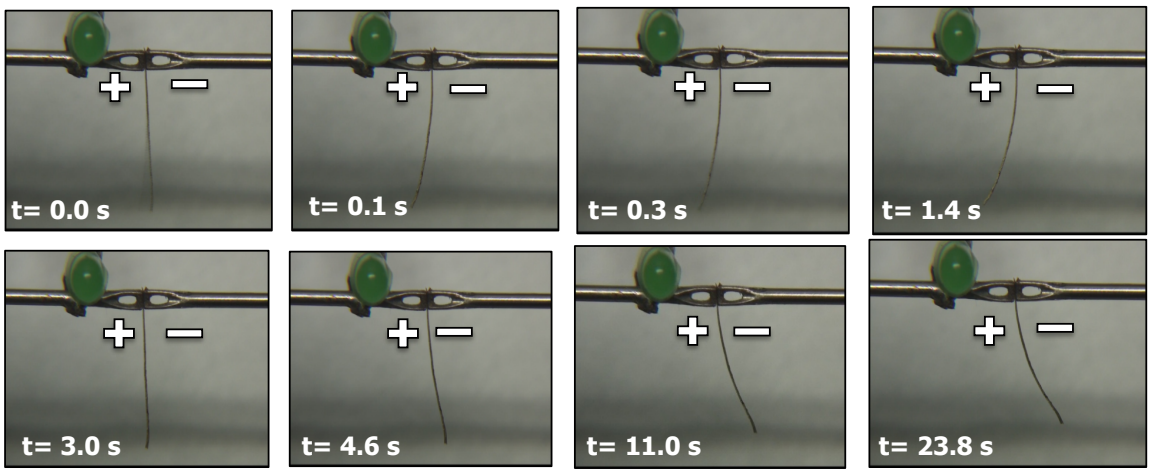

Figure 2.11 Still images of electromechanical transducer fabricated from polymer with 35-80-35 composition film casted with 32 wt.% ionic liquid under applied potential of 4 V. (Used with permission of John Wiley and Sons, 2015).

The bending performance of the actuator of the polymer with 35-80-35 composition triblock copolymer membrane, and a Nafion® membrane swollen with 32% ionic liquid as control are shown in Figure 2.10. Due the different size and migration speed of the cation and anion of IL in the actuator, the triblock copolymer actuator experienced the same bi-directional bending behavior as the Nafion® actuator[27] under the 4V DC applied voltage. Although the triblock copolymer actuator showed smaller bending curvature as compared to Nafion®, the actuation speed was fairly rapid and comparable to the Nafion® actuator. The fast actuation speed indicates the triblock copolymer had good ion conductivity, while the smaller bending curvature was presumably due to lower IL uptake. The calculations of the IL uptake are slightly different for these two cases because of the different fabrication process. The uptake of the reported polymer is for the membrane only while the Nafion® is for the membrane plus CNC layer. As a result, although the uptake of Nafion® (34 %) seems just slightly higher than the one

of the reported polymer (32 %), the net amount of the IL in the Nafion® should be clearly higher than in the reported polymer.

2.5 *Conclusions*

A series of well-defined ABA triblock copolymers with different compositions of central and external blocks were synthesized using nitroxide-mediated polymerization. These are microphase-separated triblock copolymers, exhibiting good mechanical stability and well-defined structure as observed using dynamic mechanical analysis and small angle X-ray scattering, respectively. For the first time, a detailed study of ion transport in these triblock copolymers was performed using dielectric relaxation spectroscopy to understand the contributions of mobile ion concentration, static dielectric constant, and ionic mobility. Polymer with 47 wt.% styrene external blocks exhibited a VFT temperature dependence of ionic conductivity and mobility, indicating coupling between ionic conductivity and segmental motion. This triblock copolymer also displayed the highest ionic conductivity, mobile ion concentration, and static dielectric constant of the triblock copolymers studied. When cast with 32 wt.% ionic liquid, polymer with 40-35-40 composition showed actuation for the first time in the literature.

2.6 *Acknowledgements*

This material is based on work supported by the U.S. Army Research Laboratory and the U.S. Army Research Office under contract/grant number W911NF-07-1-0452 Ionic Liquids in Electro-Active Devices Multidisciplinary University Research Initiative (ILEAD MURI). The authors acknowledge the Laboratory for Research on the Structure of Matter at Penn (MRSEC NSF DMR11-20901) for instrument support.

2.7 *References*

(1) Duncan, A. J.; Leo, D. J.; Long, T. E. *Macromolecules* **2008**, *41*, 7765.
(2) Tudryn, G. J.; Liu, W.; Wang, S.-W.; Colby, R. H. *Macromolecules* **2011**, *44*, 3572.
(3) Wang, S.-W.; Liu, W.; Colby, R. H. *Chemistry of materials* **2011**, *23*, 1862.
(4) Akle, B. J.; Bennett, M. D.; Leo, D. J.; Wiles, K. B.; McGrath, J. E. *Journal of Materials Science* **2007**, *42*, 7031.
(5) Akle, B. J.; Leo, D. J. *Smart materials and structures* **2007**, *16*, 1348.
(6) Bar-Cohen, Y.; Zhang, Q. *MRS bulletin* **2008**, *33*, 173.
(7) Park, I.-S.; Jung, K.; Kim, D.; Kim, S.-M.; Kim, K. J. *MRS bulletin* **2008**, *33*, 190.
(8) Montazami, R.; Liu, S.; Liu, Y.; Wang, D.; Zhang, Q.; Heflin, J. R. *Journal of Applied Physics* **2011**, *109*, 104301.
(9) Green, M. D.; Choi, J.-H.; Winey, K. I.; Long, T. E. *Macromolecules* **2012**, *45*, 4749.
(10) Liu, S.; Montazami, R.; Liu, Y.; Jain, V.; Lin, M.; Heflin, J. R.; Zhang, Q. *Applied Physics Letters* **2009**, *95*, 023505.
(11) Wu, T.; Wang, D.; Zhang, M.; Heflin, J. R.; Moore, R. B.; Long, T. E. *ACS applied materials & interfaces* **2012**, *4*, 6552.
(12) Green, M. D.; Wang, D.; Hemp, S. T.; Choi, J.-H.; Winey, K. I.; Heflin, J. R.; Long, T. E. *Polymer* **2012**.
(13) Nemat-Nasser, S.; Li, J. Y. *Journal of Applied Physics* **2000**, *87*, 3321.
(14) Weiland, L. M.; Leo, D. J. *Smart materials and structures* **2004**, *13*, 323.
(15) Duncan, A. J.; Leo, D. J.; Long, T. E.; Akle, B. J.; Park, J. K.; Moore, R. B. In *The 16th International Symposium on: Smart Structures and Materials & Nondestructive Evaluation and Health Monitoring*; International Society for Optics and Photonics: 2009, p 728711.
(16) Lin, J.; Liu, Y.; Zhang, Q. *Polymer* **2011**, *52*, 540.
(17) Eisenberg, A.; Hird, B.; Moore, R. *Macromolecules* **1990**, *23*, 4098.
(18) Mauritz, K. A.; Moore, R. B. *Chemical reviews* **2004**, *104*, 4535.
(19) Green, M. D.; Schreiner, C.; Long, T. E. *The Journal of Physical Chemistry A* **2011**, *115*, 13829.
(20) Cheng, S.; Beyer, F. L.; Mather, B. D.; Moore, R. B.; Long, T. E. *Macromolecules* **2011**, *44*, 6509.
(21) Green, M. D.; Salas‐de la Cruz, D.; Ye, Y.; Layman, J. M.; Elabd, Y. A.; Winey, K. I.; Long, T. E. *Macromolecular Chemistry and Physics* **2011**, *212*, 2522.
(22) Weber, R. L.; Ye, Y.; Banik, S. M.; Elabd, Y. A.; Hickner, M. A.; Mahanthappa, M. K. *Journal of Polymer Science Part B: Polymer Physics* **2011**, *49*, 1287.
(23) Allen Jr, M. H.; Wang, S.; Hemp, S. T.; Chen, Y.; Madsen, L. A.; Winey, K. I.; Long, T. E. *Macromolecules* **2013**, *46*, 3037.
(24) Weber, R. L.; Ye, Y.; Schmitt, A. L.; Banik, S. M.; Elabd, Y. A.; Mahanthappa, M. K. *Macromolecules* **2011**, *44*, 5727.
(25) Ye, Y.; Choi, J.-H.; Winey, K. I.; Elabd, Y. A. *Macromolecules* **2012**, *45*, 7027.
(26) Heiney, P. A. *Commission on Powder Diffraction Newsletter* **2005**, *32*, 9.

(27) Liu, Y.; Liu, S.; Lin, J.; Wang, D.; Jain, V.; Montazami, R.; Heflin, J. R.; Li, J.; Madsen, L.; Zhang, Q. *Applied Physics Letters* **2010**, *96*, 223503.
(28) Mather, B. D.; Lizotte, J. R.; Long, T. E. *Macromolecules* **2004**, *37*, 9331.
(29) Grimaldi, S.; Finet, J.-P.; Le Moigne, F.; Zeghdaoui, A.; Tordo, P.; Benoit, D.; Fontanille, M.; Gnanou, Y. *Macromolecules* **2000**, *33*, 1141.
(30) Ye, Y.; Elabd, Y. A. *Macromolecules* **2011**, *44*, 8494.
(31) Ye, Y.; Elabd, Y. A. *Polymer* **2011**, *52*, 1309.
(32) Roe, R.; New York: Oxford University Press.
(33) Allen Jr, M. H.; Wang, S.; Hemp, S. T.; Chen, Y.; Madsen, L. A.; Winey, K. I.; Long, T. E. *Macromolecules* **2013**.
(34) Lee, M.; Choi, U. H.; Colby, R. H.; Gibson, H. W. *Chemistry of Materials* **2010**, *22*, 5814.
(35) Macdonald, J. R. *Physical review* **1953**, *92*, 4.
(36) Coelho, R. *Rev. Phys. Appl. (Paris)* **1983**, *18*, 137.
(37) Coelho, R. *Journal of Non-Crystalline Solids* **1991**, *131*, 1136.
(38) Macdonald, J. R. *Solid State Ionics* **2005**, *176*, 1961.
(39) Klein, R. J.; Zhang, S.; Dou, S.; Jones, B. H.; Colby, R. H.; Runt, J. *The Journal of chemical physics* **2006**, *124*, 144903.
(40) Fragiadakis, D.; Dou, S.; Colby, R. H.; Runt, J. *Macromolecules* **2008**, *41*, 5723.
(41) Fragiadakis, D.; Dou, S.; Colby, R. H.; Runt, J. *The Journal of chemical physics* **2009**, *130*, 064907.
(42) Choi, U. H.; Lee, M.; Wang, S.; Liu, W.; Winey, K. I.; Gibson, H. W.; Colby, R. H. *Macromolecules* **2012**, *45*, 3974.
(43) Van Krevelen, D. W.; Te Nijenhuis, K. *Properties of polymers: their correlation with chemical structure; their numerical estimation and prediction from additive group contributions*; Elsevier Science, 2009.
(44) Slattery, J. M.; Daguenet, C.; Dyson, P. J.; Schubert, T. J.; Krossing, I. *Angewandte Chemie* **2007**, *119*, 5480.
(45) Chen, H.; Choi, J.-H.; Salas-de la Cruz, D.; Winey, K. I.; Elabd, Y. A. *Macromolecules* **2009**, *42*, 4809.
(46) Nakamura, K.; Saiwaki, T.; Fukao, K. *Macromolecules* **2010**, *43*, 6092.
(47) Ishida, Y.; Matsuo, M.; Yamafuji, K. *Kolloid-Zeitschrift und Zeitschrift für Polymere* **1962**, *180*, 108.
(48) Sasabe, H.; Saito, S. *Journal of Polymer Science Part A‐2: Polymer Physics* **1968**, *6*, 1401.
(49) Williams, G. *Transactions of the Faraday Society* **1963**, *59*, 1397.

Chapter 3: **Imidazole-Containing Triblock Copolymers With a Synergy of Ether and Imidazolium Sites**

Reproduced from *Journal of Material Chemistry C* **2015,** *3(16)*, 3891-3901

Used with permission of Elsevier, 2015

Chainika Jangu[1], Jing-Han Helen Wang[2], Dong Wang[3], Gregory Fahs[1], James R. Heflin[3], Robert B. Moore[1], Ralph H. Colby[2] and Timothy E. Long[1*]

[1]*Department of Chemistry & Macromolecules and Interfaces Institute (MII), Virginia Tech., Blacksburg, VA 24061*
[2]*Department of Chemical Engineering, The Pennsylvania State University, University Park, Pennsylvania 16802*
[3]*Department of Physics & MII, Virginia Tech., Blacksburg, VA 24061*

*To whom the correspondence should be addressed Email telong@vt.edu. TEL: (540) 231-2480 FAX: (540) 231-8517

Keywords: RAFT; ABA triblock copolymers; electromechanical transducers

3.1 *Abstract*

Reversible addition-fragmentation chain transfer (RAFT) polymerization strategy enabled the synthesis of well-defined A-BC-A triblock copolymers containing a synergy of pendant ether and imidazolium sites. The soft central BC block comprises low T_g di(ethylene glycol) methyl ether methacrylate (DEGMEMA) and 1-(4-vinylbenzyl) methyl imidazolium units. External polystyrene blocks provide mechanical reinforcement within a nanoscale morphology. Dynamic mechanical analysis (DMA) of the A-BC-A triblock copolymers exhibited a rubbery plateau, which suggested the formation of a microphase-separated morphology. Atomic force microscopy (AFM) and small angle X-ray scattering (SAXS) collectively probed the morphology of the A-BC-A triblock copolymers, revealing long-range order at the nanoscale dimensions. Dielectric relaxation

spectroscopy (DRS) examined the ion-transport properties of ionomeric A-BC-A triblock copolymers and random copolymers with different compositions. The role of morphology was demonstrated with block copolymer nanoscale structures providing superior conductivity and mechanical performance compared to random copolymers. Under a 4 V direct current (DC) applied voltage, electromechanical transducers derived from these triblock copolymer membranes showed superior performance compared to a benchmark Nafion® membrane, suggesting potential for ionic polymer device applications. This was attributed to optimum modulus, improved ionic conductivity, and microphase-separated morphology of triblock copolymers.

3.2 *Introduction*

The design and synthesis of "smart" macromolecules that respond to external stimuli such as temperature, pH, electrolytes, light, mechanical stress, and applied potential remains an area of intense interest for biological and engineering applications.[1-4] In many cases, these macromolecules are designed to mimic behavior of biological polymers and outperform commercially available materials. Prior to the development of controlled radical polymerization (CRP) techniques, lack of structural and molecular weight control with broad polydispersity indices (PDI) limited the discovery of well-defined macromolecules with requisite features for designing smart macromolecules for various applications.[5-12] CRP facilitated the synthesis of a broad range of triblock copolymers with well-defined architecture and controlled molecular weights.[1] Reversible addition-fragmentation chain transfer (RAFT) provides versatility to effectively control molecular weight with judicious chain-transfer agent (CTA) and monomer combinations,

solvent, and initiator concentration. RAFT polymerization is currently one of the most versatile CRP synthetic methods capable of affording complex macromolecules with controlled architectures, leading to a tailored range of response to external stimuli. For example, mechanical deformation under applied voltage for electromechanical transducers provides potential energy harvesting devices, biomimetic materials, and sensors.[13-17] Currently, Nafion® serves as a benchmark material for the electrically stimulated electromechanical transducers due to optimal performance.[18] The microphase[19]-separated morphology in Nafion® membranes provides superior performance as an electromechanical transducer. Microphase-separated block copolymers synthesized using CRP techniques present a facile strategy to mimic the semi-crystalline morphology of Nafion® through the inclusion of high modulus domains for mechanical reinforcement and ion-rich soft phases that facilitate ion migration.[13,20-25] Thus, recent efforts focus on the synthesis of novel ionomeric block copolymers with the potential for preparing electroactive devices.

The synthesis of a difunctional CTA for a divergent chain growth strategy for ABA triblock copolymers was described in our earlier literature.[26] Divergent chain growth maintains thiocarbonylthio groups at the propagating chain end, which results in a polymer main chain that is both thermally and hydrolytically stable. Our group has established suitable conditions for the RAFT polymerization of di(ethylene glycol) methyl ether methacrylate (DEGMEMA) with 1,6-bis(4-cyano-4-(ethylsulfanyl-thiocarbonylsulfanyl)pentanoic acid) hexane diamide (*d*CEP-NH_2) as a CTA.[26] Our group has also described ABA triblock copolymers using nitroxide-mediated polymerization (NMP) with polystyrene external blocks and a charged imidazolium-containing central

block. These well-defined triblock copolymers exhibited sufficient modulus and ionic conductivity for electromechanical transducers.[2,27] We also reported the synthesis of high molecular weight poly[Sty-*b*-(*n*BA-*co*-DMAEMA)-*b*-Sty] using RAFT synthesis, and triblock copolymers with tunable properties showed electro-responsiveness under the application of low voltage (2-4 V).[3] Elabd, Winey and co-workers recently synthesized block copolymers containing 1-[(2-methacryloyloxy)ethyl]-3-butylimidazolium bis(trifluoromethane sulfonyl)imide (MEBIm-TFSI) and methyl methacrylate (MMA) utilizing RAFT polymerization to understand the influence of phase separation on ionic conductivity.[28,29]

The self-assembled, nanostructured morphology of block copolymers enabled enhanced conductivity compared to random analogs for solid-state polymer electrolytes. Block copolymers provide a unique opportunity in polymer/ionic liquid mixtures, where a variety of nanoscale, self-assembled morphologies are accessible as a function of composition and thermodynamic incompatibility.[30] Elabd and Winey reported a polymerized ionic liquid diblock copolymer exhibiting nanoscale morphology with high hydroxide conductivity. The ionic conductivity was found to be higher than random copolymers with similar ion and water content, as well as its homopolymer analog.[31] Elabd *et al.* also demonstrated a two-order increase in ionic conductivity for diblock copolymers containing the same comonomers as random copolymers to reveal the importance of a well-defined morphology for improved ion-transport.[28] Gao *et al.* reported successful synthesis of PEG-based sulfonated polyurethanes containing sulfonates in either the soft or hard segment. The influence of charge placement on

thermomechanical properties, hydrogen bonding interactions, and morphologies of PEG-based sulfonated polyurethanes was demonstrated.[32]

Control over ABA triblock composition allows for tailored charge content, tunable mechanical properties, and well-defined morphology.[19,25,33,34] A fundamental study on the dependence of ionic conductivity on composition, morphology, and monomer selection in ionomeric triblock copolymers is essential to facilitate the intelligent design of ion-conducting polymers. Recent studies stressed that materials having low glass transition temperatures (T_g) are required to obtain high ionic conductivity, reflecting the coupling of ion-motion to polymer segmental dynamics.[28,35] However, these conductive materials are of limited use as devices due to lack of mechanical strength. Block copolymers self-assemble to form physically crosslinked, mechanically tough, nanostructured polymers, and thus have attracted significant attention in the design of polymer electrolytes for electromechanical devices. Mahanthappa *et al.* prepared poly(imidazolium) block copolymers, and the effects of macroscopic connectivity and morphological on conductivity was demonstrated in these materials.[33]

In this manuscript, we demonstrate the synthesis of novel, well-defined A-BC-A triblock copolymers containing soft "BC" central blocks of DEGMEMA and imidazolium sites with polystyrene external blocks. Earlier work has demonstrated that increasing the dielectric constant of the ion-containing phase with proper monomer selection without raising T_g optimizes ionic conductivity. Diluting the ion concentration of the ion-rich phase with neutral comonomers that have high dielectric constant reduces T_g, increases ion dissociation, and potentially maximizes ionic conductivity. Lowering T_g

of a charged polymer also increases segmental mobility and thus ionic conductivity.[36,37] Tendency of ethylene-oxide units to coordinate cations, forming stable crown ether-like, multi-nuclear coordination complexes, promotes solvation and dissociation of ionic aggregates.[38] Thus, understanding the synergy between T_g and electrostatic solvation of ethylene-oxide containing units is crucial to observe the influence on ionic conductivity.[36,38,39] Dynamic mechanical analysis (DMA) probed the thermomechanical properties of the triblock copolymers, and SAXS with complementary AFM examined the microphase-separation of the A-BC-A triblock copolymers. Dielectric relaxation spectroscopy (DRS) determined the ion-transport properties of charged A-BC-A triblock copolymers and random copolymer controls of various compositions. These triblock copolymers with suitable morphology and thermomechanical properties were cast into films with ionic liquid, and fabricated into electromechanical actuators. The addition of an ionic liquid (IL) diluent will alter the polymer morphology,[30] and a detailed understanding of this effect will enable precise control over the triblock copolymer morphology, ionic conductivity, and mechanical properties. For the first time to our knowledge, the devices fabricated using novel triblock copolymers performed comparably to earlier Nafion® membranes. This was attributed to optimum modulus, improved ionic conductivity, and microphase-separated morphology of triblock copolymers.

3.3 *Experimental*

3.3.1 Materials

N, N'-dicyclohexylcarbodiimide (DCC, 99%), 4-(dimethylamino)pyridine

(DMAP, >99.0%), 1,6-hexanediamine (98%), 1,6-hexanediol (99%) were purchased from Sigma-Aldrich and used as received. 4-cyano-4-(ethylsulfanylthiocarbonylsulfanyl)pentanoic acid (CEP) and VBIm were synthesized according to the previous literature. 1-ethyl-3-methylimidazolium trifluoromethane sulfonate (EMIm-TfO, IoLiTec Inc., 99%), iodomethane (Sigma, >99.0%) and lithium bis(trifluoromethane sulfonyl)imide (Tf_2N) ($LiTf_2N$, Aldrich, 99%) were used as received. Di(ethylene glycol) methyl ether methacrylate (DEGMEMA, 95%) and styrene (Sigma, 99%) were purchased from Sigma-Aldrich and passed through an alumina packed column prior to use. 4,4'-azobis(4-cyanovaleric acid) (V-501, Aldrich, 98%) and 2,2'-azobisisobutyronitrile (AIBN) were recrystallized from ethanol. Anhydrous dichloromethane (DCM) was obtained from a solvent purification system (Pure Solv, Innovative Technology) and all other solvents were obtained from Spectrum and used as received.

3.3.2 Synthesis of Ionomeric A-BC-A Triblock Copolymer Poly[Sty-*b*-(MVBIm-Tf_2N-*co*-DEGMEMA)-*b*-Sty]

In a representative copolymerization (Scheme 3.1), VBIm and DEGMEMA (6.0 g), *d*CEP-NH_2 (42.6 mg), V-501 (17.2 mg, 53.2 μmol), and DMF (42.5 mL) were added to a 100-mL, round-bottomed flask equipped with a stir bar. The reaction was sparged with argon for 30 min and placed in an oil bath thermostated at 70 °C for 4 h. Different compositions of VBIm and DEGMEMA were targeted to obtain poly(VBIm-*co*-DEGMEMA) copolymers. The resulting polymers were dialyzed (MWCO= 3500 g/mol) for 3 d against methanol while changing the solvent every 24 h. Aqueous SEC was used

to determine the absolute molecular weights of random copolymers of VBIm and DEGMEMA (PDI < 1.1) (SEC chromatographs are shown in supporting information).

Scheme 3.1 Synthesis of central 'BC' block comprising VBIm and DEGMEMA using RAFT polymerization. V-501 (4-cyanovaleric acid) is an azo-initiator and TTC is a difunctional trithio CTA. (Used with permission of Elsevier, 2015).

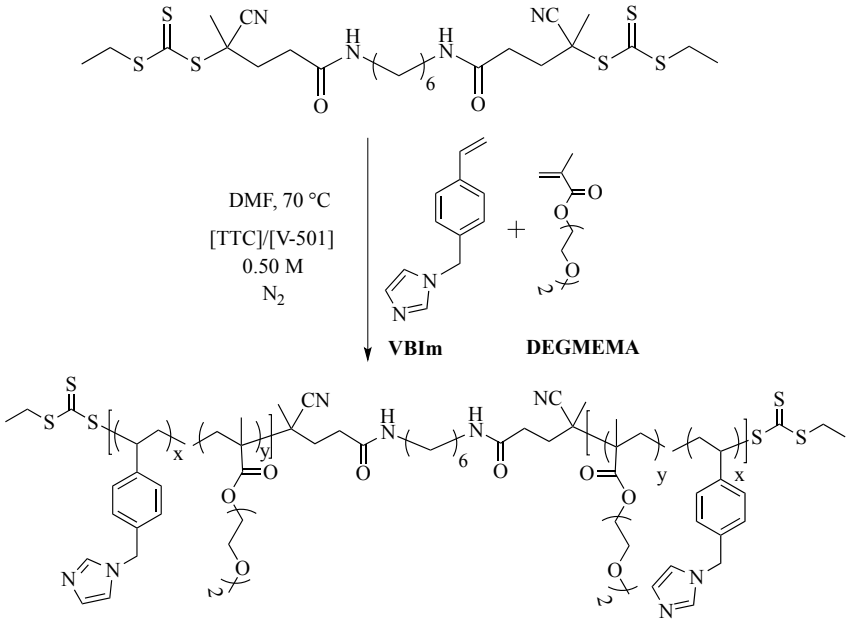

Poly[(VBIm-*co*-DEGMEMA)]

The purified macroCTA (400 mg) was redissolved in DMF (23 mL) in a 50-mL round-bottomed flask equipped with a stir bar. Styrene (0.5 g) and V-501 (3.12 mg) were added to the flask and the reaction was sparged with argon for 30 min at room temperature. The reaction was immersed in an oil bath at 70 °C for 6 h to obtain the desired amount of styrene in the external blocks. Poly[Sty-*b*-(VBIm-*co*-DEGMEMA)-*b*-Sty] and methyl iodide were dissolved in THF. The solution was purged with argon, and reacted at 23 °C for 24 h. The product was precipitated into ethyl acetate. Poly[Sty-*b*-(MVBIm-I-*co*-DEGMEMA)-*b*-Sty] was isolated through filtration and dried under

reduced pressure (0.5 mm Hg) at 40 °C for 18 h. Poly[Sty-*b*-(MVBIm-I-*co*-DEGMEMA)-*b*-Sty (3.0 g) and $LiTf_2N$ (67.03 g) were dissolved in separate solutions of water (50 mL each). The solutions were mixed together, immediately forming a white precipitate, and stirred at 23 °C for 24 h. Poly[Sty-*b*-(MVBIm-Tf_2N-*co*-DEGMEMA)-*b*-Sty] was dialyzed against methanol for 3 d to ensure removal of ionic impurities and dried at 60 °C for 24 h. The synthetic route is shown in .

Scheme 3.2.

Scheme 3.2 Chain extension and quaternization of poly(VBIm-*co*-DEGMEMA) to synthesize charged A-BC-A triblock copolymer poly[Sty-*b*-(MVBIm-Tf_2N-*co*-DEGMEMA)-*b*-Sty]. (Used with permission of Elsevier, 2015)

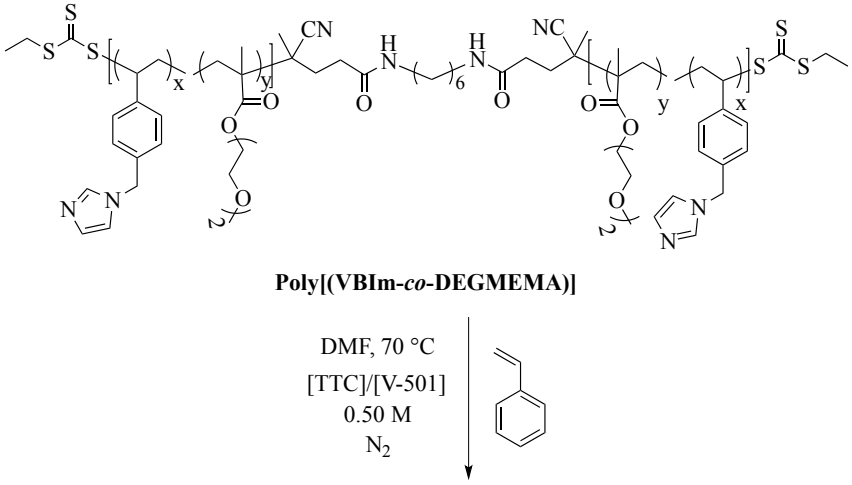

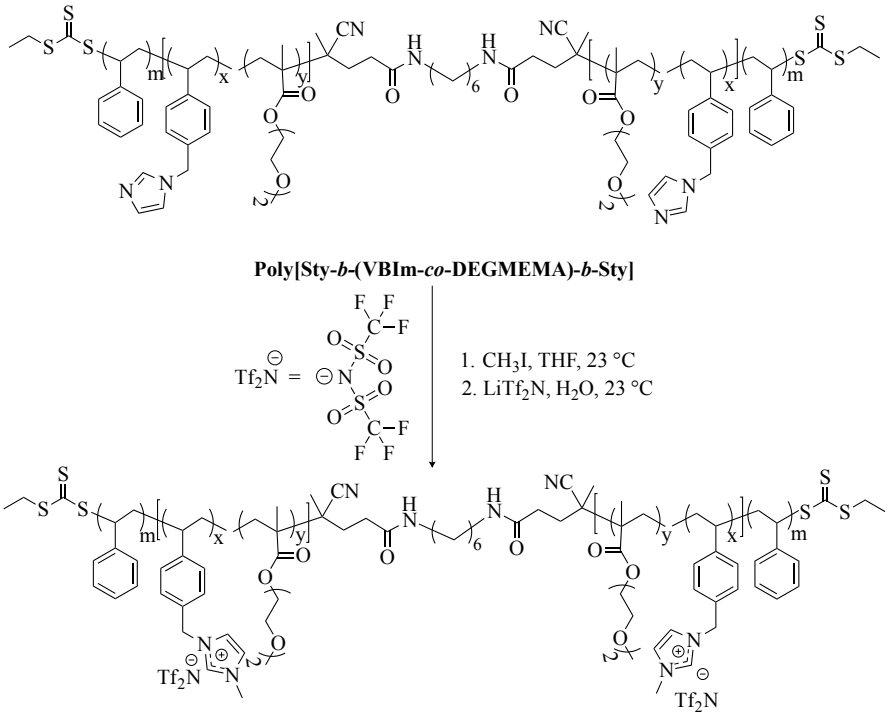

3.3.3 Synthesis of Random Copolymers Poly(Sty-*co*-MVBIm-Tf_2N-*co*-DEGMEMA)

To a round-bottomed flask all monomers, styrene, VBIm and DEGMEMA were added. To dissolve the monomers, 85 mL of DMF was added. To this reaction mixture, AIBN (0.01 mol%) was added and dissolved for 5 min. The flask was sealed and sparged with argon for 30 min to remove oxygen. The polymerization was then conducted at 65 °C for 24 h. The resulting polymer was quaternized using methyl iodide and anion exchange with $LiTf_2N$ using the previously mentioned procedure. The resulting polymer solution was dialyzed against methanol for 2 d to remove monomer and DMF, which was confirmed using ^1H NMR spectroscopy. The synthesis is shown in Scheme 3.3.

Scheme 3.3 Synthesis and quaternization of random copolymers of VBIm, DEGMEMA and styrene using free radical copolymerization. (Used with permission of Elsevier, 2015).

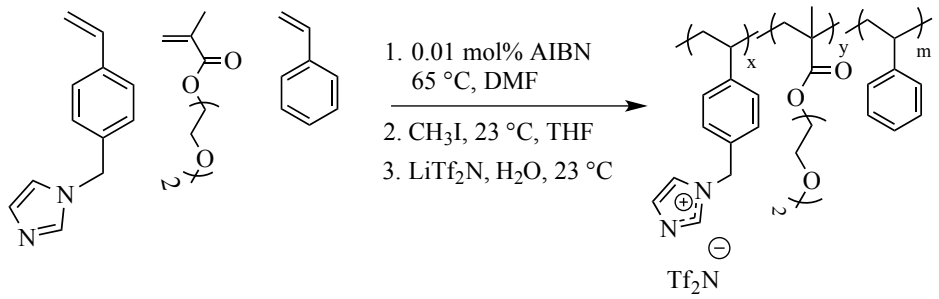

3.3.4 Analytical Methods

^{1}H NMR spectroscopy (Varian Inova, 400 MHz) determined CTA, monomer, and polymer composition. Thermogravimetric analysis (TGA) of the triblock copolymers was performed on a TA Instruments thermogravimetric analyzer (TGA Q50) with a heating rate of 10 °C/min to 600 °C under a nitrogen atmosphere after holding the sample at 100 °C for 60 min. A TA Instruments Q5000 sorption analyzer (TGA-SA) was used to measure water uptake of triblock copolymer and random copolymer samples (relative humidity (RH) 0-95%, 5% increments) at 25 °C. Thermal transitions were determined on a TA Instruments Q1000 differential scanning calorimeter (DSC, heating rate 10 °C/min) utilizing a heat/cool/heat cycle. T_g was determined from the second heat cycle of the DSC thermogram. Dynamic mechanical analysis (DMA) (TA Instruments Q800, 3 °C/min heating rate, -50 °C to 150 °C) was performed on the triblock copolymer films in tension mode at 1 Hz, oscillatory amplitude of 10 μm, and a static force of 0.01 N. Polymer molecular weight was measured using aqueous size exclusion chromatography (SEC) through two Waters ultrahydrogel linear columns with one Waters ultrahydrogel 250 column in a solvent consisting of 54/23/23 water/methanol/acetic acid (v/v/v%) with 0.1

M sodium acetate. The instrumentation consisted of a Waters 1515 isocratic HPLC pump operating at a flow rate of 0.8 mL/min, a Waters 717plus Autosampler, a Wyatt miniDAWN multiangle light scattering detector operating at a wavelength of 690 nm. Waters 2414 differential refractive index detector was used to determine the *dn/dc* for absolute molecular weight determination. Dynamic light scattering (DLS) (Malvern Zetasizer NanoZS) indicated the absence of polymer aggregation in the aqueous mobile phase prior to injection onto the SEC columns. A Wyatt Optilab refractive index detector operating at 658 nm and 35 °C determined the offline specific refractive index increment values. Wyatt ASTRA SEC/LS software was used to calculate absolute polymer molecular weights and PDIs.

All triblock copolymer were dissolved in a 80:20 $CHCl_3$: CH_3OH solvent mixture and cast from a 30 wt.% solution. Films were slowly dried at ambient conditions for 2 d under reduced pressure. The films were annealed at temperatures at 120 °C for 3 d. The films were then stored in a dry box until analyzed.

A Veeco MultiMode scanning microscope in tapping mode provided atomic force microscopy (AFM) images of the A-BC-A triblock copolymers. Samples were imaged with a set-point ratio of 0.6 at 3 μm x 3 μm and 1 μm x 1 μm magnifications using a nanosensor silicon tip with a spring constant of 42 N/m.

A Rigaku S-Max 3000 3 pinhole small-angle X-ray scattering (SAXS) instrument outfitted with a rotating anode generated Cu K_α irradiation at a wavelength of 1.54 Å to perform bulk morphology analysis on triblock copolymer films. The sample-to-detector distance was 1.5 m and was calibrated with a silver behenate standard. Two-dimensional data sets were collected using a fully integrated 2D multiwire area detector with an hour

exposure time, which was corrected for detector noise, background scattering, and sample absorption. All data processing and analysis was performed with the SAXSGUI software package to obtain intensity *vs* scattering vector *q* plots, where $q=4\pi \sin(\theta)/\lambda$ and 2θ is the scattering angle.

Samples for dielectric relaxation spectroscopy (DRS) measurements were solvent-cast films from mixtures of 80:20 $CHCl_3$: CH_3OH and vacuum annealed for 5 d at 120 °C. The samples were placed on a freshly polished brass electrode and dried in a vacuum oven at 353 K for 48 h, and a second brass electrode was finally placed on top of the sample. A Novocontrol GmbH Concept 40 broadband dielectric spectrometer was used to measure the dielectric permittivity. Frequency sweeps were performed isothermally from 10 MHz to 0.01 Hz in the temperature range from 233 to 453 K under dry nitrogen. The samples were initially held at a temperature above 393 K for at least 30 min to minimize water in the samples and avoid a change in water content during the experiment. The measurements were performed during subsequent cooling under a flow of dry N_2. The sample was heated to the starting temperature, revealing perfectly reproducible data during the second heating to the highest temperature.

For electromechanical bending actuator fabrication, two conductive network composite (CNC) layers were coated on both sides of the poly[Sty-*b*-(MVBIm-Tf_2N-*co*-DEGMEMA)-*b*-Sty] membrane. A layer-by-layer self-assembly technique was used to fabricate CNC layers consisting of negatively-charged gold nanoparticles (Au NPs, 3 nm diameter, 20 ppm, Purest Colloids) alternating with positively charged inert long chain poly(allylamine hydrochloride) (PAH, 10 mM, Sigma-Aldrich) to form a highly porous and conductive structure. The detailed process is described in a previous publication.

Briefly, an automatic dipping system (StratoSequence VI Robot, nanoStrata Inc) was used to alternatively dip a framed polymer membrane into respective solutions of PAH and Au NPs with three DI water rinses steps in between. After coating with 30 CNC bi-layers, the membrane was soaked with 1-ethyl-3-methylimidazolium trifluoromethanesulfonate (EMIm TfO) ionic liquid (>98%, Sigma-Aldrich) at 90 °C for 30 min to weight uptake of 30% as electrolyte. The transportation and accumulation of the $EMIm^+$ cations and TfO^- under the applied external electric field are responsible for the bending behavior of the actuator. Finally, the membrane was hot-pressed (90 °C, 700 psi) with 50 nm thick gold foil on both sides to provide outer electrodes for connection to the power supply and cut into 1 mm × 1 cm strips for testing. The electric stimulation was 4 V DC input, and the bending behavior was recorded using an HD CCD camera for further analysis. As a control, a second actuator was fabricated using a commercially available Nafion® membrane (N111-IP, EW 1100, 25 μm thick, Ion Power, Inc.) with an identical CNC layer and EMIm-TfO IL as electrolyte (34.2 wt.%) and tested under identical condition.

3.4 *Results and Discussion*

Initial polymerizations involved the synthesis of poly(DEGMEMA-*co*-VBIm) copolymers mediated with a difunctional CTA, *d*CEP-NH_2 in DMF to generate the low-T_g central block as shown in Scheme 3.1. The copolymerization of VBIm and DEGMEMA using RAFT ([DEGMEMA]/[TTC]/[V-501] ratio = 400/2/1) displayed linear, pseudo-first-order polymerization kinetics. These polymerizations proceeded at conversions 75-80% with narrow PDIs and demonstrated good agreement between

experimental and theoretical molecular weights. A series of low-T_g central blocks was prepared with varying molar ratio of VBIm and DEGMEMA. All the copolymers exhibited narrow PDIs as shown in Table 3.1.

Table 3.1 Molecular weights and PDI of poly(VBIm-*co*-DEGMEMA) at various compositions of VBIm and DEGMEMA. (Used with permission of Elsevier, 2015)

Polymer	VBIm (mol%)[a]	M_n (g/mol)[b]	PDI
Poly($VBIm_{80}$-*co*-$DEGMEMA_{20}$)	80	37,000	1.02
Poly($VBIm_{72}$-*co*-$DEGMEMA_{28}$)	72	36,100	1.04
Poly($VBIm_{52}$-*co*-$DEGMEMA_{48}$)	52	35,200	1.06
Poly($VBIm_{35}$-*co*-$DEGMEMA_{65}$)	35	28,600	1.06

[a] ^{1}H NMR spectroscopy: 400 MHz, DMSO-d_6, 25 ˚C
[b] SEC: 35 ˚C, 1 mL/min, MALLS detector, 54/23/23 (v/v/v%)H_2O/CH_3OH/AcOH, 0.1 M NaOAc

The soft central block incorporating the low T_g monomer DEGMEMA and VBIm was chain extended with styrene to obtain A-BC-A triblock copolymers, where the external polystyrene blocks provide mechanical stability and the central block poly(DEGMEMA-*co*-VBIm) introduces charge in the soft phase to increase ion-transport. Chain extension using styrene was accomplished using RAFT polymerization and PDI values remained relatively narrow after chain extension with increasing molecular weights as shown in Table 3.2.

Table 3.2 Molecular weight and PDI of A-BC-A triblock copolymer poly[Sty-*b*-(MVBIm-Tf_2N-*co*-DEGMEMA)-*b*-Sty].(Used with permission of Elsevier, 2015).

Polymer	M_n (g/mol)[a]	DP of Polystyrene	Styrene (wt.%)[b]	PDI
Poly[Sty-*b*-($VBIm_{72}$-*co*-$DEGMEMA_{28}$)-*b*-Sty]	16k-*b*-36k-*b*-16k	307	47	1.12
Poly[Sty-*b*-($VBIm_{52}$-*co*-$DEGMEMA_{48}$)-*b*-Sty]	18k-*b*-35k-*b*-18k	338	50	1.23
Poly[Sty-*b*-($VBIm_{35}$-*co*-$DEGMEMA_{65}$)-*b*-Sty]	18k-*b*-28k-*b*-18k	348	56	1.26

[a]SEC: 35 ˚C, 1 mL/min, MALLS detector, 54/23/23 (v/v/v %) H_2O/CH_3OH/AcOH, 0.1 M NaOAc
[b]^{1}H NMR spectroscopy: 400 MHz, DMSO-d_6, 25 ˚C

The thermal properties depended on the composition, presence of charge, and counterion selection. As observed in the earlier literature, T_g of the copolymers increased after quaternization with methyl iodide and decreased after anion exchange to Tf_2N^- due to a large counterion size.[24,28] Table 3.3 summarizes the thermal transitions and molecular weights of central blocks as well as A-BC-A triblock copolymers. Different charge concentration enabled investigations of ionic content on thermal properties. Although the number-average molecular weight (M_n) of the charged triblock copolymer remained similar with increasing ion content from 35 to 72 mol%, the T_g of the central block increased from 10 to 35 °C. Incorporation of ionic groups within the soft block restricts polymer segmental mobility and consequently, increases T_g.[40] The charge placement in the soft block at various concentrations did not affect the high-T_g transition, suggesting an absence of appreciable phase mixing in the triblock copolymers. For the triblock copolymers, we observed two T_gs indicating the presence of a phase-separated morphology. The lower transition was attributed to the soft ionic block and the transition at higher temperature was assigned to the polystyrene block. The random copolymer analog did not exhibit a second T_g, suggesting the absence of phase-separation in the

random copolymers. TGA showed that thermal stability decreased after quaternization due to the presence of the more basic I^- anion and increased after anion exchange to the less basic couteranion Tf_2N^-, consistent with earlier literature.[28] Table 3.3 includes the thermal transitions and molecular weight data for random copolymers of styrene, DEGMEMA and VBIm. The random copolymer serves as a comparative control for the A-BC-A triblock copolymers.

Table 3.3 Thermal transitions and molecular weights of A-BC-A triblock copolymer poly[Sty-*b*-(MVBIm-Tf_2N-*co*-DEGMEMA)-*b*-Sty]. (Used with permission of Elsevier, 2015).

Polymer	M_n (g/mol)[a]	Styrene[b] (wt.%)	T_{g1} (℃)[c]	T_{g2} (℃)[c]	$T_{d,5\%}$ (℃)[d]
Poly(VBIm)	ND	-	107	-	354
Poly($VBIm_{72}$-*co*-$DEGMEMA_{28}$)	36,100	-	64	-	390
Poly($VBIm_{52}$-*co*-$DEGMEMA_{48}$)	35,200	-	43	-	341
Poly($VBIm_{35}$-*co*-$DEGMEMA_{65}$)	28,600	-	31	-	327
Poly[Sty-*b*-($VBIm_{72}$-*co*-$DEGMEMA_{28}$)-*b*-Sty]	16k-*b*-36k-*b*-16k	47	57	109	345
Poly[Sty-*b*-($VBIm_{52}$-*co*-$DEGMEMA_{48}$)-*b*-Sty]	18k-*b*-35k-*b*-18k	50	40	96	415
Poly[Sty-*b*-($VBIm_{35}$-*co*-$DEGMEMA_{65}$)-*b*-Sty]	18k-*b*-28k-*b*-18k	56	28	112	428
Poly[Sty-*b*-(MVBIm-Tf_2N_{72}-*co*-$DEGMEMA_{28}$)-*b*-Sty]	16k-*b*-56k-*b*-16k	37	35	110	332
Poly[Sty-*b*-(MVBIm-Tf_2N_{52}-*co*-$DEGMEMA_{48}$)-*b*-Sty]	18k-*b*-55k-*b*-18k	40	26	108	350
Poly[Sty-*b*-(MVBIm-Tf_2N_{35}-*co*-$DEGMEMA_{65}$)-*b*-Sty]	18k-*b*-40k-*b*-18k	47	10	111	375
Poly[Sty-*co*-VBIm-*co*-DEGMEMA]-18 mol% ion content	ND	48	19	-	368
Poly[Sty-*co*-VBIm-*co*-DEGMEMA]-26 mol% ion content	ND	45	20	-	376
Poly[Sty-*co*-VBIm-*co*-DEGMEMA]-36 mol% ion content	ND	43	23	-	365

[a] SEC: 35 ˚C, 1 mL/min, MALLS detector, 54/23/23 (v/v/v %) H_2O/CH_3OH/AcOH, 0.1 M NaOAc; dn/dc=0.2310 mL/g

[b] ^1H NMR spectroscopy: 400 MHz, DMSO-d_6, 25 ˚C

[c] DSC: 10 ˚C/min, N_2, second heat

[d] TGA: 10 ˚C/min, N_2

Dynamic mechanical analysis (DMA) indicated microphase-separation in the triblock copolymers at various styrene contents as shown in Figure 3.1 and Figure 3.2. The storage modulus (G') *vs* temperature for the charged triblock copolymers is shown in Figure 3.1. The triblock copolymer exhibited two distinctive transitions, i.e. T_g of the soft central block, poly(DEGMEMA-*co*-MVBIm-Tf_2N), while the second terminal flow transition at ~ 100 °C is consistent with the T_g of polystyrene hard phase. Figure 3.1 depicts the DMA results for 37, 40, and 47 wt.% polystyrene. Increasing the hard segment content from 37 to 47 wt.% increased the breadth of the lower $T_{g,}$ indicating phase mixing. The styrenic comonomer, VBIm, is presumably more compatible with polystyrene, thus an increase in the styrenic comonomer was expected to promote phase mixing. The triblock copolymer films exhibited significantly improved mechanical strength compared to either poly(VBIm-*co*-DEGMEMA) or poly(DEGMEMA) homopolymers as neither polymers formed a ductile film for mechanical property characterization.[41]

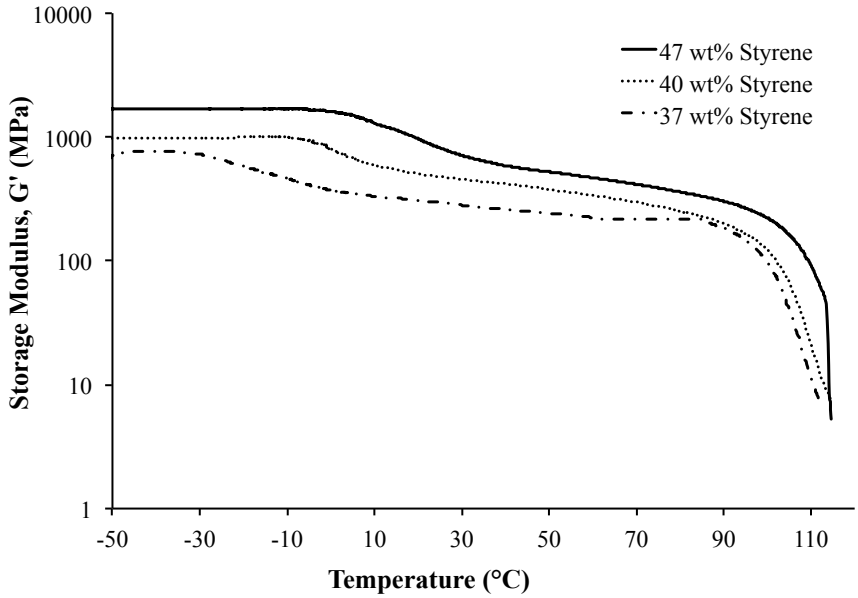

Figure 3.1 Dynamic mechanical analysis (DMA) of charged A-BC-A triblock copolymer poly[Sty-*b*-(MVBIm-Tf_2N-*co*-DEGMEMA)-*b*-Sty] with varying compositions. (Used with permission of Elsevier, 2015).

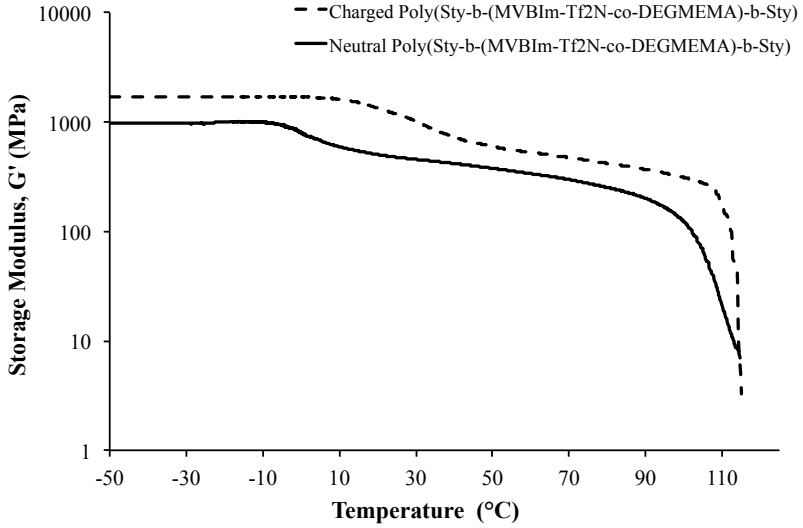

Figure 3.2 Dynamic mechanical analysis (DMA) of neutral and charged A-BC-A triblock copolymer poly[Sty-*b*-(MVBIm-Tf_2N_{52}-*co*-$DEGMEMA_{48}$)-*b*-Sty]. (Used with permission of Elsevier, 2015).

Earlier studies in the literature employed AFM to elucidate the multiphase morphology of triblock copolymers.[42-45] Morphological investigations using AFM uncovered a microphase-separated surface morphology. AFM (Figure 3.3) indicates the

presence of lamellar morphology in a triblock copolymer with 18 mol% ion content, and morphological features changed with varying ion content. With an increase in composition of VBIm in the central block, phase mixing was observed presumably due to increased styrenic comonomer compatibility with polystyrene in the external block. The morphology became less ordered and the domain size was smaller, which is apparent in both AFM and also in SAXS data. The literature extensively describes the dynamics and structural parameters that dictate block copolymer microphase-separation.[46]

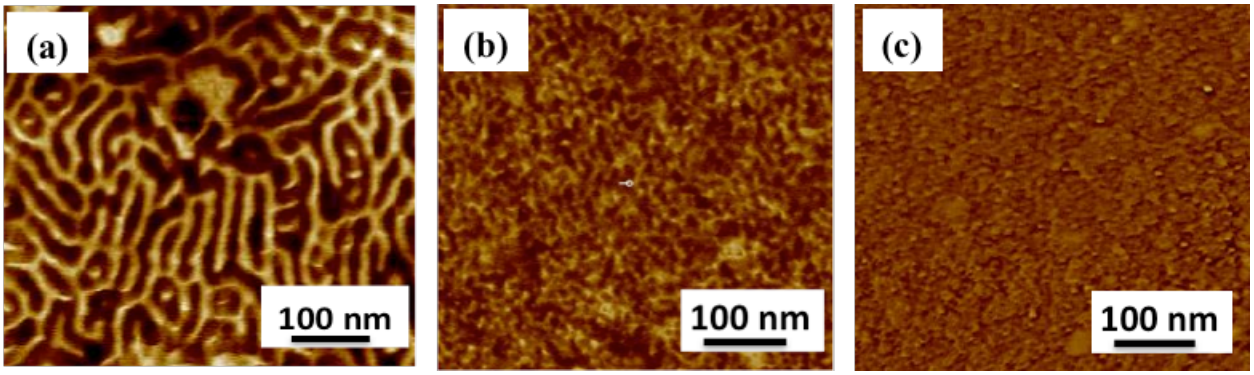

Figure 3.3 Atomic force microscopy (AFM) of charged A-BC-A triblock copolymer poly[Sty-*b*-(MVBIm-Tf_2N-*co*-DEGMEMA)-*b*-Sty] going from (a) 18 mol% (b) 26 mol% (c) 36 mol% ion content. (Used with permission of Elsevier, 2015).

SAXS experiments complemented AFM morphological findings and determined the presence of bulk microphase-separation (Figure 3.4). X-ray scattering data plotted as intensity, *I(q)*, *vs* the momentum transfer vector, *q,* confirmed microphase-separation in the A-BC-A triblock copolymers. For all three triblock copolymers, scattering maxima were observed, indicating the presence of microphase-separation in the A-BC-A triblock copolymer films. The triblock copolymers with 18 mol% ion content exhibited peak maxima at *q*, 2q*, 3q**and *4q*,* indicating a well-ordered, lamellar morphology. The triblock copolymer with 26 mol% ion content, second peak maxima was still observed,

which diminishes at 36 mol% ion content, indicating phase mixing.

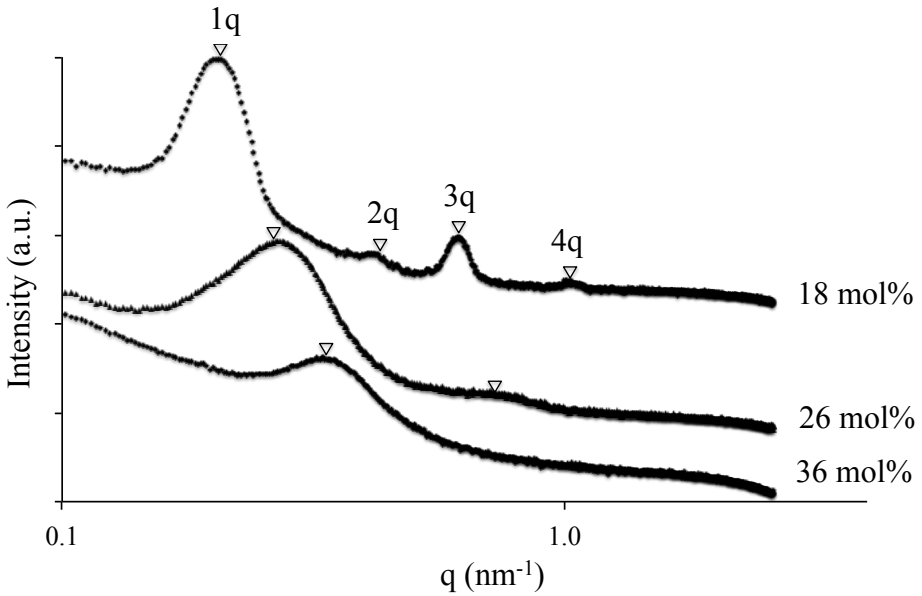

Figure 3.4 Small angle X-ray scattering (SAXS) of charged A-BC-A triblock copolymer poly[Sty-*b*-(MVBIm-Tf_2N-*co*-DEGMEMA)-*b*-Sty] with various ion contents 18, 26 and 36 mol%. (Used with permission of Elsevier, 2015).

The principal q peak shifted to higher q values with lamellar spacing d of 75.43 nm, largest for 18 mol% ion content, and decreased to 23.12 nm for 36 mol% ion content, also observed in AFM data. With an increase in VBIm composition in the central block, we observed a less ordered system, since the styrenic comonomer was presumably more compatible to polystyrene external blocks, inducing phase mixing. The SAXS results agreed well with AFM images and DMA analysis of the triblock copolymer. Furthermore, there was no peak observed for ionic aggregation at q of 1.0-2.0 nm, indicating the A-BC-A triblock copolymer system behaving as single ion conductors with superior properties as opposed to a "channel-network morphology" in Nafion®.

Charged polymers typically exhibit the ability to absorb moisture, which is quantified using TGA-sorption analysis. These triblock copolymers showed less than 1%

weight gain due to water at 25 ˚C and 10% relative humidity. Ionic conductivity also strongly depends on frequency and temperature for single-ion conductors.[47] The DC conductivity, defined as the in-phase part of the conductivity where it is independent of frequency in a ~3-decade frequency range, is plotted in Figure 3.5. For both triblock and random copolymer ionomers, ionic conductivity increased with increasing ion content and did not correlate with the T_g of the ion-containing block; the triblock copolymer poly[Sty-*b*-(VBIm$_{72}$-*co*-DEGMEMA$_{28}$)-*b*-Sty] with the highest ion content exhibited the highest ionic conductivity. Further, addition of ethylene oxide units diluted the ion content and also changed ion aggregation behavior and morphology, resulting in decreased ionic conductivity. Moreover, all triblock copolymers showed higher ionic conductivity than random copolymers at identical monomer composition, which suggested the microphase-separated morphologies of triblock copolymers provide a continuous path to facilitate ion conduction.

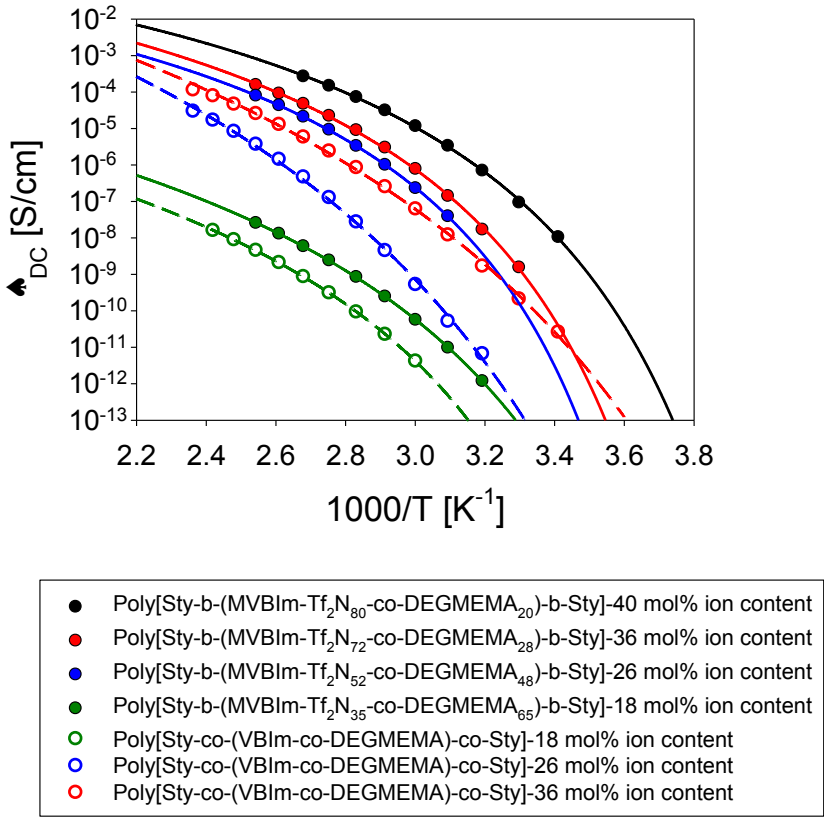

Figure 3.5 Temperature dependence of ionic conductivity, which increases with increase in ion content and found to be more than random copolymers. (Used with permission of Elsevier, 2015).

The ionic conductivity (σ) is simply expressed by

$$\sigma = pe\mu \qquad 1$$

where p, e, and μ are total number density of conducting ions, elementary electric charge, and conducting ion mobility, respectively. It is crucial to determine whether the increase in ionic conductivity has a larger contribution from the number density of simultaneously conducting ions or their mobility in order to understand counter anion conduction. This is assessed with electrode polarization at very low frequencies in dielectric relaxation spectroscopy (DRS).[47]

In DRS, a sinusoidal ac field is applied to a thin-film sample sandwiched between two blocking electrodes. The electrode polarization (EP) occurs at frequencies low enough such that the transporting ions have sufficient time to polarize at the electrodes during each cycle. A physical model of EP,[48-51] which has been applied to a number of single-ion conductors recently,[14,15,47,52-55] determined the number density of simultaneous conductors and their mobility. The time scale for full polarization at the electrode is

$$\tau_{EP} \equiv \frac{\varepsilon_{EP}\varepsilon_0}{\sigma_{DC}} \qquad 2$$

where ε_{EP} is the effective permittivity after the electrode polarization is complete, ε_0 is the permittivity of vacuum, and σ_{DC} is the DC conductivity. The time scale of conduction or when the ion motion becomes diffusive is

$$\tau_{\sigma} \equiv \frac{\varepsilon_s\varepsilon_0}{\sigma_{DC}} \qquad 3$$

where ε_s is the static dielectric constant. EP is regarded as a simple Debye relaxation in the Macdonald and Coelho model[48-51] with the loss tangent peak expressed as

$$\tan\delta = \frac{\varepsilon''}{\varepsilon'} = \frac{\omega\tau_{EP}}{1+\omega^2\tau_{\sigma}\tau_{EP}} \qquad 4$$

where the peak maximum frequency relates to the geometric mean of the two fitting parameters τ_{EP} and τ_{σ}, demonstrated in Figure 3.6.

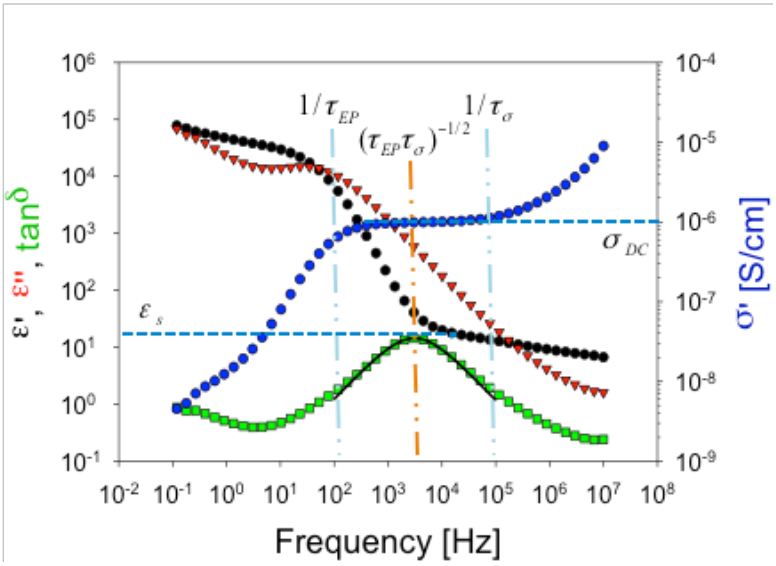

Figure 3.6 Dielectric spectra and fitting of the loss tangent peak with Equation 4 for triblock copolymer poly[Sty-*b*-(VBIm$_{52}$-*co*-DEGMEMA$_{48}$)-*b*-Sty] at 70 °C. (Used with permission of Elsevier, 2015).

Since one type of ion is attached to the polymer chain and assumed to be immobilized, the counterion's mobility μ and number density of simultaneous conducting ions *p* are then determined from the fitting parameters,

$$\mu = \frac{eL^2\tau_\sigma}{4\tau_{EP}{}^2 kT} \qquad 5$$

$$p = \frac{\sigma_{DC}}{e\mu} = \frac{4\sigma_{DC}\tau_{EP}{}^2 kT}{e^2L^2\tau_\sigma} \qquad 6$$

where *L* is the sample thickness between electrodes, *k* is Boltzmann's constant, and *T* is the absolute temperature.

The temperature dependence of the number density of simultaneously conducting ions calculated from Equation 6 is plotted in Figure 3.7 and is well-described by the Arrhenius equation,

$$p = p_{\infty} \exp(-\frac{E_a}{RT}) \quad (7)$$

where p_{∞} is the conducting ion concentration as T approaches ∞ and E_a is the activation energy for conducting ions listed in Table 3.4. The activation energy is related to the Coulomb energy of a cation-anion pair, and this electrostatic attraction is the main driving force for pair and aggregate formation, mediated by an effective dielectric constant of the ion-conducting block. The Arrhenius temperature dependence of the conducting ion concentration suggests the conducting ions would be fully dissociated at infinite temperature, thus the intercept of the Arrhenius fit in Figure 3.7 is fixed to p_0, the total ion concentration calculated from a group contribution method[56,57] with stoichiometry determined from the chemical structure. The number density of simultaneously conducting ions of all random copolymers is higher than triblock copolymers, suggesting ions in random copolymers are better solvated by ether oxygen atoms. The ethylene oxide side chains in triblock copolymers are likely stretched to form the microphase-separated morphologies shown in SAXS, and the ether oxygen atoms on the stretched side chains has less ability to solvate the attached cations than the ether oxygen atoms on random copolymers because of the restricted mobility.

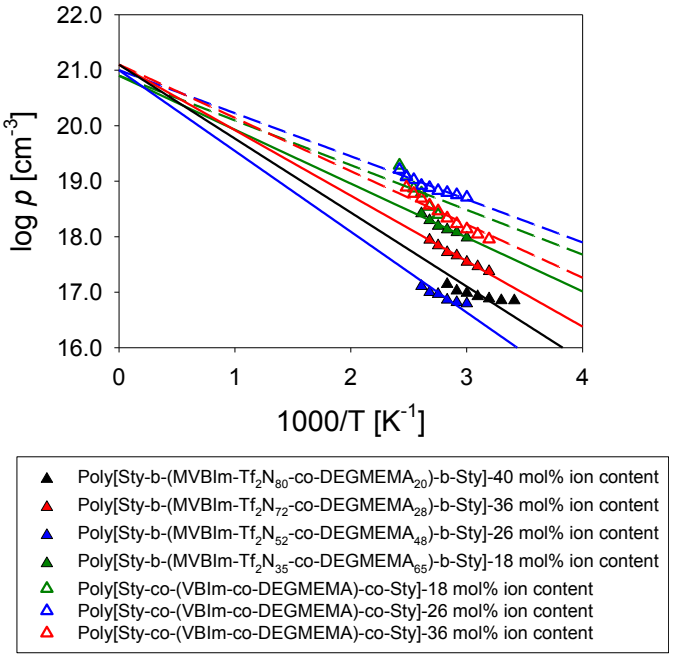

Figure 3.7 Temperature dependence of conducting ion concentration for A-BC-A triblock copolymer determined using EP model. (Used with permission of Elsevier, 2015).

Table 3.4 Fitting parameters (Equation 7) for the temperature dependence of the number density of simultaneously conducting ions with intercept p_∞ fixed to p_0. (Used with permission of Elsevier, 2015).

Sample	$\log p_\infty (cm^{-3})$	$E_a (kJ/mol)$
Poly[Sty-*b*-(MVBIm-Tf_2N_{80}-*co*-$DEGMEMA_{20}$)-*b*-Sty]	21.1	25.8
Poly[Sty-*b*-(MVBIm-Tf_2N_{72}-*co*-$DEGMEMA_{28}$)-*b*-Sty]	21.1	22.8
Poly[Sty-*b*-(MVBIm-Tf_2N_{52}-*co*-$DEGMEMA_{48}$)-*b*-Sty]	21.0	28.1
Poly[Sty-*b*-(MVBIm-Tf_2N_{35}-*co*-$DEGMEMA_{65}$)-*b*-Sty]	20.9	18.8
Poly[Sty-*co*-VBIm-*co*-DEGMEMA]-18 mol% ion content	20.9	15.6
Poly[Sty-*co*-VBIm-*co*-DEGMEMA]-26 mol% ion content	21.0	15.0
Poly[Sty-*co*-VBIm-*co*-DEGMEMA]-36 mol% ion content	21.1	18.6

Since ionic conductivity is obtained over a much wider temperature range than the EP model allows, the activation energies obtained from the Arrhenius fit to the number

density of simultaneously conducting ions where the intercept is not fixed are used to fit the temperature dependence of ionic conductivity with

$$\sigma_{DC} = e\mu_{\infty}p_{\infty}\exp(-\frac{DT_0}{T-T_0})\exp(-\frac{E_a}{RT}) \qquad 8$$

where μ, T_0, and D, listed in Table 3.5, is the highest temperature limit of mobility, Vogel temperature, and the strength parameter that is reciprocally related to fragility, respectively.

Table 3.5 Fitting parameter (Equation 8) for the temperature dependence of ionic conductivity. (Used with permission of Elsevier, 2015).

Sample	$e\mu_{\infty}p_{\infty}$ (S/cm)	D	T_0 (K)	Ea (kJ/mol)
Poly[Sty-*b*-(MVBIm-Tf_2N_{80}-*co*-$DEGMEMA_{20}$)-*b*-Sty]	4.4	5.4	226	28.7
Poly[Sty-*b*-(MVBIm-Tf_2N_{72}-*co*-$DEGMEMA_{28}$)-*b*-Sty]	5.8	4.9	240	21.1
Poly[Sty-*b*-(MVBIm-Tf_2N_{52}-*co*-$DEGMEMA_{48}$)-*b*-Sty]	1.7	4.7	246	15.4
Poly[Sty-*b*-(MVBIm-Tf_2N_{35}-*co*-$DEGMEMA_{65}$)-*b*-Sty]	5.7E-3	6.8	231	20.3
Poly[Sty-*co*-VBIm-*co*-DEGMEMA]-18 mol% ion content	9.3E-3	4.4	252	51.1
Poly[Sty-*co*-VBIm-*co*-DEGMEMA]-26 mol% ion content	2.8E+2	14	213	15.4
Poly[Sty-*co*-VBIm-*co*-DEGMEMA]-36 mol% ion content	1.5E+2	12	198	25.7

The temperature dependence of the counterion mobility calculated from Equation 5 is plotted in Figure 3.8. The VFT temperature dependence observed in Figure 3.8 for all ionomers in this study indicates the coupling of ion transport to segmental motion of the polymer. All triblock copolymers had significantly higher ion mobility than the corresponding random copolymers at the same ion content, and this confirms our claim

that the microphase-separated morphologies formed in triblock copolymers provide continuous conducting pathways that increases counterion mobility, while ions in random copolymers are hindered by polystyrene segments randomly distributed in the polymer matrix.

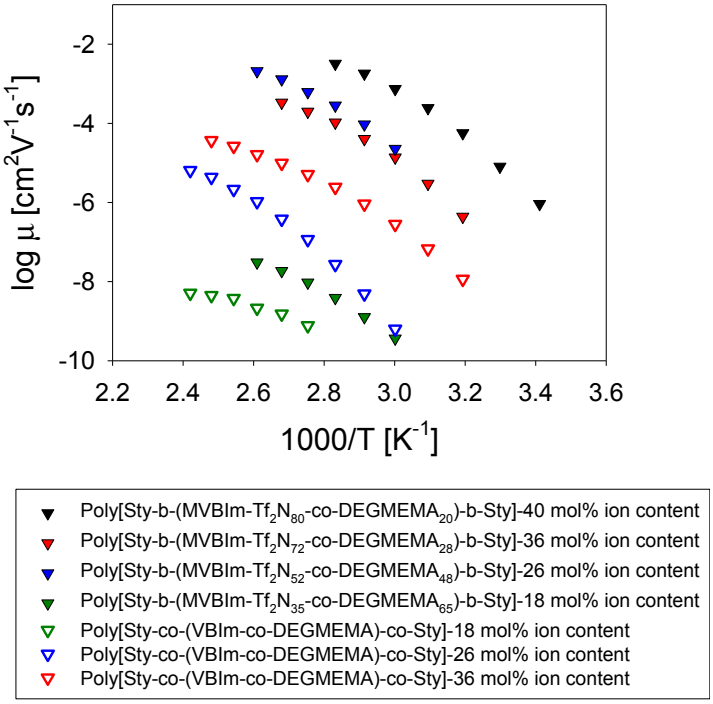

Figure 3.8 Temperature-dependence of ion mobility for A-BC-A triblock copolymer determined using EP model. (Used with permission of Elsevier, 2015).

The static dielectric constant ε_s shown in Figure 3.9, was calculated from τ_σ in Equation 3 and defined as the low-frequency plateau of the dielectric constant $\varepsilon'(\omega)$ before EP begins. The temperature dependence of static dielectric constant of all copolymers did not obey the Onsager prediction where thermal randomization of dipoles results in ε_s inversely proportional to temperature and is only applicable to segments with polar groups in the liquid state where their motion is unrestricted by neighbors (far

above T_g). The very low $\varepsilon_s \cong 10$ for the random and triblock copolymers with ~18 mol% and their extremely low ionic conductivities suggested that the lamellar morphology formed have one microphase, most likely polystyrene, favoring the electrodes or failing to form continuous microphase of the ion conducting block, thus resulting in much lower ionic conductivity than other ionomers.

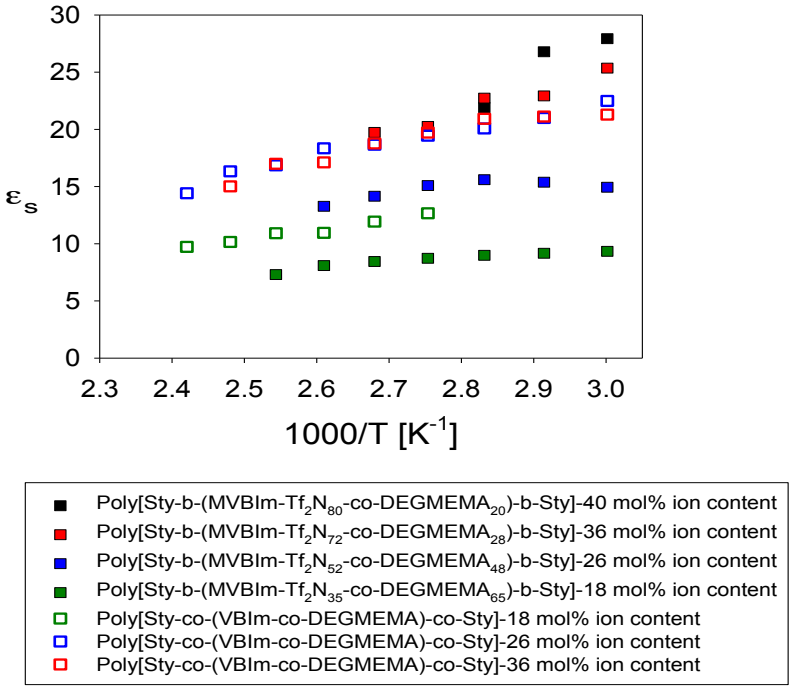

Figure 3.9 Temperature-dependence of static dielectric constant for A-BC-A triblock copolymer determined using EP model. (Used with permission of Elsevier, 2015).

At ambient conditions (20 ˚C and ~ 43% RH), the actuator prepared from a poly[Sty-*b*-(MVBIm-Tf_2N_{52}-*co*-$DEGMEMA_{48}$)-*b*-Sty] membrane showed bi-directional bending under a 4 V DC input. Distinct from the widely reported relaxation of actuators, this bi-directional behavior is due to difference in size and transport of the two ions of the IL in the actuator, as reported previously.[58] Images of the bending performance are shown in supporting figure, where the actuator bends first toward the anode after the DC

input was applied. The actuator then reverses in the opposite direction and achieves strong curvature towards the cathode. The smaller but faster cations move through the membrane and rapidly accumulate on the cathode side of the CNC to swell the cathode side of the actuator and cause initial bending in the anode direction. The larger, slower anions complete their transport and accumulate on the anode side of the CNC. Increased swelling on the anode side of the actuator thus causes the final bending in the cathode direction. Although similar behavior was found in the Nafion® actuators in our previous study,[58] as shown in Figure 3.10 and Figure 3.11, actuators made with poly[Sty-*b*-(MVBIm-Tf_2N_{52}-*co*-$DEGMEMA_{48}$)-*b*-Sty] membrane show greater curvature and faster response in the anode direction compared to the cathode direction. This implies a more efficient transport channel for electrolytes provided by the poly[Sty-*b*-(MVBIm-Tf_2N_{52}-*co*-$DEGMEMA_{48}$)-*b*-Sty] membrane and thus results in faster and larger accumulation of the cations in the cathode side of the CNC. Considering that the poly[Sty-*b*-(MVBIm-Tf_2N_{52}-*co*-$DEGMEMA_{48}$)-*b*-Sty] actuator contains fewer ions (29.9% weight uptake, as compared to 34.2% of Nafion® actuator), these triblock copolymers are promising candidates for replacing Nafion® in electroactive device applications. The triblock copolymers exhibited electrochemical stability between +4 V and -4 V, as observed with cyclic voltammetry.

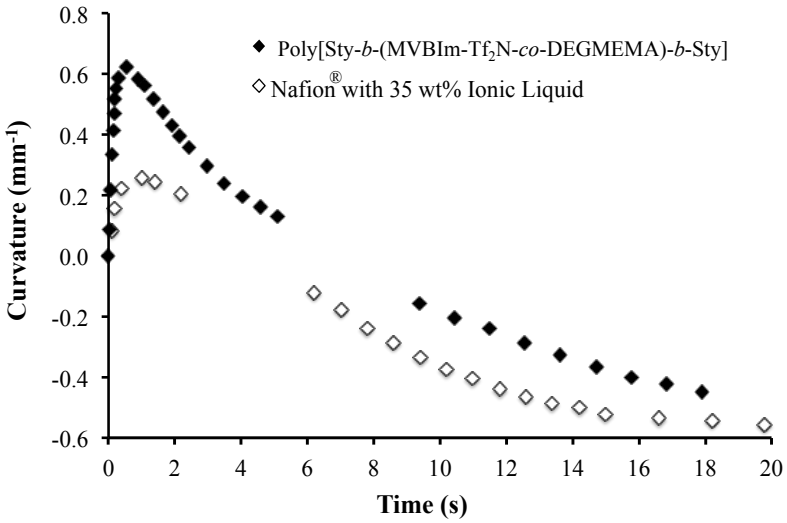

Figure 3.10 Curvature observed for electromechanical actuators made from poly[Sty-*b*-(MVBIm-Tf_2N_{52}-*co*-$DEGMEMA_{48}$)-*b*-Sty] having 26 mol% ion content at ambient conditions (20℃ and ~ 43% RH) under a 4 V applied voltage. The films were casted with 35 wt.% ionic liquid [EMIm][TfO]. (Used with permission of Elsevier, 2015).

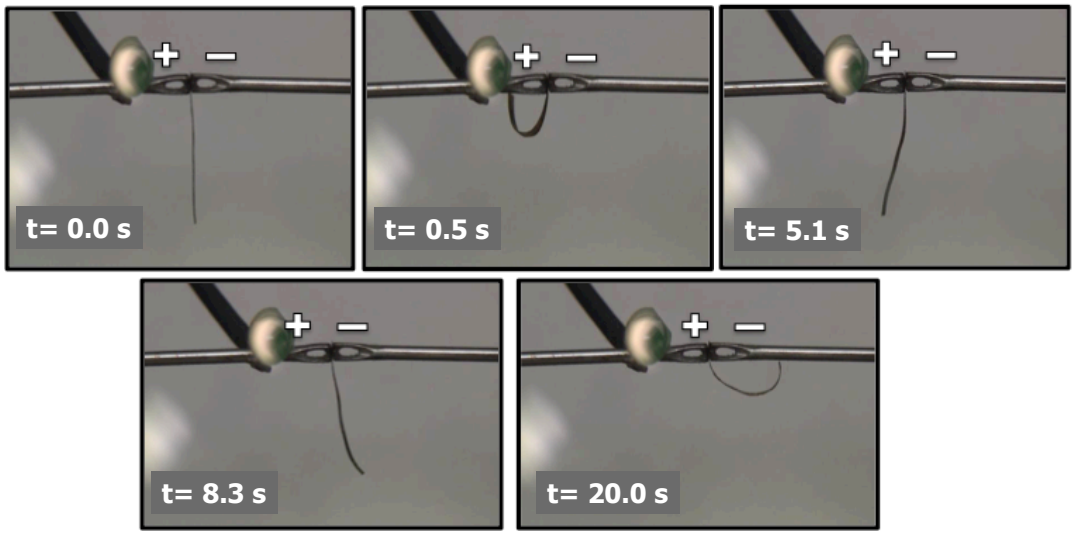

Figure 3.11 Still images of electromechanical transducer made from poly[Sty-*b*-(MVBIm-Tf_2N_{52}-*co*-$DEGMEMA_{48}$)-*b*-Sty] having 26 mol% ion content under applied potential of 4 V. (Used with permission of Elsevier, 2015).

3.5 *Conclusions*

RAFT polymerization enabled the synthesis of well-defined ABA triblock copolymers using a difunctional CTA containing a low T_g monomer DEGMEMA in the central block to increase segmental motion and improve ion transport. Controlling the composition of the polystyrene external block and ion content enabled the tuning of thermomechanical properties. SAXS and AFM confirmed the microphase separation and showed that the morphology can be tuned with change in ion content in the triblock copolymer system. DRS demonstrated the importance of triblock copolymer architecture as compared to random copolymers. Ionic conductivity of the copolymers was dependent on morphology, composition and ion-content. The data suggested that these triblock copolymers provide more efficient ion transport channels for electrolytes resulting in faster and greater accumulation of the cations on the anode side of the CNC. The development of these new ABA triblock copolymer systems enables the design of future electroactive devices by changing morphology, ion-content and composition to tune the macromolecular properties.

3.6 *Acknowledgements*

This material is based on work supported by the U.S. Army Research Laboratory and the U.S. Army Research Office under contract/grant number W911NF-07-1-0452 Ionic Liquids in Electro-Active Devices Multidisciplinary University Research Initiative (ILEAD MURI). The authors acknowledge the Laboratory for Research on the Structure of Matter at Penn (MRSEC NSF DMR11-20901) for instrument support.

3.7 *References*

(1) Smith, A. E.; Xu, X.; McCormick, C. L. *Progress in Polymer Science* **2010**, *35*, 45.
(2) Green, M. D.; Wang, D.; Hemp, S. T.; Choi, J.-H.; Winey, K. I.; Heflin, J. R.; Long, T. E. *Polymer* **2012**.
(3) Wu, T.; Wang, D.; Zhang, M.; Heflin, J. R.; Moore, R. B.; Long, T. E. *ACS applied materials & interfaces* **2012**, *4*, 6552.
(4) Wang, D.; Wu, T.; Wan, X.; Wang, X.; Liu, S. *Langmuir* **2007**, *23*, 11866.
(5) Hawker, C. J.; Bosman, A. W.; Harth, E. *Chemical Reviews* **2001**, *101*, 3661.
(6) Chung, T.; Janvikul, W.; Lu, H. *Journal of the American Chemical Society* **1996**, *118*, 705.
(7) Kamigaito, M.; Ando, T.; Sawamoto, M. *Chemical reviews* **2001**, *101*, 3689.
(8) Matyjaszewski, K.; Xia, J. *Chemical reviews* **2001**, *101*, 2921.
(9) Chiefari, J.; Chong, Y.; Ercole, F.; Krstina, J.; Jeffery, J.; Le, T. P.; Mayadunne, R. T.; Meijs, G. F.; Moad, C. L.; Moad, G. *Macromolecules* **1998**, *31*, 5559.
(10) Moad, G.; Rizzardo, E.; Thang, S. H. *Australian journal of chemistry* **2005**, *58*, 379.
(11) Mitsukami, Y.; Donovan, M. S.; Lowe, A. B.; McCormick, C. L. *Macromolecules* **2001**, *34*, 2248.
(12) McCormick, C. L.; Lowe, A. B. *Accounts of Chemical Research* **2004**, *37*, 312.
(13) Duncan, A. J.; Leo, D. J.; Long, T. E. *Macromolecules* **2008**, *41*, 7765.
(14) Tudryn, G. J.; Liu, W.; Wang, S.-W.; Colby, R. H. *Macromolecules* **2011**, *44*, 3572.
(15) Wang, S.-W.; Liu, W.; Colby, R. H. *Chemistry of Materials* **2011**, *23*, 1862.
(16) Akle, B. J.; Bennett, M. D.; Leo, D. J.; Wiles, K. B.; McGrath, J. E. *Journal of Materials Science* **2007**, *42*, 7031.
(17) Akle, B. J.; Leo, D. J. *Smart materials and structures* **2007**, *16*, 1348.
(18) Lin, J.; Liu, Y.; Zhang, Q. *Polymer* **2011**, *52*, 540.
(19) Green, M. D.; Choi, J.-H.; Winey, K. I.; Long, T. E. *Macromolecules* **2012**, *45*, 4749.
(20) Duncan, A. J.; Leo, D. J.; Long, T. E.; Akle, B. J.; Park, J. K.; Moore, R. B. In *The 16th International Symposium on: Smart Structures and Materials & Nondestructive Evaluation and Health Monitoring*; International Society for Optics and Photonics: 2009, p 728711.
(21) Eisenberg, A.; Hird, B.; Moore, R. *Macromolecules* **1990**, *23*, 4098.
(22) Mauritz, K. A.; Moore, R. B. *Chemical reviews* **2004**, *104*, 4535.
(23) Green, M. D.; Schreiner, C.; Long, T. E. *The Journal of Physical Chemistry A* **2011**, *115*, 13829.
(24) Green, M. D.; Salas‐de la Cruz, D.; Ye, Y.; Layman, J. M.; Elabd, Y. A.; Winey, K. I.; Long, T. E. *Macromolecular Chemistry and Physics* **2011**, *212*, 2522.
(25) Green, M. D.; Long, T. E. *Journal of Macromolecular Science®, Part C: Polymer Reviews* **2009**, *49*, 291.

(26) Allen, M. H.; Hemp, S. T.; Zhang, M.; Zhang, M.; Smith, A. E.; Moore, R. B.; Long, T. E. *Polymer Chemistry* **2013**, *4*, 2333.
(27) Jangu, C.; Wang, J. H. H.; Wang, D.; Sharick, S.; Heflin, J. R.; Winey, K. I.; Colby, R. H.; Long, T. E. *Macromolecular Chemistry and Physics* **2014**.
(28) Ye, Y.; Elabd, Y. A. *Polymer* **2011**, *52*, 1309.
(29) Ye, Y.; Choi, J.-H.; Winey, K. I.; Elabd, Y. A. *Macromolecules* **2012**, *45*, 7027.
(30) Gwee, L.; Choi, J.-H.; Winey, K. I.; Elabd, Y. A. *Polymer* **2010**, *51*, 5516.
(31) Ye, Y.; Sharick, S.; Davis, E. M.; Winey, K. I.; Elabd, Y. A. *ACS Macro Letters* **2013**, *2*, 575.
(32) Gao, R.; Zhang, M.; Dixit, N.; Moore, R. B.; Long, T. E. *Polymer* **2012**, *53*, 1203.
(33) Weber, R. L.; Ye, Y.; Schmitt, A. L.; Banik, S. M.; Elabd, Y. A.; Mahanthappa, M. K. *Macromolecules* **2011**, *44*, 5727.
(34) Weber, R. L.; Ye, Y.; Banik, S. M.; Elabd, Y. A.; Hickner, M. A.; Mahanthappa, M. K. *Journal of Polymer Science Part B: Polymer Physics* **2011**, *49*, 1287.
(35) Yoshizawa, M.; Ohno, H. *Electrochimica Acta* **2001**, *46*, 1723.
(36) Wang, W.; Tudryn, G. J.; Colby, R. H.; Winey, K. I. *Journal of the American Chemical Society* **2011**, *133*, 10826.
(37) Wang, J.-H. H.; Colby, R. H. *Soft Matter* **2013**, *9*, 10275.
(38) Meyer, W. H. *Advanced materials* **1998**, *10*, 439.
(39) Zhang, L.; Chaloux, B. L.; Saito, T.; Hickner, M. A.; Lutkenhaus, J. L. *Macromolecules* **2011**, *44*, 9723.
(40) Eisenberg, A. *Macromolecules* **1971**, *4*, 125.
(41) Wu, L.; Cochran, E. W.; Lodge, T. P.; Bates, F. S. *Macromolecules* **2004**, *37*, 3360.
(42) Klinedinst, D. B.; Yilgör, E.; Yilgör, I.; Beyer, F. L.; Wilkes, G. L. *Polymer* **2005**, *46*, 10191.
(43) Sheth, J. P.; Wilkes, G. L.; Fornof, A. R.; Long, T. E.; Yilgor, I. *Macromolecules* **2005**, *38*, 5681.
(44) McLean, R. S.; Sauer, B. B. *Macromolecules* **1997**, *30*, 8314.
(45) Sheth, J. P.; Unal, S.; Yilgor, E.; Yilgor, I.; Beyer, F. L.; Long, T. E.; Wilkes, G. L. *Polymer* **2005**, *46*, 10180.
(46) Gehlsen, M. D.; Almdal, K.; Bates, F. S. *Macromolecules* **1992**, *25*, 939.
(47) Lee, M.; Choi, U. H.; Colby, R. H.; Gibson, H. W. *Chemistry of Materials* **2010**, *22*, 5814.
(48) Macdonald, J. R. *Physical review* **1953**, *92*, 4.
(49) Coelho, R. *Rev. Phys. Appl. (Paris)* **1983**, *18*, 137.
(50) Coelho, R. *Journal of Non-Crystalline Solids* **1991**, *131*, 1136.
(51) Macdonald, J. R. *Solid State Ionics* **2005**, *176*, 1961.
(52) Klein, R. J.; Zhang, S.; Dou, S.; Jones, B. H.; Colby, R. H.; Runt, J. *The Journal of chemical physics* **2006**, *124*, 144903.
(53) Fragiadakis, D.; Dou, S.; Colby, R. H.; Runt, J. *The Journal of chemical physics* **2009**, *130*, 064907.
(54) Fragiadakis, D.; Dou, S.; Colby, R. H.; Runt, J. *Macromolecules* **2008**, *41*, 5723.
(55) Choi, U. H.; Lee, M.; Wang, S.; Liu, W.; Winey, K. I.; Gibson, H. W.; Colby, R. H. *Macromolecules* **2012**, *45*, 3974.

(56) Van Krevelen, D. W.; Te Nijenhuis, K. *Properties of polymers: their correlation with chemical structure; their numerical estimation and prediction from additive group contributions*; Elsevier Science, 2009.
(57) Slattery, J. M.; Daguenet, C.; Dyson, P. J.; Schubert, T. J.; Krossing, I. *Angewandte Chemie* **2007**, *119*, 5480.
(58) Liu, Y.; Liu, S.; Lin, J.; Wang, D.; Jain, V.; Montazami, R.; Heflin, J. R.; Li, J.; Madsen, L.; Zhang, Q. *Applied Physics Letters* **2010**, *96*, 223503.

Chapter 4: **Thermal Polymerization and Block Copolymerization of 1-(4-vinylbenzyl)imidazole and Poly(ethylene glycol) methyl ether acrylate**

Chainika Jangu, Alison R. Schultz, and Timothy E. Long*

Macromolecules and Interfaces Institute, Department of Chemistry, Virginia Tech., Blacksburg, VA 24061, United States

*To whom correspondence should be addressed, *Email: telong@vt.edu TEL: (540) 231-2480; FAX: (540) 231-8517*

Keywords: thermal polymerization, *in situ* FTIR, nitroxide-mediated polymerization, controlled radical polymerization

4.1 *Abstract*

Controlled polymerization route permits the synthesis of well-defined macromolecules with controlled composition, predictable molecular weights, and narrow molecular weight distributions. Nitroxide-mediated polymerization (NMP) is based on reversible activation-deactivation equilibrium and has the advantage of being only governed by a thermal process and does not require any catalyst or bimolecular exchange. The feasibility of utilizing NMP polymerization in the synthesis of well-defined copolymers of 1-(4-vinylbenzyl) imidazole (VBIm) and poly(ethylene glycol)methyl ether acrylate (EG_9MEA) is investigated in this paper. *In situ* Fourier transform infrared spectroscopy (FTIR) was used to monitor the thermal polymerization in acrylate and methacrylate monomers and Arrhenius equation was used to calculate activation energies of monomers. It was found that acrylates have lower activation energy than methacrylates. The copolymerizations of EG_9MEA and VBIm were attempted,

resulted in linear increase in molecular weight *vs* conversion with narrow molecular weight distributions.

4.2 *Introduction*

Nitroxide-mediated polymerization (NMP) is a well-established controlled radical polymerization technique in which the molecular weight control relies on equilibrium between dormant propagating chains and a low concentration of propagating radicals.[1,2] NMP offers functional group tolerance providing versatility and less stringent purification techniques compared to living anionic polymerization.[2-7] A significant complication in NMP is the contribution of thermally initiated polymerization as a result of elevated reaction temperatures required for the propagation step.[8,9] Styrene is well known to undergo thermal initiation at typical reaction temperatures for NMP.[10] Initiation occurs *via* Mayo mechanism, where two free radicals capable of initiation are produced when a monomer unit reacts with a Diels–Alder adduct initially formed from two monomer units. The adjacent aromatic ring provides resonance stabilization to both resulting radicals.[10-13] Strong acids such as camphor sulfonic acid have been used to reduce the propensity for thermal polymerization because it reduces the concentration of the free nitroxide.[14] Long *et al.* also investigated thermal polymerization of 2-vinylnaphthalene (2VN), where activation energy was ~30 kJ/mol less than styrene due to significant thermal contributions.[15-17]

Recently with the development of new acyclic alkoxyamines initiators, NMP polymerization is possible with wide range of monomers such as acrylates and acrylamides.[18] The use of small amount (~ 5-10 mol% in the feed) of comonomer results in controlled copolymerizations, characterized by a linear increase in M_n with conversion (X) along with narrow molecular weight distributions. For styrene-methyl methacrylate (MMA)

copolymerizations mediated with SG1-based initiator, Blocbuilder®, 4.4-8.8 mol% of styrene is required to have control in the polymerization.[18] Lessard *et. al* also investigated the effects of using styrenic comonomer 9-(4-vinylbenzyl)-9H-carbazole (VBK) in the polymerization of MMA. The synthesis of MMA copolymers was observed to have controlled kinetics using VBK as a comonomer.[19-21]

In this work, we demonstrate the synthesis of poly(VBIm-*co*-EG_9MEA) using free radical and controlled radical copolymerizations. The study of rate constants and activation energies of acrylates and methacrylates using *in situ* FTIR spectroscopy, revealed the contribution from thermal polymerizations. The thermal polymerization is observed to have contribution in NMP of EG_9MEA. When VBIm was used as a "controlling" comonomer with EG_9MEA, the polymerization kinetics of copolymerizations showed linear increase in molecular weight with conversion and narrow molecular weight distributions.

4.3 *Experimental*

4.3.1 Materials

4-Vinylbenzyl chloride (VBCl 90%) and imidazole (99%) were purchased from Sigma-Aldrich and used as received. Poly(ethylene glycol) methyl ether acrylate (EG_9MEA), poly(ethylene glycol) methyl ether methacrylate (EG_9MEMA), di(ethylene glycol) methyl ether acrylate (DEGA) and di(ethylene glycol) methyl ether methacrylate (DEGMEMA) was obtained from Sigma-Aldrich and passed through alumina to remove inhibitor prior to use. *n*-butyl acrylate (*n*-BA) (99%) and *n*-butyl methacrylate (*n*-BMA) was purchased from Sigma-Aldrich and was vacuum distilled from calcium hydride. *α, α'*-Azobis(isobutyronitrile) (AIBN) was

purchased from Fluka and recrystallized from methanol. All solvents were purchased from Fischer and used without further purification.

4.3.2 Analytical Methods

^{1}H NMR spectroscopy was performed in DMSO-d_6 using a Varian Unity 400 MHz spectrometer at 25 °C. Thermogravimetric analysis (TGA) was performed on TA Instruments TGA Q50 from 25 to 600 °C at a heating rate of 10 °C/min. Differential scanning calorimetry (DSC) was performed using a TA Instruments DSC Q1000 and scans were performed under a N_2 atm. with heating rate of 10 °C/min and cooling rate of 100 °C/min. T_gs were recorded from the second heating cycle. Aqueous size exclusion chromatography (SEC) utilized a ternary mixture of water/methanol/acetic acid (54:23:23 v/v/v %) with 0.1 M sodium acetate at 35 °C, and a flow rate of 0.8 mL/h, determined the absolute weight-average molecular weights (M_w) of polymer using the refractive index detector and a multi-angle laser light scattering (MALLS) detector. The aqueous SEC included a Waters 717 plus autosampler, a Waters 1515 isocratic HPLC pump, two Waters ultrahydrogel linear columns, and one Waters ultrahydrogel 250 columns. Offline refractive index increment (d*n*/d*c*) measurements were performed using a Wyatt Optilab T-rEX equipped with a 690 nm laser at 35 °C. *In situ* FTIR monitoring was performed with an ASI Applied Systems ReactIR^{TM} 1000 reaction analysis system with a stainless steel DiComp^{TM} probe. The reaction vessel was sealed with rubber septa and the DiComp^{TM} probe was inserted into the third fitted neck of the flask and sealed tight. The solvent, DMF was added using a syringe, and the flask was purged with nitrogen for 10-15 min. The probe tip was positioned below the surface of the solvent to collect spectra of the reaction mixture. The reaction vessel was then placed in an oil bath heated at different temperatures, and FTIR data collection was

commenced. The ReactIR analysis system was programmed to collect a spectrum every 5 min for 24 h.

4.3.3 Synthesis of Poly(VBIm-*co*-EG_9MEA)

Poly(VBIm-*co*-EG_9MEA) with different compositions of VBIm and EG_9MEA were synthesized using conventional free radical polymerizations. For a representative copolymerization, the monomers, VBIm (4 g) and EG_9MEA (2 g) and azo initiator AIBN (0.1 mol%) were dissolved in DMF (80 wt%). The reaction flask was sealed with a rubber septum, purged with argon for 30 min and then placed in an oil bath at 65 °C for 24 h with constant stirring. After polymerization, the product was dialyzed against methanol for 3 d. The final product was dried at 50 °C under reduced pressure (0.5 mm Hg) for 24 h. ^{1}H NMR confirmed mol fractions incorporation of VBIm and EG_9MEA in the copolymer series. The synthetic strategy is presented in Scheme 4.1.

Scheme 4.1 Free radical copolymerization of VBIm and EG_9MEA

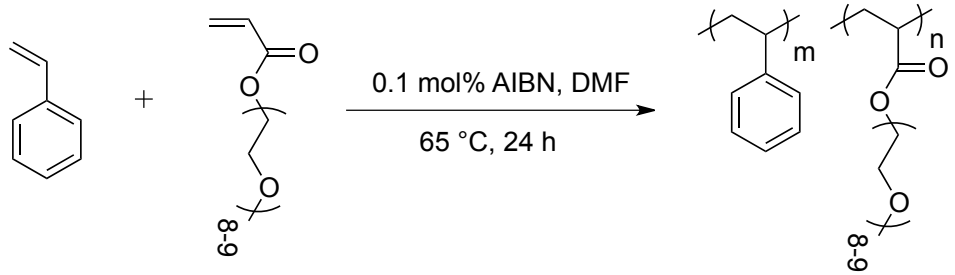

4.3.4 Synthesis of Poly(VBIm-*co*-EG_9MEA) using Nitroxide-Mediated Polymerization (NMP)

Several copolymers were synthesized with various concentrations of VBIm relative to EG_9MEA. As an example, VBIm (2 g), Blocbuilder® (0.54 g) and DEPN (23 mg) were dissolved in DMF (25 mL) and degassed using three freeze pump thaw cycles. The flask was back-filled with argon, and heated to 125 °C. The solution was cooled to 23 °C, diluted with DMF (20 mL),

and dialyzed against methanol for 7 d. The reaction conditions were optimized and the copolymerization kinetics was probed using ^{1}H NMR spectroscopy and SEC. The overall synthetic route is shown in Scheme 4.2.

Scheme 4.2 Nitroxide-mediated copolymerization of VBIm and EG_9MEA using Blocbuilder®

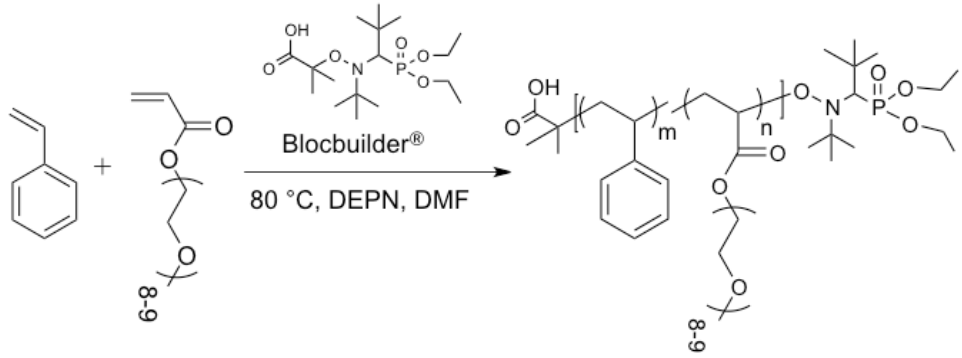

4.4 *Results and Discussions*

The synthesis of VBIm monomer was adopted from previous literature.[22] Conventional free radical copolymerization enabled the synthesis of poly(VBIm-*co*-EG_9MEA) as displayed in Scheme 4.1. The copolymers were investigated providing useful insights into the copolymerization behavior of these two monomers. The molecular weight analysis and thermal properties of the copolymers are listed in Table 4.1. All of the copolymers have a single T_g and T_g was observed to increase with increased incorporation of VBIm. The copolymers are thermally stable up to 300 ˚C determined using TGA. The copolymers obtained are high molecular weight polymers with PDIs expected from a typical conventional free radical copolymerization.

Table 4.1 Thermal properties and molecular weight analysis of poly(VBIm-*co*-EG_9MEA)

EG_9MEA[a] (mol%)	VBIm[a] (mol%)	$T_{d,5\%}$[b] (°C)	T_g[c] (°C)	M_w[d] (g/mol)	M_n[d] (g/mol)	PDI[d]
0	100	370	103	452,000	668,000	1.48
10.9	89.1	317	101	434,000	616,000	1.42
44.6	55.4	395	-37	411,000	560,000	1.36
75.4	24.6	302	-55	389,000	537,000	1.38
100	0	305	-69	309,000	426,000	1.38

[a] ^1H NMR spectroscopy: 400 MHz, $CDCl_3$, 25 °C
[b] TGA: 10 °C/min, N_2 atmosphere
[c] DSC: 10 °C/min, N_2 atmosphere, second heat
[d] SEC: 35 °C, 1 mL/min, MALLS detector, 54/23/23 (v/v/v %) H_2O/CH_3OH/AcOH, 0.1 M NaOAc

Figure 4.1 showed experimentally determined T_g of poly(VBIm-*co*-EG_9MEA) as compared to theoretically calculated T_g predicted using Fox-equation. The copolymers appeared random based on their adherence to theoretical Fox equation, which predicts T_g for random copolymers. To further confirm the random copolymerization behavior, reactivity ratios for these monomers were determined. The product of reactivity ratios, r_1 and r_2 is equal to one, $r_1r_2 = 1$ indicates ideal copolymerization. *In situ* FTIR was used to determine reactivity ratio of VBIm with EG_9MEA. *In situ* FTIR monitors instantaneous monomer conversion in real time for each polymerization with varying monomer molar ratios.[11] Mayo-Lewis analysis of three different copolymerizations with different monomer compositions (40, 50 and 60 mol% of VBIm) was used to determine reactivity ratios. The peaks located at 898 cm^{-1} and 1094 cm^{-1} were followed for vinyl group conversion of VBIm and EG_9MEA, respectively. Plotting *r vs* assumed *r* for different molar feed ratio gave three intersecting lines shown in Figure 4.2. The intersection point estimated the reactivity ratios, $r_{VBIm} = 0.9$ and $r_{EG9MEA} = 1.1$. Since the product of the reactivity ratios is close to one and also T_gs of the copolymers adhered with predictions from Fox

equation, random behavior of these copolymers was confirmed.

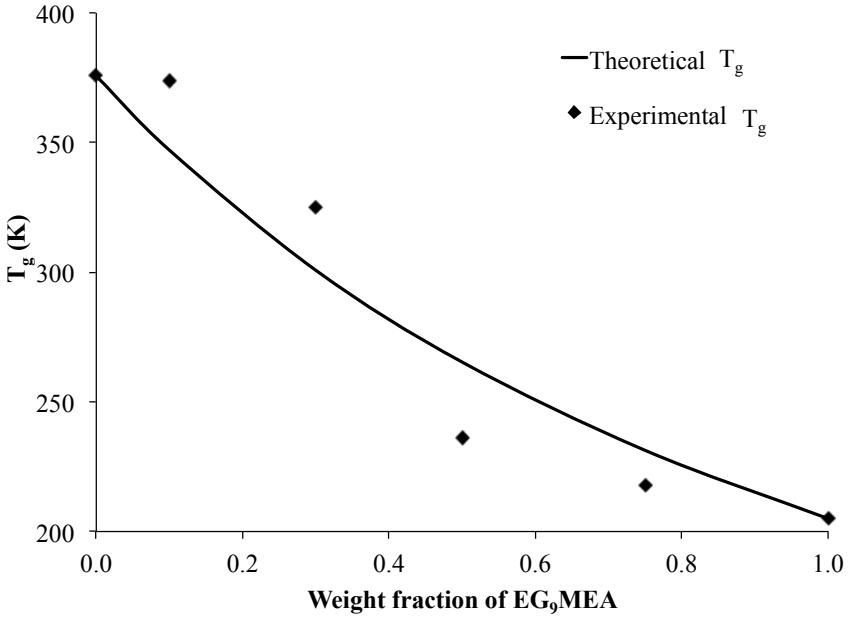

Figure 4.1 Experimentally determined T_g of poly(VBIm-*co*-EG_9MEA) as compared to theoretically calculated T_g predicted using the Fox-equation

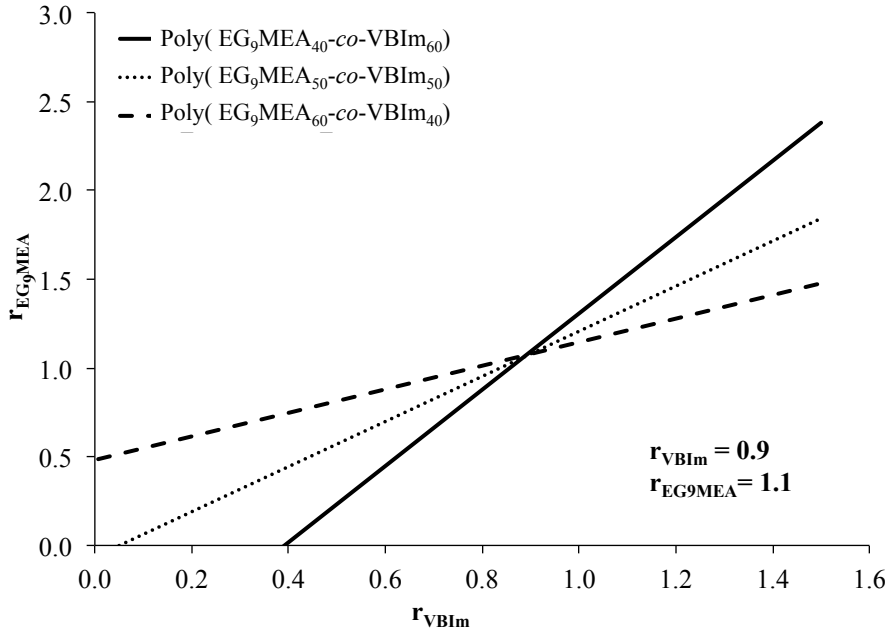

Figure 4.2 Monomer reactivity ratio determination of VBIm and EG_9MEA using the Mayo-Lewis method

In situ FTIR spectroscopy is an efficient analytical method for elucidating polymerization kinetic processes.[11,23] A ReactIR 1000 *in situ* FTIR spectrometer was used to monitor the thermal polymerizations of *n*-butyl acrylate (*n*-BA), EG_9MEA, diethylene glycol acrylate (DEGA) along with their methacrylate analogues. The thermal polymerization of monomers was monitored at 90, 100, and 110 °C to elucidate the thermal initiation over a range of temperatures. The polymerizations were monitored using *in situ* FTIR spectroscopy and the observed rate constants for the pseudo-first-order thermal polymerization kinetics were determined.

A representative plot is shown in Figure 4.3**,** where the rate of DEGA consumption displayed a substantial degree of thermal initiation and polymerization at all reaction temperatures, although decreasing the reaction temperature resulted in lower monomer conversion. Thermal polymerization activation energies were calculated to quantitatively ascertain the relative rates of thermal polymerization as recorded in Table 4.2.

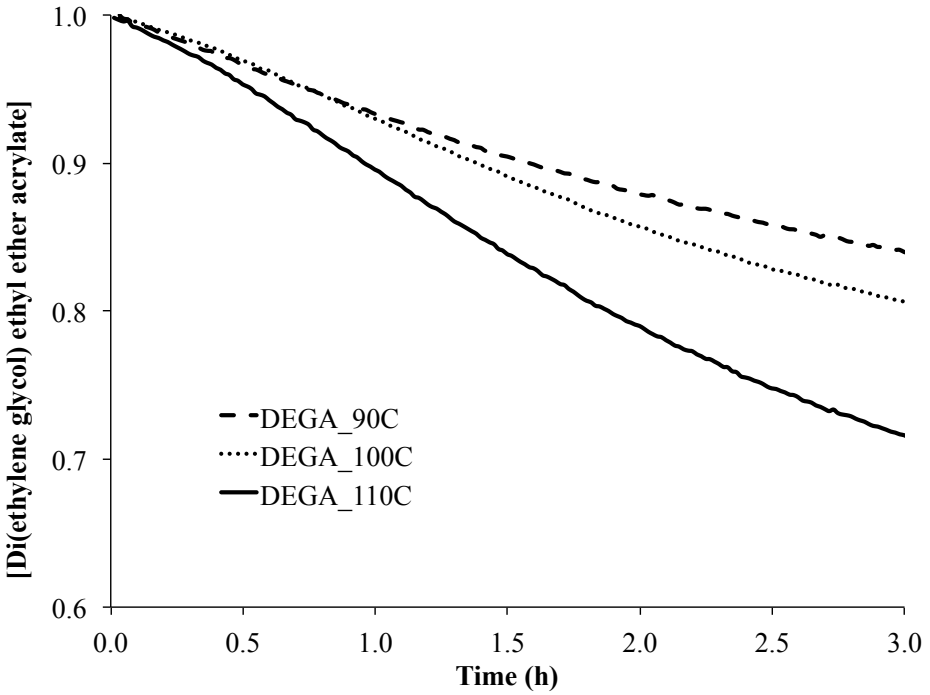

Figure 4.3 A representative plot of monomer disappearance of di(ethylene glycol) ethyl ether acrylate (DEGA) with time determined using *in situ* FTIR at different temperatures

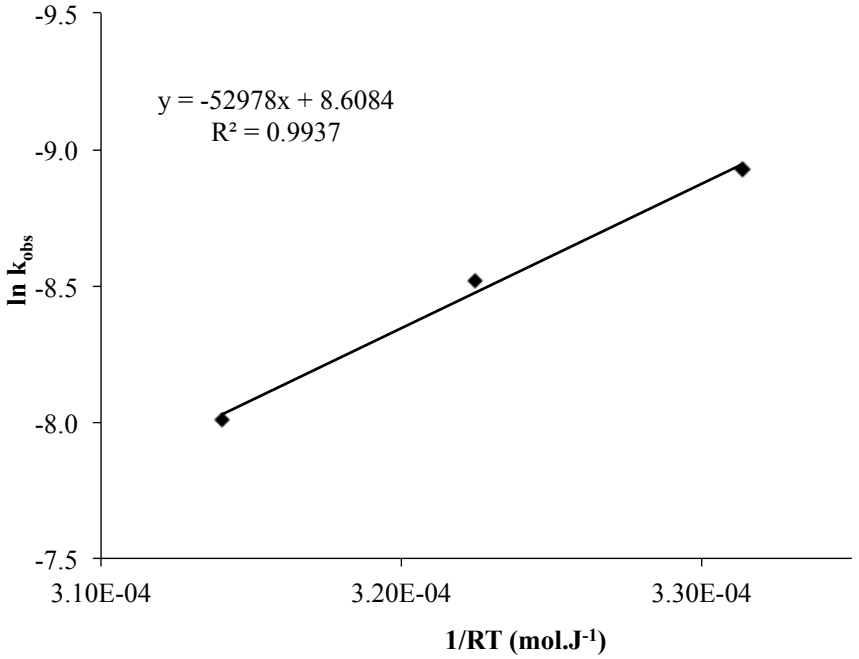

Figure 4.4 Arrhenius plot for thermal polymerization of DEGA at different temperatures

Table 4.2 Summary of activation energies for thermal initiation and polymerization of various acrylic and methacrylic monomers

Monomer	Temperature (°C)	k_{obs} (s^{-1})	E_{act} (kJ/mol)
n-Butyl acrylate 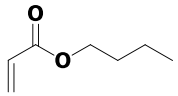	90	1.67×10^{-5}	77.2
	100	3.33×10^{-5}	
	110	6.33×10^{-5}	
Di(ethylene glycol) methyl ether acrylate 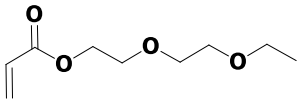	90	1.33×10^{-4}	52.9
	100	2.0×10^{-4}	
	110	3.33×10^{-4}	
Poly(ethylene glycol) methyl ether acrylate 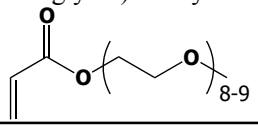	90	3.13×10^{-3}	34.2
	100	4.95×10^{-3}	
	130	1.13×10^{-2}	
n-Butyl methacrylate 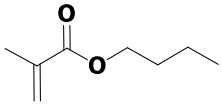	80	5.0×10^{-6}	92.9
	90	2.0×10^{-5}	
	110	2.33×10^{-5}	
Di(ethylene glycol) methyl ether methacrylate 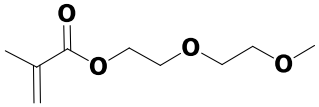	80	2.33×10^{-6}	78.9
	100	4.17×10^{-6}	
	120	4.83×10^{-5}	

The activation energy for thermal polymerization of acrylates is low as observed using *in situ* FTIR. Recently, it was postulated and computationally verified that the self-initiation of methyl acrylate is likely initiating mechanism in spontaneous thermal polymerization of methyl acrylate.[24] The Flory's mechanism of self-initiation proposes two monomers to combine and form a diradical, which either undergoes ring closure to form a cyclobutane derivative or undergoes hydrogen transfer or abstraction with a third monomer to form monoradical species. They postulated that the diradical self-initiation is the most likely mechanism of initiation in spontaneous thermal polymerization of alkyl acrylates.[18] Pryor and Lasswell postulated that spontaneous initiation in non-styrenic monomers would occur *via* Flory's mechanism to generate monoradicals. In non-styrenic monomers such as MMA, Diels-Alder adducts lack the tendency to undergo hydrogen abstraction. [25]

Once the thermal polymerizations of acrylates and methacrylates were defined, NMP controlled radical polymerization strategy was used for the synthesis of copolymers. The polymerization of EG_9MEA in literature shows lack of molecular weight control over a broad range of initiator concentrations, further suggesting the presence of an alternative initiation process.[21] We wish to obtain polymerizations that are controlled and exhibit the characteristics of a controlled polymerization. The estimation of kinetic parameters was done by plotting ln(1/(1-X) (where X is monomer conversion) *vs* time and determining the slopes in the linear region. Such plots are shown in Figure 4.5 at various initial VBIm concentrations relative to EG_9MEA. The effect of VBIm as a comonomer on the copolymerization kinetics, the control of the polymerization and the "livingness" of the resulting copolymer were investigated.

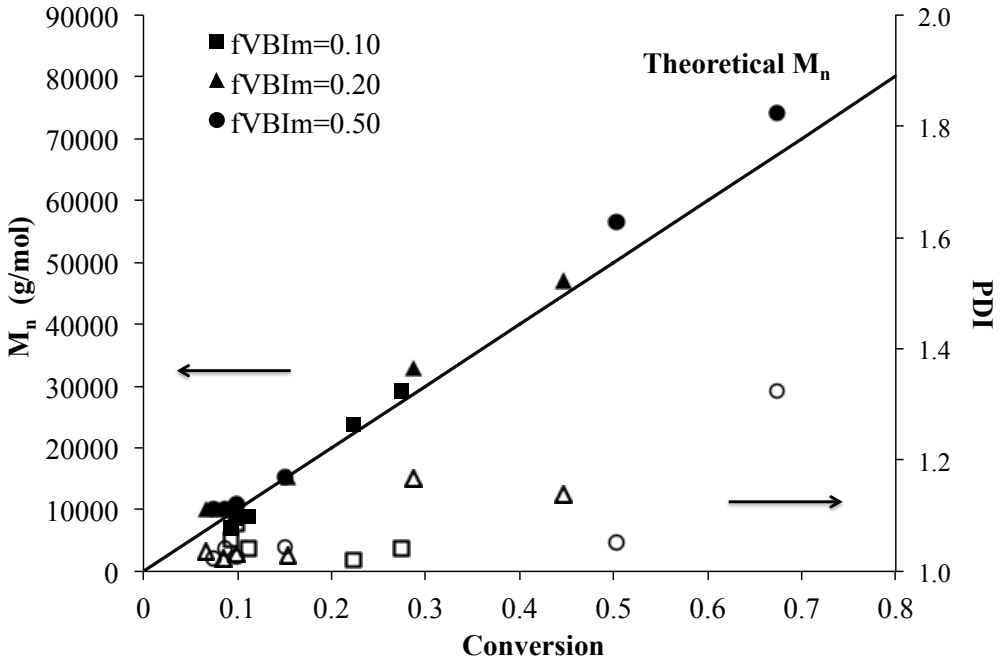

Figure 4.5 Number-average molecular weight (M_n) (filled symbols) and PDI (open symbols) *vs* conversion for NMP of VBIm and EG_9MEA initiated by Blocbuilder®. (a) $f_{VBIm} = 0.10$ (b) $f_{VBIm} = 0.20$ (c) $f_{VBIm} = 0.50$, where f_{VBIm} is the initial molar composition of VBIm in the feed

Figure 4.5 and Figure 4.6 shows the kinetic plots indicating controlled polymerization behavior. The M_n values for all copolymerizations in this study were found to increase linearly with conversion, which when paired with the relatively narrow PDIs, is indicative of a controlled polymerization. SEC chromatograms also highlighted the controlled shift with increasing target M_n values, monomodal chromatograms, and narrow polydispersities for the copolymer series as shown in Figure 4.7.

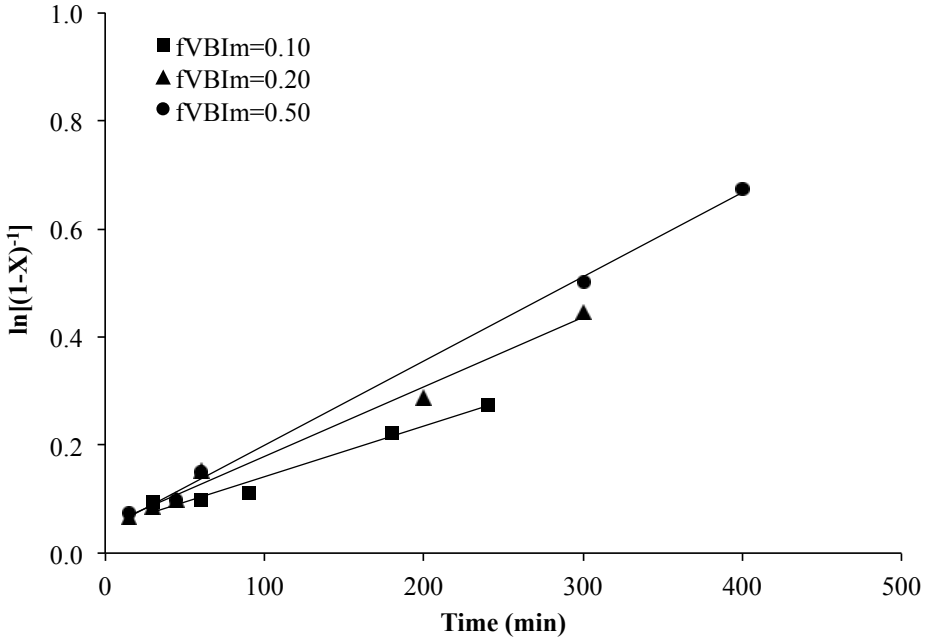

Figure 4.6 Conversion ln[1/(1-X)] (where X is monomer conversion) *vs* time for copolymerization of VBIm and EG_9MEA at 85 °C in DMF with [DEPN]/[Blocbuilder®] = 0.20. (a) $f_{VBIm} = 0.10$ (b) $f_{VBIm} = 0.20$ (c) $f_{VBIm} = 0.50$, where f_{VBIm} is the initial molar composition of VBIm in the feed. The solid lines are linear fits to the data taken at early points in the polymerization to calculate the apparent rate constant $k_p[P]$ where k_p is the propagation rate constant and [P] is the concentration of propagating macro-radicals

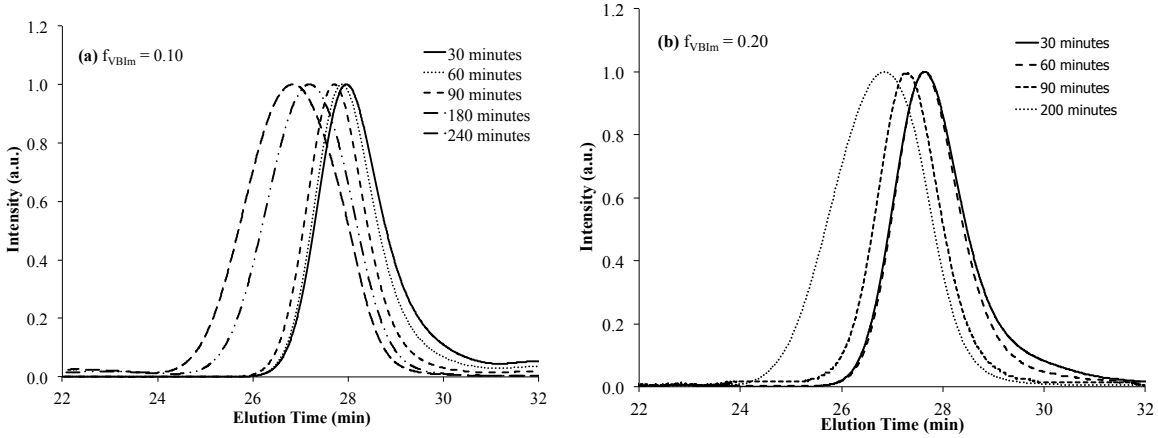

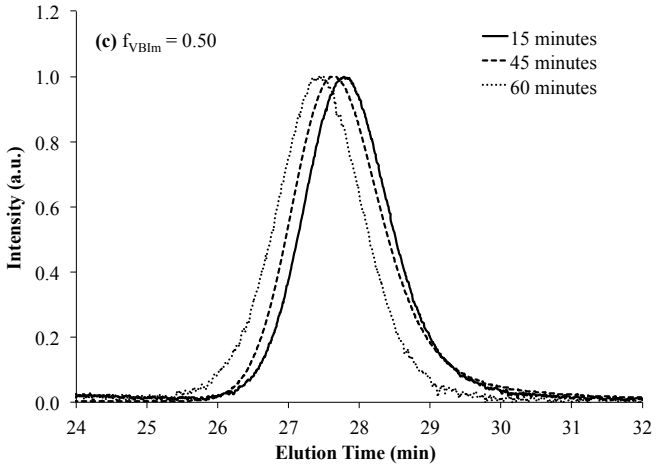

Figure 4.7 Evolution of SEC curves with conversion for copolymerization of EG_9MEA with different incorporations of VBIm. (a) $f_{VBIm} = 0.10$ (b) $f_{VBIm} = 0.20$ (c) $f_{VBIm} = 0.50$, where f_{VBIm} is the initial molar composition of VBIm in the feed

The kinetics behavior of NMP is often characterized in the literature by k_pK values, where k_p is the propagation rate constant and K is the activation-deactivation equilibrium constant.[15,21] The k_pK was estimated using following procedure. The equilibrium constant *K* for the reaction shown in Scheme 4.2 is defined as:

$$K = \frac{[DEPN][P]}{[P - Blocbuilder]}$$

where [DEPN] is equal to the concentration of free nitroxide, [P] is the concentration of propagating radicals, and [P-Blocbuilder] is the concentration of DEPN-polymer capped species. Early in the polymerization, it is very likely that the concentration of free nitroxide radicals is high and relatively constant and therefore can be substituted with the initial concentration of added nitroxide that is $[DEPN]_0$. During the early portion of the polymerization when the chains are relatively short, homotermination is negligible and therefore the concentration of reversibly deactivated alkoxyamine-terminated species can be assumed to be equal to the initial concentration of the alkoxyamine initiator, thus [P-N] will be same as $[Blocbuilder]_0$. All of these

assumptions are most relevant when the polymerization behaves in a controlled fashion (if M_n *vs* X is linear). Since the polymerization shown in Scheme 4.2 behaves in a controlled fashion (Figure 4.6), thus the above equation becomes:

$$K = \frac{[DEPN]_0[P]}{[Blocbuilder]_0}$$

Multiplying the above equation by the propagation rate constant (k_p) gives the following expression.

$$k_pK = k_p \frac{[DEPN]_0[P]}{[Blocbuilder]_0} = \frac{[DEPN]_0}{[Blocbuilder]_0} k_p[P]$$

$k_p[P]$ can be determined using the slopes of the scaled conversion *vs* time. Table 4.3 lists the apparent constant values of copolymerizations with different incorporations of VBIm. The k_pK constant value decreased with increase in amount of VBIm in copolymers. The decrease in k_pK constant values indicates slower polymerization kinetics, and likely to contribute towards controlled behavior of copolymerizations.

Table 4.3 The apparent rate constants (k_pK) of copolymers with different incorporations of VBIm

Polymer	f_{VBIm} [a]	F_{VBIm} [b]	k_pK [c] (s^{-1})
Poly(EG_9MEA)	-	-	4.6×10^{-3}
Poly(EG_9MEA_{90}-*co*-$VBIm_{10}$)	0.10	0.13	3.0×10^{-4}
Poly(EG_9MEA_{80}-*co*-$VBIm_{20}$)	0.20	0.25	1.3×10^{-4}
Poly(EG_9MEA_{50}-*co*-$VBIm_{50}$)	0.50	0.66	1.6×10^{-4}

[a] f_{VBIm} is the initial VBIm monomer feed composition. [b] F_{VBIm} is the final molar composition of VBIm in copolymer determined using ^{1}H NMR spectroscopy. [c] k_pK is the apparent rate constant calculated using $k_pK = k_p[P] \times [DEPN]/[Blocbuilder^{®}]$. $k_p[P]$ were determined from the slope for fits in the linear regions of the semilogarithmic kinetic plots of ln[1/(1-X)] (where X is monomer conversion) *vs* time.

4.5 *Conclusions*

Conventional free radical copolymerizations enabled the synthesis of poly(VBIm-*co*-EG_9MA). *In situ* FTIR was used to confirm random incorporation of the two monomers and also to investigate thermal polymerization behavior of acrylates and their methacrylates analogues. The acrylates were found to have lower activation energies than methacrylates suggesting relatively less control in the polymerizations. NMP copolymerizations of EG_9MA with VBIm as comonomer exhibited controlled polymerization behavior confirmed by kinetic plots coupled with narrow molecular weight distributions observed from SEC chromatograms. The control behavior of the copolymerization is likely attributed to the observed decrease in calculated apparent rate constants for the copolymerizations with addition of VBIm as comonomer.

4.6 *Acknowledgements*

This material is based on work supported by the U.S. Army Research Laboratory and the U.S. Army Research Office under contract/grant number W911NF-07-1-0452 Ionic Liquids in Electro-Active Devices Multidisciplinary University Research Initiative (ILEAD MURI). The authors acknowledge the Laboratory for Research on the Structure of Matter at Penn (MRSEC NSF DMR11-20901) for instrument support

4.7 *References*

(1) Nicolas, J.; Guillaneuf, Y.; Lefay, C.; Bertin, D.; Gigmes, D.; Charleux, B. *Progress in Polymer Science* **2012**.
(2) Hawker, C. J.; Bosman, A. W.; Harth, E. *Chemical Reviews* **2001**, *101*, 3661.
(3) Anderson, E. B.; Long, T. E. *Polymer* **2010**, *51*, 2447.
(4) Benoit, D.; Grimaldi, S.; Robin, S.; Finet, J.-P.; Tordo, P.; Gnanou, Y. *Journal of the American Chemical Society* **2000**, *122*, 5929.
(5) Cheng, S.; Beyer, F. L.; Mather, B. D.; Moore, R. B.; Long, T. E. *Macromolecules* **2011**, *44*, 6509.

(6) Mather, B. D.; Baker, M. B.; Beyer, F. L.; Berg, M. A.; Green, M. D.; Long, T. E. *Macromolecules* **2007**, *40*, 6834.
(7) Mather, B. D.; Lizotte, J. R.; Long, T. E. *Macromolecules* **2004**, *37*, 9331.
(8) Grubbs, R. B. *Polymer Reviews* **2011**, *51*, 104.
(9) Hadjichristidis, N.; Pitsikalis, M.; Iatrou, H. In *Block Copolymers I*; Springer: 2005, p 1.
(10) Katzer, J.; Pauer, W.; Moritz, H. U. *Macromolecular Reaction Engineering* **2012**, *6*, 213.
(11) Pasquale, A. J.; Long, T. E. *Macromolecules* **1999**, *32*, 7954.
(12) Chong, Y. K.; Rizzardo, E.; Solomon, D. H. *Journal of the American Chemical Society* **1983**, *105*, 7761.
(13) Mayo, F. R. *Journal of the American Chemical Society* **1968**, *90*, 1289.
(14) Buzanowski, W.; Graham, J.; Priddy, D.; Shero, E. *Polymer* **1992**, *33*, 3055.
(15) Lizotte, J. R.; Erwin, B. M.; Colby, R. H.; Long, T. E. *Journal of Polymer Science Part A: Polymer Chemistry* **2002**, *40*, 583.
(16) Lizotte, J. R.; Long, T. E. *Macromolecular Chemistry and Physics* **2003**, *204*, 570.
(17) Lizotte, J. R.; Long, T. E. *Macromolecular Chemistry and Physics* **2004**, *205*, 692.
(18) Guillaneuf, Y.; Gigmes, D.; Marque, S. R.; Astolfi, P.; Greci, L.; Tordo, P.; Bertin, D. *Macromolecules* **2007**, *40*, 3108.
(19) Lessard, B.; Graffe, A.; Maric, M. *Macromolecules* **2007**, *40*, 9284.
(20) Lessard, B. H.; Ling, E. J. Y.; Marić, M. *Macromolecules* **2012**, *45*, 1879.
(21) Lessard, B. t.; Maric, M. *Macromolecules* **2008**, *41*, 7870.
(22) Green, M. D.; Allen Jr, M. H.; Dennis, J. M.; Cruz, D. S.-d. l.; Gao, R.; Winey, K. I.; Long, T. E. *European Polymer Journal* **2011**, *47*, 486.
(23) Pasquale, A. J.; Long, T. E. *Journal of Polymer Science Part A: Polymer Chemistry* **2001**, *39*, 216.
(24) Srinivasan, S.; Lee, M. W.; Grady, M. C.; Soroush, M.; Rappe, A. M. *The Journal of Physical Chemistry A* **2009**, *113*, 10787.
(25) Pryor, W. A.; Lasswell, L. D. *Advances in Free Radical Chemistry* **1975**, *5*, 27.

Chapter 5: **Phosphonium Cation-containing Polymers: From Ionic Liquids to Polyelectrolytes**

(Published in *Polymer* **2014**, *55*(13), 3298-3304)

Chainika Jangu and Timothy E. Long*

Department of Chemistry, Macromolecules and Interfaces Institute
Virginia Tech., Blacksburg, Virginia 24061

*To whom correspondence should be addressed E-mail: telong@vt.edu. TEL: (540)231-2480 FAX: (540)231-8517

Keywords: macromolecules; ionic liquids; polyelectrolytes.

5.1 *Abstract*

Phosphonium cation-based ionic liquids (ILs) are a readily available family of ILs that in some applications offer superior properties as compared to ammonium cation-based ILs. Recently investigated applications include extraction solvents, electrolytes in batteries and super-capacitors, and in corrosion protection. At the same time, the range of cation–anion combinations available commercially has also increased in recent years. Polymerized ionic liquids and polyelectrolytes play a major role in a broad range of biological applications including antimicrobials, non-viral gene delivery, synthetic enzymes, metal chelation, and drug delivery. Ammonium- and phosphonium-containing macromolecules will be reviewed with a focus on structure-property relationships of these polyelectrolytes and ionic liquids. Phosphonium-containing macromolecules display a broad range of improved properties compared to ammonium macromolecules.

5.2 *Introduction*

Recently ammonium or phosphonium ion-containing polymers have gained technological importance since they serve as potential phase-transfer catalyst, anti-static agents, biocides, humidity sensors, and water filtration membranes.[1-5] Recently, broader commercial phosphine library facilitated the synthesis of low viscosity, high conductivity phosphonium ILs.[4] Nitrogen and phosphorus atoms have different atomic radii and electronegativity that leads to widely different cationic structures. Row 2 element in the periodic table, nitrogen has an atomic weight of 14.01 g/mol as compared to phosphorus in the row 3 of periodic table below nitrogen with an atomic weight of 30.97 g/mol. Phosphorus has a larger atomic radius than nitrogen[6], and electronegativity differences result in a different charge distribution within the cation. Colby *et al.* determined the specific charges found upon each atom within the ammonium and phosphonium cation using *ab initio* calculations.[7] The nitrogen in ammonium cations exhibited a slightly negative partial charge of -0.5 eV while the surrounding alpha carbons displayed a slightly positive charge of 0.3 eV because nitrogen is more electronegative than carbon. Conversely, phosphonium cations contained a reversed charge density because phosphorus is less electronegative than carbon; therefore, the phosphorus atom displayed a partial positive charge of +1.1 eV and the adjacent carbon atoms exhibited a partial negative charge of -0.2 eV. These differences are expected to markedly alter properties in emerging technologies.[8]

Due to the difference in the cationic structures, ammonium and phosphonium cation-based macromolecules exhibit different properties. Ammonium ionic liquids (IL) are often limited by their poor thermal stability.[4] Phosphonium cation-based ILs potentially offer superior properties, such as higher thermal stabilities, higher conductivities, and lower viscosities compared with the corresponding ammonium ILs. Ammonium and phosphonium ionic liquids

degrade through two different pathways under alkaline conditions. The literature proposed different degradation pathways for ammonium polyelectrolytes, predominantly Hofmann elimination and reverse Menschutkin degradation. Phosphonium cations generally resist Hofmann elimination and Menschutkin degradation, leading to improved thermal stabilities. Ammonium ILs typically degrade through Hofmann elimination while phosphonium ILs degrade into tertiary phosphine oxides and alkanes.[8] The overall structure of the ammonium or phosphonium cation largely impacts its overall base stability.[9,10] Therefore, many phosphonium-containing macromolecules with improved thermal stabilities as compared to ammonium analogs are suitable for alkaline fuel cells and anion exchange membranes.[1,9,11]

Apart from the enhanced thermal stability, many researchers have examined high flame retardency of phosphorus-containing macromolecules, ideal for high temperature aerospace and transportation applications. Also, natural occurrence of phosphorus-containing macromolecules in nucleic acids highlights their importance in biological applications. The overall focus of this review revolves around phosphonium-containing macromolecules with an emphasis on ionic liquids and polyelectrolytes.

5.3 *Phosphonium Cation-Containing Polymers as Ionic Liquids*

According to the current convention, ionic liquids (ILs) are salts that exhibit a melting point (T_m) below 100 °C; however, this strict definition is often challenged in the literature.[12] These ILs are typically an organic cation (imidazolium, pyridinium, quaternary ammonium, and phosphonium) as shown in Figure 5.1 and an anion such as halide, tetrafluoroborate (BF_4), hexafluorophosphate, triflate, amidotriflate, and bis(trifluorosulfonyl)imide.[8,13,14] The literature has reported significant variation in physical properties among these salts, despite a common cation with different anions e.g. *n*-butylmethylimidazolium with hexafluorophosphate anion

[C_4mim][PF_6] is immiscible with water, whereas with tetrafluoroborate anion [C_4mim][BF_4] is water-soluble.[15] Seddon described ILs as designer solvent due to variation in physical properties with change in cation or anion.[16] Structural variation enables high thermal stabilities, low vapor pressures, high ionic conductivities and variable solubility for their applications as potential electrolytes for various electrochemical devices[5,17-26], including rechargeable lithium batteries[27,28], solar cells[29-31], actuators[32-34], and capacitors[4,35-39].

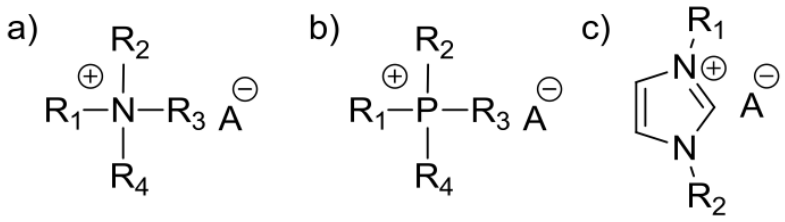

Figure 5.1 Example structures of ionic liquids (a) ammonium, (b) phosphonium, (c) imidazolium.

The phosphonium-based ILs are typically produced using two approaches of ion exchange reactions.

$$[R'PR_3]^+[X]^- + MA \longrightarrow [R'PR_3]^+[A]^- + MX$$

$$[R'PR_3]^+[X]^- + MOH + HA \longrightarrow [R'PR_3]^+[A]^- + MX + H_2O$$

where R, R′ = alkyl; X = halogen; M = alkali metal; and A = an anion such as phosphinate, carboxylate, tetrafluoroborate, and hexafluorophosphate.[4] Parshall published phosphonium ILs in 1970s using stannate and germanate salts[40-42], and in 1980s, Knifton *et al.* used molten tetrabutylphosphonium bromide as an ionic solvent.[43-45]

ILs containing a polymerizable functionality enables the polymerization of ionic liquids.[38] Polymerization of IL monomers typically results in reduced ionic conductivities due to immobilization of the cation and a higher T_g[46], but PILs result in single-ion conductors suitable

for electromechanical actuators[47], gas separation membranes[48], and ion exchange membranes[49]. Common ammonium PILs include quaternized poly(2-dimethylaminoethyl methacrylate)[50], poly(vinylbenzyl ammonium)s[51], and poly(diallyldimethylammonium chloride)[52]. Figure 5.2 depicts broad potential applications of ILs. Imidazolium ionic liquids are the most common ionic liquids with a broad range of structural diversity through substituent control and counterion structure[53]. Phosphonium cation-based ILs offer a broad range of useful properties and recently received attention in the recent literature[8]. Typically, researchers examine structure-property relationships of ammonium- and phosphonium-containing polymerized ionic liquids to examine the impact of cation structure on macromolecular properties.

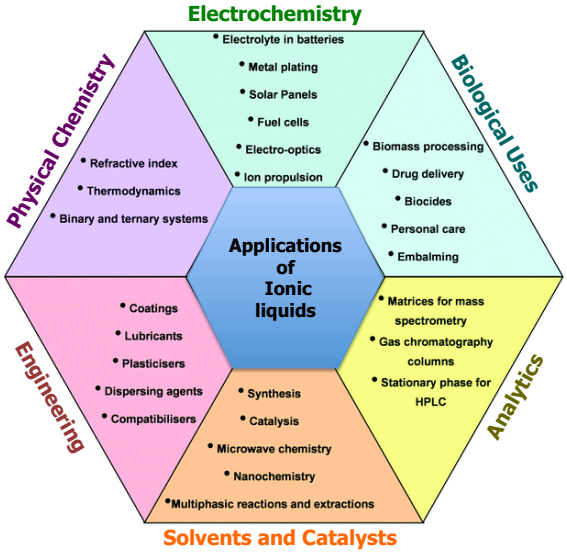

Figure 5.2 Applications of ionic liquids

MacFarlane *et al.* summarized the history, commercial synthesis, and several of the enhanced physical properties of phosphonium ILs as compared to ammonium and imidazolium ILs.[54,55] MacFarlane described the superior stability in basic environments, i.e., higher chemical, electrochemical, and thermal stabilities with typical densities less than water. The structural effects concluded that the length and symmetry of the alkyl substituents on the phosphonium cation significantly influenced the physical state, while anion selection favored smaller charge-

diffuse ions. Clyburne *et al.* studied the use of phosphonium ILs as reaction media for strong bases. Phosphonium ILs are also under consideration for their application as extraction agents[56,57], where Chen *et al.* studied the adsorption of Cr(III) and Cr(IV) onto silica-based systems embedded with phosphonium ILs. Their work displayed improved thermal stability, higher metal extraction, and quantitative desorption of chromium ions relative to ammonium IL counterparts. Frackowiak *et al.* investigated phosphonium ILs for their potential applications as super-capacitors[5]. Their findings suggested that phosphonium ILs provided an enhanced electrochemical window relative to currently available ammonium ILs, while providing suitable capacitance values at reasonable applied voltages and scan rates. Tsunashima *et al.* also studied the potential of phosphonium ILs as battery electrolytes; their studies revealed that through chemical tuning, the phosphonium IL viscosity reduced to values that provided high discharge capacities relative to ammonium IL counterparts.[58,59]

Downard et al. discussed the potential for commercialization of phosphonium ILs, citing synthetic procedures, structural tuning through phosphonium-substituent and anion choice, physical properties, and the potential for application-specific materials.[60,61] Janus and Stefaniak utilized tri(hexyl) tetradecylphosphonium TFSI as a solvent for the Diels Alder reaction, and the product is easily distilled from the IL reaction media due to the thermal stability and negligible volatility of the phosphonium IL.[62] Pawar *et al.* also analyzed the use of tri(hexyl) tetradecylphosphonium chloride as a phosphonium IL reaction media for Michael additions. They also noted the lower potential for chemical side reactions and intermolecular interactions among phosphonium ILs.[60]

Dreisinger *et al.* discussed the physical properties including density, viscosity, and conductivity of a variety of commercially available phosphonium ILs. The study showed that the

conductivity of the IL directly related to the anion volume and inversely correlated with the cation volume. They also investigated how cation symmetry influenced physical properties, and they cited a decrease in viscosity and slight increase in conductivity with the introduction of molecular asymmetry. In general, they also measured higher viscosities for phosphonium ILs relative to ammonium ILs.[63] Diamond *et al.* investigated the unique ability of ILs to solvate compounds and related the unique polar and non-polar regions within homogeneous IL solutions to solvating power.[64] Xanthos *et al.* discussed the hydrolytic and thermal degradation of poly(lactic acid) within two phosphonium ILs, tri(hexyl) tetradecylphosphonium tetrafluoroborate (BF_4) and tri(hexyl) tetradecylphosphonium decanoate. Their findings suggested that the decanoate anion resulted in pronounced degradation because the decanoate anion catalyzed the hydrolytic degradation. On the other hand, degradation in BF_4-containing phosphonium IL related to the generation of HF in the presence of atmospheric moisture, and the presence of the phosphonium IL actually increased the thermal stability.[65]

Long and coworkers presented a facile anion exchange synthetic technique, which enabled a larger toolbox of IL chemical structure. Anion exchanges shown in Figure 5.3 significantly impacted solubility, T_g, thermal stability, conductivity, and viscosity of the IL. These exchanges resulted in phase changes for the products of the metathesis reactions, simplifying purification. The IL viscosity-temperature relationship exhibited Arrhenius-type behavior with activation energies favoring bulky, fluorinated anions. Similarly, activation energies derived from ionic conductivities favored the phosphonium ILs with bulky fluorinated anions. The trend for molar conductivities of phosphonium-containing ILs were smaller than for imidazolium-based ILs presumably due to stronger intermolecular interactions.[66]

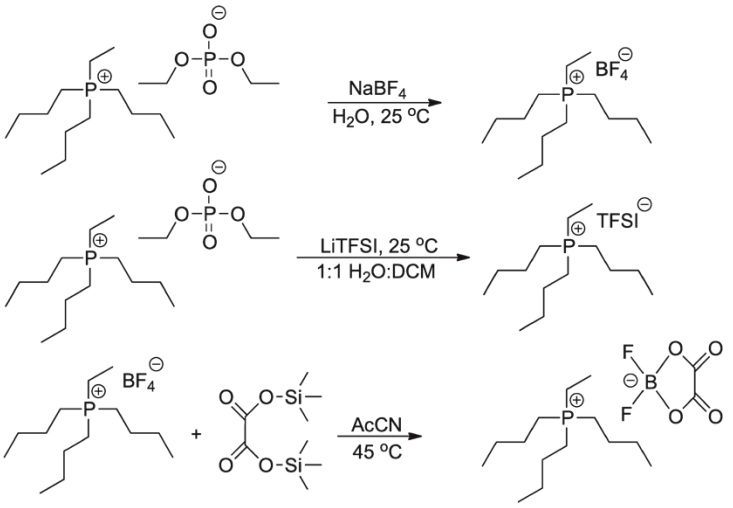

Figure 5.3 Anion exchange to produce Bu_3-based phosphonium ILs with different counter ions

Long *et al.* also discussed the synthesis of styrenic phosphonium-based ILs (Figure 5.4) possessing various alkyl substituents and counter ions. They investigated the influence of chemical structure on the thermomechanical behavior of phosphonium-containing random copolymers with *n*-butyl acrylate bearing Cl, BF_4, TFSI anions. Replacing Cl with large counterions, such as TFSI, plasticized the polymer and provided liquid-like, viscous behavior. Additionally, their corresponding scattering peaks in WAXD systematically shifted to lower *q* region, indicating an increase of ionic domain distance with the length of alkyl substituents.[67]

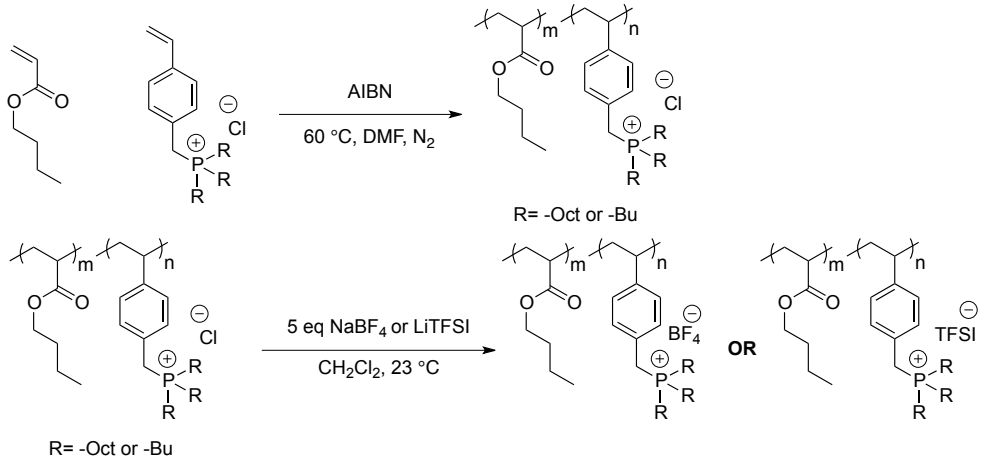

Figure 5.4 Synthesis and anion-exchange of phosphonium-containing random copolymers

Long *et al.* also performed a detailed study of structure-property relationship examining ammonium and phosphonium PILs. The ammonium and phosphonium PILs library enabled an examination of the influence of cationic site, alkyl substituent length, and counter ion on thermal properties, ionic conductivity, and morphology. The ammonium and phosphonium PILs shown in Figure 3.5 synthesized using conventional free radical polymerization with subsequent anion metathesis displayed significantly different thermal properties and ionic conductivities. Phosphonium PILs displayed higher thermal stabilities than ammonium analogs, and phosphonium PILs exhibited only a single-step degradation profile. Anion exchange to bulkier, less basic anions improved the thermal stability of all PILs and depressed the T_gs of the PILs. Phosphonium PILs displayed higher thermal stabilities and ionic conductivities than their ammonium analogs, highlighting the advantageous use of phosphonium PILs for high temperature, conductive applications.[11]

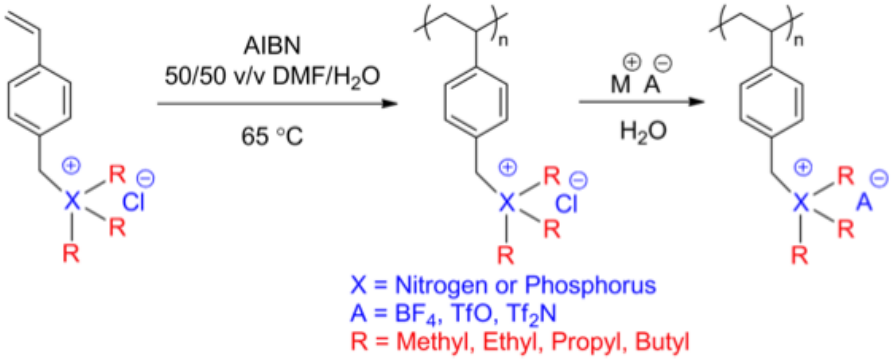

Figure 5.5 Synthesis of ammonium- and phosphonium-containing PILs using conventional free radical polymerization and anion exchange

The influence of cation structure on non-viral gene delivery was studied on free radically polymerized styrenic-based ammonium and phosphonium monomers as shown in Figure 5.6. We demonstrated the effect of varying alkyl substituent length on DNA delivery and these vectors address to a different endosomal escape mechanism other than the proton sponge effect.[68] The

polyelectrolytes were examined for their ability to bind and deliver DNA to HeLa cells using DNA binding assays, dynamic light scattering (DLS), cytotoxicity assays, luciferase expression assays, and wide-field fluorescence optical microscopy. Phosphonium vectors mediated higher gene transfection than ammonium analogs; the longer tributyl alkyl substituent lengths attached to the cationic center also imparted enhanced pDNA delivery relative to triethyl-based analogs.[69]

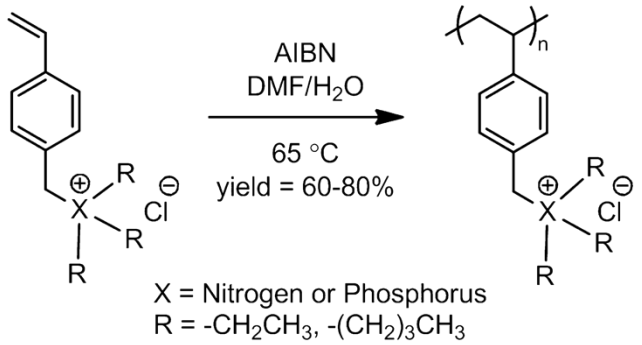

Figure 5.6 Conventional free-radical polymerization of ammonium- and phosphonium-containing styrenic homopolymers

5.4 *Phosphonium Cation-Containing Polymers as Polyelectrolytes*

Typical cationic polyelectrolytes include poly[2-(dimethylamino)ethyl methacrylate], poly(diallyldimethylammonium chloride), poly(vinyl imidazolium)s, and cationic polystyrenes. Polyelectrolytes polymers have experienced renewed interest due to their potential impact as flocculation, antimicrobials, nonviral nucleic acid delivery, and thin films.[70] Polyelectrolytes containing ammonium or phosphonium cations are typically synthesized utilizing two different pathways: a functional monomer route[71] or post-polymerization functionalization.[72] The synthesis of ammonium and phosphonium monomers typically relies on a simple nucleophilic substitution between a haloalkane and a tertiary amine or tertiary phosphine to generate the desired cationic monomer. Monomer stability tends to be a limiting factor in the suitability of a functional monomer route. Post-polymerization functionalization avoids potential monomer stability issues or polymerization hurdles, but remains disadvantageous to achieve 100%

functionalization due to steric and neighboring group effects. Tertiary amine-containing monomers are also common in the literature, and after polymerization, subsequent alkylation with a haloalkane will generate the desired ammonium polyelectrolyte. Tertiary phosphine-containing monomers are rare due to their propensity for oxidation, but 4-(diphenylphosphino)styrene is readily used in the literature.[73-75]

Endo and coworkers pioneered structure-property analysis of ammonium- and phosphonium-containing polyelectrolytes for antimicrobial applications. They directly probed the antimicrobial efficacy of ammonium- and phosphonium-containing monomers and polymers against E. coli and S. aureus.[3] Phosphonium polyelectrolytes displayed enhanced antimicrobial properties compared to ammonium analogs. Endo and coworkers also examined ammonium and phosphonium random copolymers and polymer blends. Polymer blends of ammonium and phosphonium polyelectrolytes exhibited a synergistic bactericidal effect, which resulted in improved efficacy. Interestingly, ammonium and phosphonium random copolymers failed to display any synergistic effect and higher phosphonium concentrations in the random copolymers resulted in higher antimicrobial efficacies. Kenawy and coworkers also examined crosslinked cationic materials wherein triphenylphosphonium cations displayed the highest antimicrobial efficiency. Finally, they controlled the charge density of ammonium- and phosphonium-containing copolymers, which elucidated improved antimicrobial activity for phosphonium cations and higher charge densities.[76,77]

Nitrogen-based cations such as ammonium, imidazolium, and pyridinium cations are utilized throughout the literature to electrostatically complex nucleic acids and delivery them to cells *in vitro* and *in vivo*.[78] Delivery vehicles that buffer during endosomal acidification enable polyplex escape through the proton-sponge effect, wherein endosomal acidification and

polymeric buffering capacity induces an influx of chloride anions.[79]

Our laboratories aimed to improve nucleic acid delivery under serum-containing conditions and minimize cytotoxicity through the synthesis of phosphonium-containing AB diblock copolymers as depicted in Figure 5.7. The A block consisted of either an oligo(ethylene glycol) methyl ether methacrylate (OEG) or methacryloxyphosphoryl choline (MPC) block. These represent the first phosphonium-containing AB diblock copolymers for enhanced nucleic acid delivery where the A block provides colloidal stability and the phosphonium-based B block efficiently complexes pDNA to generate core-shell nanoparticles. Cellular uptake studies demonstrated poor cellular uptake for the diblock copolymers, which led to inadequate transfection in HeLa and COS-7 cells. GFP microscopy studies in HepaRG cells showed successful transfection in a dose-dependent manner and all diblock copolymers delivered pDNA on the same order of magnitude as Jet-PEI with minimal cytotoxicity.[68]

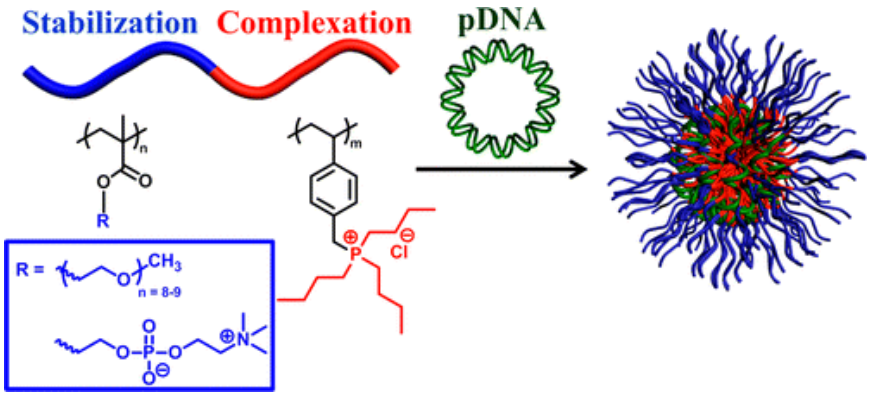

Figure 5.7 Polyplexes formed using phosphonium-containing diblock copolymers and pDNA

Our research group also synthesized phosphonium cation-containing ABA-type triblock copolymers (Figure 5.8) using nitroxide-mediated polymerization involving a difunctional initiator and a phosphonium ionic-liquid monomer. Phosphonium ion-rich domains microphase separated from amorphous rubbery matrices and evolved to various morphologies, which was

clearly shown using TEM and SAXS. The self-assembly of amphiphilic phosphonium units in block copolymer systems resulted in well-defined microphases and tuned flow behavior, which provide potential alkaline fuel cell membrane and melt processing applications.[80] Substitution of cationic phospholipid head groups from ammonium to phosphonium or arsenium in antitumor lipids decreased cytotoxicity while maintaining efficacy. Clemént *et al.* first successfully synthesized and examined ammonium-, phosphonium-, and arsenium-containing lipids for nonviral gene delivery. In these lipid-based gene delivery vectors, they found that modifying the cationic head group from ammonium to phosphonium or arsenium improved gene delivery *in vivo* and *in vitro* and decreased cytotoxicity. The phosphonium and arsenium lipid-based vectors also displayed improved solution stability.[81,82]

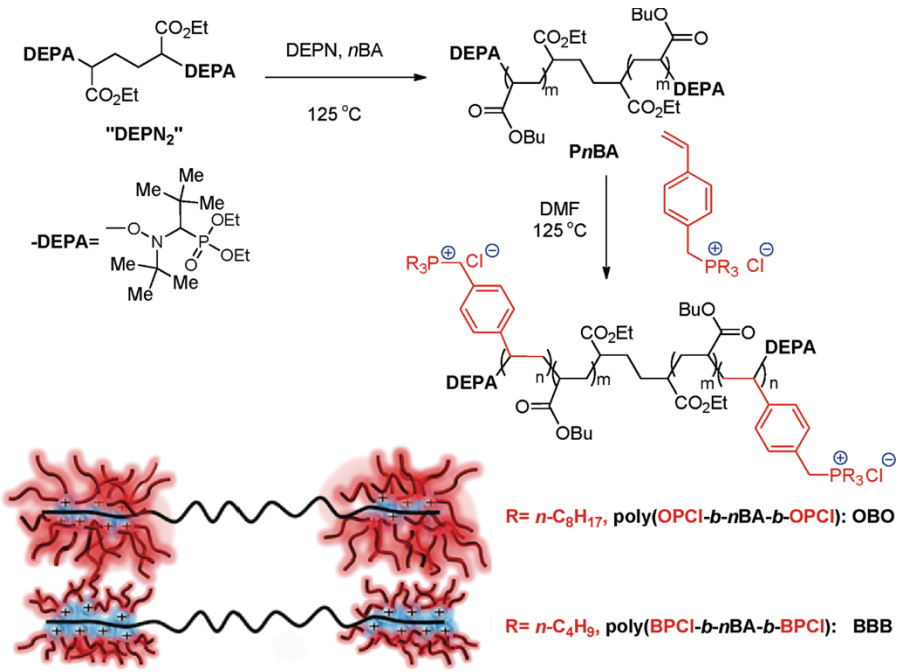

Figure 5.8 Schematic representation of synthesis of phosphonium-containing triblock copolymers

siRNA delivery is a rapidly expanding field focused on therapeutic treatment through the siRNA pathway, wherein delivered siRNA induces silencing of a specific protein through

cellular machinery.[83] Frechet *et al.* synthesized a water-soluble polyphosphonium polymer (Figure 5.9) and directly compared with its ammonium analog in terms of siRNA delivery. The triethylphosphonium polymer shows transfection efficiency up to 65% with 100% cell viability, whereas the best result obtained for the ammonium analog reached only 25% transfection with 85% cell viability. The results show that the use of positively charged phosphonium groups is a worthy choice to achieve a good balance between toxicity and transfection efficiency in gene delivery systems.[84]

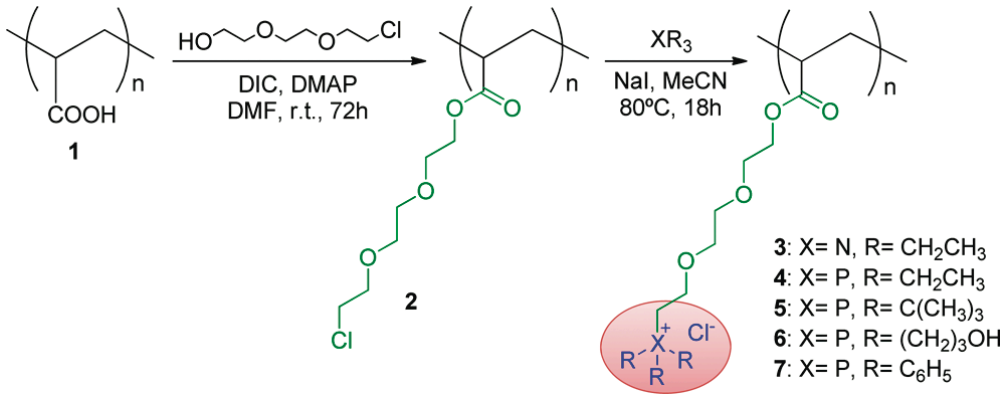

Figure 5.9 Synthesis of ammonium and phosphonium copolymers

McGrath *et al.* reported the synthesis of poly(arylene ether) main-chain phosphonium-containing ionomers for high-performance applications such as ion-exchange membranes. The phosphonium ionomers were prepared through the reduction of poly(arylene ether phosphine oxide) to phosphine/phosphine oxide copolymers with phenylsilane and subsequent quaternization of phosphines with alkyl halides as shown in Figure 5.10.[85] Novel phosphonium-containing polyurethane was synthesized using a prepolymer method shown in Figure 5.11.[86] By varying the alkyl groups and mobile counterion, it was possible to tailor the amphiphilicity of phosphonium units for self-assembly. Polymers with phosphonium units randomly distributed along the polymer main-chain are well documented for their applications for high-performance materials such as ion-exchange membranes.

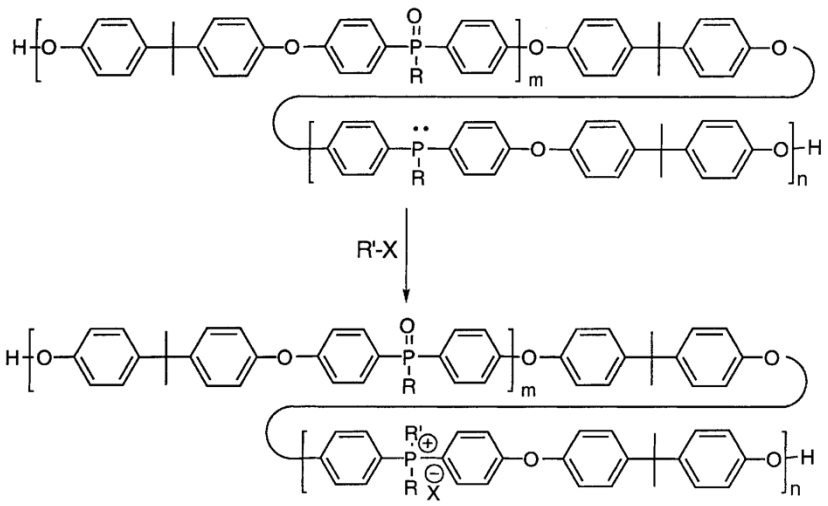

Figure 5.10 Synthesis of poly(arylene ether phosphonium salts)

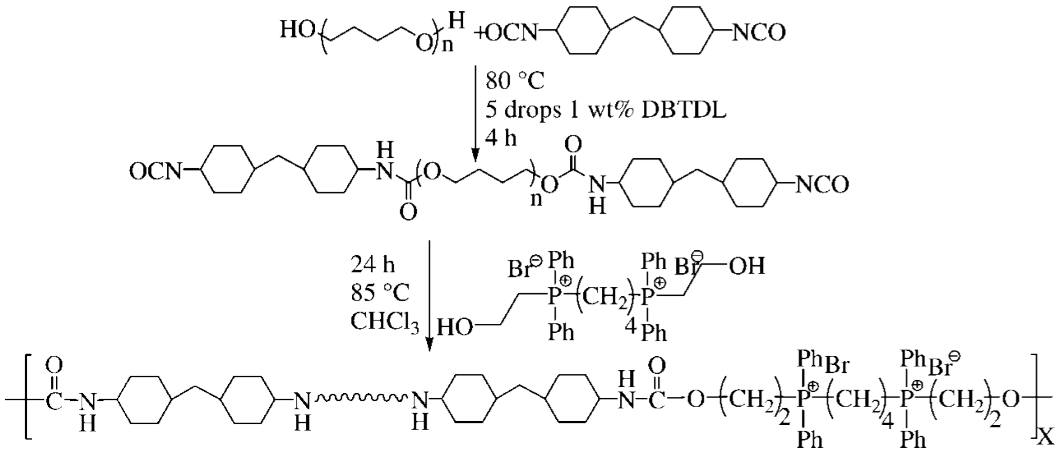

Figure 5.11 Synthesis of phosphonium-containing polyurethanes

Our group has reported the synthesis of phosphonium ionenes using Menschutkin reaction to give polymers with controlled charge density (Figure 5.12). Ionenes are a unique class of polyelectrolytes with the cationic charges located within the polymer main chain. The step-growth polymerization of bis(diphenyl)phosphinoalkanes and dibromoalkanes was used to synthesize high molecular weight phosphonium ionenes within 24 h. Control of the alkyl spacer between the phosphines or bromides generated a broad range of phosphonium ionenes with controlled alkyl spacing between cationic sites. Phosphonium ionenes demonstrated higher thermal and chemical stabilities as compared to ammonium analogs. Finally, these ionenes

demonstrated sufficient water solubility and effectively bound pDNA at a ± ratio of 1.These enable applications in non-viral nucleic acid delivery and alkaline fuel cells.

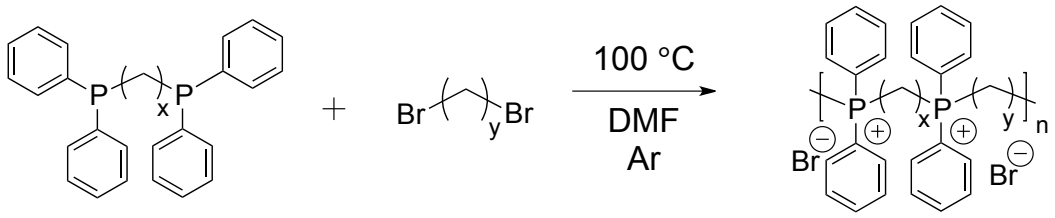

Figure 5.12 Step-growth polymerization of bis(diphenyl)phosphines and dibromides to synthesize phosphonium ionenes

5.5 *Summary*

Polyelectrolytes display a broad range of properties suitable for many applications including ionic liquids, antimicrobials and non-viral nucleic acid delivery. Due to the difference in atomic radius and electronegativity, there is a dramatic difference in the cation structure where the cationic atom is nitrogen or phosphorus. Phosphonium ILs clearly offer, in some cases, several advantages over other types of ILs, including higher thermal stability, lower viscosity, and higher stability in strongly basic or strongly reducing conditions. Phosphonium polyelectrolytes displayed enhanced thermal stability due to their resistance to Hofmann elimination. Cationic macromolecules exhibit significant antimicrobial activity and researchers found phosphonium macromolecules generally displayed higher antimicrobial efficiency. Ammonium and phosphonium macromolecules also effectively bound and delivered nucleic acids to cells; phosphonium polyelectrolytes displayed enhanced nucleic acid binding and delivery efficiency compared to ammonium analogs.

5.6 *Acknowledgements*

This material is based upon work supported in part by the U.S. Army Research Laboratory and the U.S. Army Research Office under the Army Materials Center of Excellence

Program, contract W911NF-06-2-0014. This material is based upon work supported in part by the Macromolecular Interfaces with Life Sciences (MILES) Integrative Graduate Education and Research Traineeship (IGERT) of the National Science Foundation under Agreement No. DGE-0333378. This material is also based upon work supported in part by the US Army Research Office under Grant No. W911NF-07-1-0452 Ionic Liquids in Electro-Active Devices (ILEAD) MURI.

5.7 *References*

(1) Bauer, B.; Strathmann, H.; Effenberger, F. *Desalination* **1990**, *79*, 125.
(2) Kanazawa, A.; Ikeda, T.; Endo, T. *Journal of Polymer Science Part A: Polymer Chemistry* **1993**, *31*, 1467.
(3) Kanazawa, A.; Ikeda, T.; Endo, T. *Journal of Polymer Science Part A: Polymer Chemistry* **1994**, *32*, 1997.
(4) Bradaric, C. J.; Downard, A.; Kennedy, C.; Robertson, A. J.; Zhou, Y. *Green Chemistry* **2003**, *5*, 143.
(5) Frackowiak, E.; Lota, G.; Pernak, J. *Applied physics letters* **2005**, *86*, 164104.
(6) Bondi, A. *The Journal of Physical Chemistry* **1966**, *70*, 3006.
(7) Wang, S.-W.; Liu, W.; Colby, R. H. *Chemistry of materials* **2011**, *23*, 1862.
(8) Fraser, K. J.; MacFarlane, D. R. *Australian Journal of Chemistry* **2009**, *62*, 309.
(9) Noonan, K. J.; Hugar, K. M.; Kostalik IV, H. A.; Lobkovsky, E. B.; Abruña, H. c. D.; Coates, G. W. *Journal of the American Chemical Society* **2012**, *134*, 18161.
(10) Hemp, S. T.; Zhang, M.; Tamami, M.; Long, T. E. *Polym. Chem.* **2013**, *4*, 3582.
(11) Hemp, S. T.; Zhang, M.; Allen, M. H.; Cheng, S.; Moore, R. B.; Long, T. E. *Macromolecular Chemistry and Physics* **2013**.
(12) Plechkova, N. V.; Seddon, K. R. *Chemical Society Reviews* **2008**, *37*, 123.
(13) Holbrey, J. D.; Reichert, W. M.; Reddy, R.; Rogers, R. In *ACS symposium series* 2003; Vol. 856.
(14) Earle, M. J.; Seddon, K. R. *Pure and Applied Chemistry* **2000**, *72*, 1391.
(15) Davis Jr, J. H.; Fox, P. A. *Chemical Communications* **2003**, 1209.
(16) Sheldon, R. A.; Lau, R. M.; Sorgedrager, M. J.; van Rantwijk, F.; Seddon, K. R. *Green Chemistry* **2002**, *4*, 147.
(17) Yoshizawa, M.; Xu, W.; Angell, C. A. *Journal of the American Chemical Society* **2003**, *125*, 15411.
(18) Bansal, D.; Cassel, F.; Croce, F.; Hendrickson, M.; Plichta, E.; Salomon, M. *The Journal of Physical Chemistry B* **2005**, *109*, 4492.
(19) Kim, K.; Lang, C. M.; Kohl, P. A. *Journal of The Electrochemical Society* **2005**, *152*, E56.
(20) Lee, J.; Quan, N.; Hwang, J.; Bae, J.; Kim, H.; Cho, B. W.; Kim, H.; Lee, H. *Electrochemistry communications* **2006**, *8*, 460.

(21) Lu, W.; Norris, I. D.; Mattes, B. R. *Australian Journal of Chemistry* **2005**, *58*, 263.
(22) MacFarlane, D.; Meakin, P.; Amini, N.; Forsyth, M. *Journal of physics: condensed matter* **2001**, *13*, 8257.
(23) MacFarlane, D. R.; Forsyth, M. *Advanced materials* **2001**, *13*, 957.
(24) Marwanta, E.; Mizumo, T.; Nakamura, N.; Ohno, H. *Polymer* **2005**, *46*, 3795.
(25) Kawano, R.; Watanabe, M. *Chemical Communications* **2005**, 2107.
(26) Wasserscheid, P.; Welton, T. *Ionic liquids in synthesis*; Wiley Online Library, 2008; Vol. 1.
(27) van Schalkwijk, W.; Scrosati, B. *Advances in lithium-ion batteries*; Springer, 2002.
(28) Matsumoto, H.; Sakaebe, H.; Tatsumi, K. *Journal of power sources* **2005**, *146*, 45.
(29) Papageorgiou, N.; Athanassov, Y.; Armand, M.; Bonho, P.; Pettersson, H.; Azam, A.; Grätzel, M. *Journal of The Electrochemical Society* **1996**, *143*, 3099.
(30) Wang, P.; Zakeeruddin, S. M.; Exnar, I.; Grätzel, M. *Chemical Communications* **2002**, 2972.
(31) Zakeeruddin, S. M.; Grätzel, M. *Advanced Functional Materials* **2009**, *19*, 2187.
(32) Lu, W.; Fadeev, A. G.; Qi, B.; Smela, E.; Mattes, B. R.; Ding, J.; Spinks, G. M.; Mazurkiewicz, J.; Zhou, D.; Wallace, G. G. *Science* **2002**, *297*, 983.
(33) Ding, J.; Zhou, D.; Spinks, G.; Wallace, G.; Forsyth, S.; Forsyth, M.; MacFarlane, D. *Chemistry of materials* **2003**, *15*, 2392.
(34) Zhou, D.; Spinks, G. M.; Wallace, G. G.; Tiyapiboonchaiya, C.; MacFarlane, D. R.; Forsyth, M.; Sun, J. *Electrochimica acta* **2003**, *48*, 2355.
(35) Welton, T. *Chemical reviews* **1999**, *99*, 2071.
(36) Dupont, J.; de Souza, R. F.; Suarez, P. A. *Chemical reviews* **2002**, *102*, 3667.
(37) Wasserscheid, P.; Keim, W. *Angewandte Chemie* **2000**, *39*, 3772.
(38) Mecerreyes, D. *Progress in Polymer Science* **2011**, *36*, 1629.
(39) Marcilla, R.; Sanchez‐Paniagua, M.; Lopez‐Ruiz, B.; Lopez‐Cabarcos, E.; Ochoteco, E.; Grande, H.; Mecerreyes, D. *Journal of Polymer Science Part A: Polymer Chemistry* **2006**, *44*, 3958.
(40) Gosser, L.; Knoth, W.; Parshall, G. *Journal of Molecular Catalysis* **1977**, *2*, 253.
(41) Muetterties, E.; Gerlach, D.; Kane, A.; Parshall, G.; Jesson, J. *Journal of the American Chemical Society* **1971**, *93*, 3543.
(42) Manzer, L. E.; Parshall, G. W. *Inorganic Chemistry* **1976**, *15*, 3114.
(43) Knifton, J. F. *Journal of the American Chemical Society* **1981**, *103*, 3959.
(44) Knifton, J. F.; Grigsby Jr, R. A.; Lin, J. *Organometallics* **1984**, *3*, 62.
(45) Knifton, J. In *Aspects of Homogeneous Catalysis*; Springer: 1988, p 1.
(46) Lu, J.; Yan, F.; Texter, J. *Progress in Polymer Science* **2009**, *34*, 431.
(47) Ricks-Laskoski, H. L.; Snow, A. W. *Journal of the American Chemical Society* **2006**, *128*, 12402.
(48) Bara, J. E.; Gabriel, C. J.; Hatakeyama, E. S.; Carlisle, T. K.; Lessmann, S.; Noble, R. D.; Gin, D. L. *Journal of Membrane Science* **2008**, *321*, 3.
(49) Ye, Y.; Elabd, Y. A. *Macromolecules* **2011**, *44*, 8494.
(50) Hunley, M. T.; England, J. P.; Long, T. E. *Macromolecules* **2010**, *43*, 9998.
(51) Tang, J.; Shen, Y.; Radosz, M.; Sun, W. *Industrial & Engineering Chemistry Research* **2009**, *48*, 9113.
(52) Valade, D.; Boschet, F.; Roualdès, S.; Ameduri, B. *Journal of Polymer Science Part A: Polymer Chemistry* **2009**, *47*, 2043.

(53) Huddleston, J. G.; Visser, A. E.; Reichert, W. M.; Willauer, H. D.; Broker, G. A.; Rogers, R. D. *Green Chemistry* **2001**, *3*, 156.
(54) Canal, J. P.; Ramnial, T.; Dickie, D. A.; Clyburne, J. A. *Chemical Communications* **2006**, 1809.
(55) Ramnial, T.; Taylor, S. A.; Bender, M. L.; Gorodetsky, B.; Lee, P. T.; Dickie, D. A.; McCollum, B. M.; Pye, C. C.; Walsby, C. J.; Clyburne, J. A. *The Journal of organic chemistry* **2008**, *73*, 801.
(56) YANG, X.-y.; ZHANG, J.-p.; GUO, L.; ZHAO, H.; ZHANG, Y.; CHEN, J. *Transactions of Nonferrous Metals Society of China* **2012**, *22*, 3126.
(57) Campos, K.; Vincent, T.; Bunio, P.; Trochimczuk, A.; Guibal, E. *Solvent Extraction and Ion Exchange* **2008**, *26*, 570.
(58) Tsunashima, K.; Yonekawa, F.; Sugiya, M. *Electrochemical and Solid-State Letters* **2009**, *12*, A54.
(59) Tsunashima, K.; Yonekawa, F.; Sugiya, M. *Chemistry letters* **2008**, *37*, 314.
(60) Sarda, S. R.; Jadhav, W. N.; Shete, A. S.; Dhopte, K. B.; Sadawarte, S. M.; Gadge, P. J.; Pawar, R. P. *Synthetic Communications*® **2010**, *40*, 2178.
(61) Ramnial, T.; Taylor, S. A.; Clyburne, J. A.; Walsby, C. J. *Chemical Communications* **2007**, 2066.
(62) Qiang, H.; Lili, W.; Baozhong, Z.; Quan, L. *化学进展* **2009**, *21*, 1782.
(63) Vaughan, J. W.; Dreisinger, D.; Haggins, J. *ECS Transactions* **2006**, *2*, 381.
(64) Thompson, D.; Coleman, S.; Diamond, D.; Byrne, R. *Physical Chemistry Chemical Physics* **2011**, *13*, 6156.
(65) Park, K.; Xanthos, M. *Polymer Degradation and Stability* **2009**, *94*, 834.
(66) Green, M. D.; Schreiner, C.; Long, T. E. *The Journal of Physical Chemistry A* **2011**, *115*, 13829.
(67) Cheng, S.; Zhang, M.; Wu, T.; Hemp, S. T.; Mather, B. D.; Moore, R. B.; Long, T. E. *Journal of Polymer Science Part A: Polymer Chemistry* **2012**, *50*, 166.
(68) Hemp, S. T.; Smith, A. E.; Bryson, J. M.; Allen Jr, M. H.; Long, T. E. *Biomacromolecules* **2012**, *13*, 2439.
(69) Hemp, S. T.; Allen Jr, M. H.; Green, M. D.; Long, T. E. *Biomacromolecules* **2011**, *13*, 231.
(70) Smith, A. E.; Hemp, S. T.; Allen, M. H.; Bryson, J. M.; Long, T. E. In *MOLECULAR THERAPY*; NATURE PUBLISHING GROUP 75 VARICK ST, 9TH FLR, NEW YORK, NY 10013-1917 USA: 2012; Vol. 20, p S246.
(71) Hatakeyama, E. S.; Ju, H.; Gabriel, C. J.; Lohr, J. L.; Bara, J. E.; Noble, R. D.; Freeman, B. D.; Gin, D. L. *Journal of Membrane Science* **2009**, *330*, 104.
(72) Parent, J. S.; Penciu, A.; Guillén-Castellanos, S. A.; Liskova, A.; Whitney, R. A. *Macromolecules* **2004**, *37*, 7477.
(73) Bütün, V.; Armes, S. P.; Billingham, N. C. *Macromolecules* **2001**, *34*, 1148.
(74) Choi, M. K. W.; He, H. S.; Toy, P. H. *The Journal of organic chemistry* **2003**, *68*, 9831.
(75) Guinó, M.; Hii, K. K. M. *Chemical Society Reviews* **2007**, *36*, 608.
(76) Kenawy, E. R.; Mahmoud, Y. A. G. *Macromolecular Bioscience* **2003**, *3*, 107.
(77) Kenawy, E.-R.; Abdel-Hay, F. I.; El-Magd, A. A.; Mahmoud, Y. *Reactive and Functional Polymers* **2006**, *66*, 419.
(78) Mintzer, M. A.; Simanek, E. E. *Chemical reviews* **2008**, *109*, 259.
(79) Behr, J.-P. *CHIMIA International Journal for Chemistry* **1997**, *51*, 1.

(80) Cheng, S.; Beyer, F. L.; Mather, B. D.; Moore, R. B.; Long, T. E. *Macromolecules* **2011**, *44*, 6509.
(81) Floch, V.; Loisel, S.; Guenin, E.; Hervé, A. C.; Clément, J. C.; Yaouanc, J. J.; des Abbayes, H.; Férec, C. *Journal of medicinal chemistry* **2000**, *43*, 4617.
(82) Mevel, M.; Breuzard, G.; Yaouanc, J. J.; Clément, J. C.; Lehn, P.; Pichon, C.; Jaffrès, P. A.; Midoux, P. *ChemBioChem* **2008**, *9*, 1462.
(83) Whitehead, K. A.; Langer, R.; Anderson, D. G. *Nature reviews Drug discovery* **2009**, *8*, 129.
(84) Ornelas-Megiatto, C. t.; Wich, P. R.; Fréchet, J. M. *Journal of the American Chemical Society* **2012**, *134*, 1902.
(85) Ghassemi, H.; Riley, D.; Curtis, M.; Bonaplata, E.; McGrath, J. M. **1998**.
(86) Williams, S. R.; Wang, W.; Winey, K. I.; Long, T. E. *Macromolecules* **2008**, *41*, 9072.

Chapter 6: **Diphenylphosphino Styrene-containing Homopolymers: Influence of Alkylation and Mobile Anions on Physical Properties**

Chainika Jangu[2], Alison R. Schultz[1, 2], Candace Wall[1], Alan Esker[1, 2], and Timothy E. Long[1, 2*]

[1]Department of Chemistry, [2]Macromolecules and Interfaces Institute (MII), Virginia Tech., Blacksburg, VA 24061-0212

[*]To whom correspondence should be addressed E-mail: telong@vt.edu. TEL: (540)231-2480 FAX: (540)231-8517

Keywords: Free radical polymerization, anion metathesis, phosphonium, contact angle, rheology

6.1 *Abstract*

Homopolymerization of DPPS using conventional free radical polymerization and anion metathesis leads to interesting variations in thermal and rheological properties. In this investigation, conventional free radical polymerization and anion metathesis of 4-(diphenylphosphino) styrene (DPPS) generated high molecular weight triaryl phosphine-containing copolymers. Alkylation with subsequent anion exchange to BF_4^-, TfO^-, and Tf_2N^- improved thermal stability due to the decreased basicity of the mobile counteranion. Bulkier anions also depressed the T_g of homopolymers, with the counteranion Tf_2N^- displaying the lowest T_g at 100 °C. Longer alkyl chain lengths led to decreased thermal stability and lower T_g values. Rheological characterization facilitated the generation of time-temperature-superposition (TTS) pseudomaster curves. Subsequent TTS analysis of phosphonium-containing polystyrenes generated using frequency sweeps at various temperatures revealed two relaxation modes. The first transition corresponds to long-range segmental motion, while the second transition at the higher temperature represents the onset of viscous flow. Contact angle measurements confirmed that the wetting properties of phosphonium-containing polystyrenes varied as a function of

counteranion. This investigation of these novel polymers provides a fundamental understanding of the counteranion effects on thermal, viscoelastic, and wetting properties of phosphonium-containing polystyrenes.

6.2 *Introduction*

Ammonium and phosphonium ion-containing polymers are gaining interest due to their unique physical properties and potential applications in advanced technologies. In particular, the unique properties of phosphonium-containing macromolecules include their enhanced thermal stability, potential biocompatibility, and improved conductivity over ammonium analogs.[1-6] Their increasingly widespread use in biological applications reinforces the importance of phosphorus-containing macromolecules.[7-12] A broader commercial library of phosphines enables the design and synthesis of low-viscosity, high-conductivity phosphonium ILs.[13,14] Phosphonium-containing macromolecules also show improvements in thermal and chemical stability in alkaline environments as compared to their ammonium analogs, which could render them useful in energy generation and storage devices.[2,4,15-19] Therefore, a number of phosphonium-based materials are suitable for use as anion-exchange membranes in alkaline fuel cells, as well as for use in high-temperature aerospace applications.[13,18-24]

Ammonium ionic liquids are less suitable in comparison to phosphonium analogs for many industrial applications due to their poor thermal stability. Ammonium ionic liquids typically degrade through a reverse nucleophilic substitution mechanism or a Hoffman elimination mechanism, wherein the counterion abstracts a β-hydrogen in the first step.[25] According to previous reports, ammonium- and phosphonium-containing macromolecules typically exhibit distinct physical properties due to the minor structural change from cationic nitrogen to cationic phosphorus. For example, Long *et al.* detailed structure-property

relationships in ammonium and phosphonium polymerized ionic liquids (PILs), demonstrating their improved thermal stability, ion conductivity, and other properties in comparison to ammonium analogs.[4,26,27] Kenawy *et al.* and Endo *et al.* documented improved antimicrobial activity for phosphonium-containing polyelectrolytes as compared to ammonium-containing polyelectrolytes.[28-30] Moreover, Long and coworkers recently confirmed improved nucleic acid binding and cellular delivery using phosphonium-containing vehicles.[9-12] In this investigation, we synthesized phosphonium-containing random copolymers with *n*-butyl acrylate bearing BF_4^-, Cl^-, and Tf_2N^- as counteranions in order to demonstrate the influence of chemical structure on thermomechanical behavior.[3,27,31]

As documented in the literature, ammonium and phosphonium polystyrenes rely solely on the attachment of the ammonium or phosphonium cation at the *para*-benzylic position of the monomer. While benzylic substitution affords facile synthesis, it also results in thermal and chemical instability due to the acidity of benzylic hydrogens.[25] 4-(diphenylphosphino)styrene (DPPS) is a commercially available monomer with no $-CH_2$ group at the *para* position, eliminating the possibility of the Hoffman elimination mechanism. Conventional free radical polymerization of DPPS successfully generates phosphine-containing polystyrene homopolymers, wherein the phosphino group is directly at the *para*-position. The alkylation of the phosphine group with a broad range of alkyl halides creates a library of phosphonium-containing polystyrenes. Counterion exchange with bulky fluorinated counteranions further broadens the library of polyelectrolytes, leading to enhanced thermal stabilities, lower glass transition temperatures, and tunable wetting behavior.

6.3 *Experimental*

6.3.1 Materials.

Iodomethane (CH_3I, >99.0%), lithium bis(trifluoromethane sulfonyl) imide ($LiTf_2N$, 99%), sodium tetrafluoroboric acid ($NaBF_4$), sodium trifluoromethanesulfonate (NaTfO), all bromoalkanes, 4-(diphenylphosphino) styrene (DPPS, 95%) were purchased from Sigma Aldrich and used as received. 2,2'-azobisisobutyronitrile (AIBN) was recrystallized from ethanol. All solvents were obtained from Spectrum Chemicals and used as received.

6.3.2 Analytical Methods.

^1H NMR spectroscopy (Varian Inova, 400 MHz) determined monomer and polymer composition. Thermogravimetric analysis (TGA) of polymers was performed on a TA Instruments thermogravimetric analyzer (TGAQ50) with a heating rate of 10 °C/min to 600 °C under a N_2 atmosphere after holding the sample at 100 °C for 60 min. Thermal transitions were determined using a TA Instruments Q1000 differential scanning calorimeter (DSC) with a heating rate of 10 °C/min utilizing a heat/cool/heat cycle. T_g was determined from the second heat cycle. Polymer molecular weight was measured using both aqueous and THF size exclusion chromatography (SEC). The aqueous solvent was a combination of water/methanol/acetic acid (54/23/23 v/v/v %) with 0.1 M sodium acetate to minimize the aggregation of charged polymer systems. A Waters 2414 differential refractive index detector was used to determine the *dn/dc* for absolute molecular weight determination. Dynamic light scattering (DLS) (Malvern Zetasizer NanoZS) confirmed the absence of polymer aggregations in the mobile phase before injection into the SEC columns.

Melt rheology using a TA Instruments DHR-2 strain-controlled rheometer with disposable 8 mm diameter aluminum parallel plate geometry directly probed viscoelastic

properties of the copolymers and generated time-temperature-superposition (TTS) curves. All measurements were performed at a constant nominal strain value within the linear viscoelastic regime, determined with strain sweeps (0.004 to 2.0 % oscillatory strain) at 1 Hz. The samples were subjected to temperature step, frequency sweep experiments at 10 °C/step. The time-temperature superposition method was utilized to investigate the frequency dependence over a wide frequency range. The resulting storage and loss moduli for each polymer were shifted using the TA Instruments TRIOS software package and horizontal shift factors (a_T). Master curves based on shifting and overlapping both storage and loss moduli generated horizontal shift factors, which were fitted to the WLF equation using TRIOS.

Contact angle measurements were performed with a FTA 200 contact angle analyzer (First Ten Angstroms, Portsmouth, VA) using a sessile drop technique. The polymer coatings on Teflon were placed on an adjustable platform and ≈ 5 μL of Milli-Q water (Millipore Gradient A10) was placed on the surface using a 3 mL 22 gauge syringe. For contact angle analysis, a single frame movie was taken using a video CCD camera. Afterwards, the contact angle was measured using a mathematical expression and fitting it to the shape of the drop, and then calculating the slope of the tangent to the drop at the liquid-solid-vapor interface (FTA Operator's and Installation Manuals, revision 2.0, May 30, 1997). Four replicates were performed to determine the average contact angle.

6.3.3 Synthesis of Charged Poly((4-diphenylphosphino)styrene).

In a representative synthesis, DPPS and DMF were added to a round-bottomed flask. To this reaction mixture, AIBN (0.1 mol%) was added and dissolved for 5 min. The flask was sealed and sparged with argon for 30 min to remove oxygen. The polymerization was then conducted at 65 °C for 24 h. The polymer solution was dialyzed against THF for 3 d. Poly(DPPS) was

recovered after rotovaping THF and impurities, dried at 40 °C under reduced pressure (0.5 mm Hg) for 24 h. The resulting polymer and methyl iodide were dissolved in THF. The solution was purged with argon and reacted at 23 °C for 24 h. The product was precipitated in ether. The polymer solution was dialyzed in water for 3 d and then lyophilized to obtain a white powder. Poly(DPPS-I) and $LiTf_2N$ were then dissolved in separate solutions of water (50 mL each). The solutions were mixed together, immediately forming a white precipitate, and stirred at 23 °C for 48 h. The complete synthetic scheme is shown in Scheme 6.1. The polymers were characterized using ^1H NMR spectroscopy and silver nitrate test to ensure complete anion exchange.

Scheme 6.1 Conventional free radical polymerization generated phosphonium polystyrenes for subsequent alkylation and anion exchange

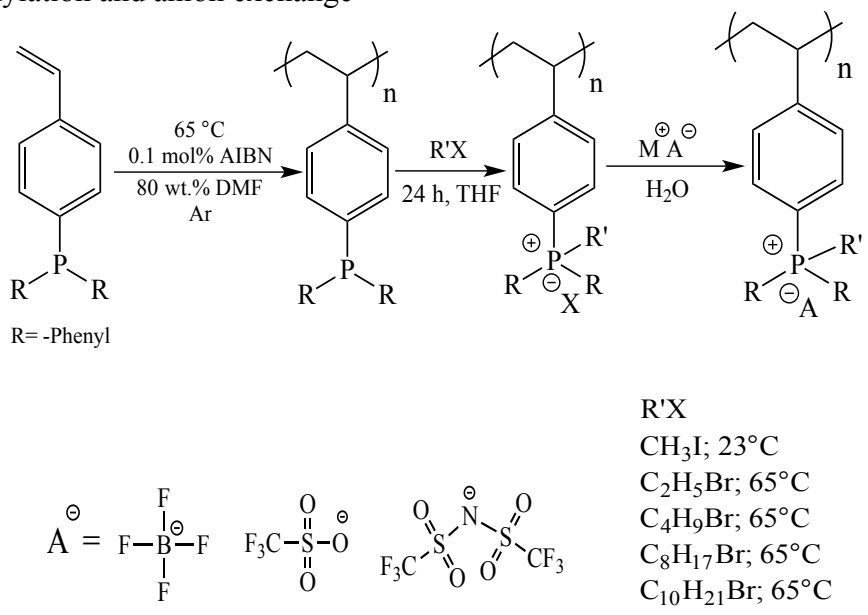

6.4 *Results and Discussions*

Conventional free-radical polymerization generated a library of phosphonium-containing polystyrenes, thus enabling the investigation of the influence of counteranions and alkyl substituent lengths on physical and rheological properties. Scheme 6.1 depicts the synthetic pathway for generating phosphonium-containing polystyrene wherein the phosphonium group

was located at the *para*-position. Anion metathesis with an excess of desired salt enabled facile anion exchange.

SEC analysis proved challenging for the highly charged macromolecules due to aggregation, column interaction, and poor solubility. In order to minimize polymer aggregation and column interaction, we utilized aqueous SEC with a ternary mobile phase mixture of water/methanol/acetic acid (54/23/23 v/v/v%) and 0.1 M sodium acetate salt**.** Table 1 **(**found in Supplementary Information) summarizes the molecular weight analysis of the phosphonium-containing polystyrenes. All polymers displayed high molecular weight ranging from 108-173 kg/mol with molecular weight distribution (PDI), as expected from conventional free radical polymerization.

The absence of β-hydrogens in DPPS, alkyl substituent lengths, and counteranion properties influenced the thermal stability and thermal transitions of the macromolecules. Figure 6.1 shows charged poly(DPPS) (without hydrogen at the β-carbon) featuring a one-step degradation, as compared to poly(triphenyl phosphonium chloride) (poly(TPP-Cl)) with a two-step degradation due to the presence of β-hydrogens at the benzylic position. Phosphonium-containing polystyrene with I^- as the counteranion displays thermal stability above 400 °C. Poly(DPPS) fails to undergo Hoffman elimination due to the absence of β-hydrogens. Ammonium-containing macromolecules exhibit poor thermal stability, and the literature suggests two possible degradation pathways: Hoffman elimination and reverse Menschutkin (nucleophilic) degradation. Hoffman elimination occurs when the counteranion abstracts a hydrogen from the β-carbon causing subsequent elimination.

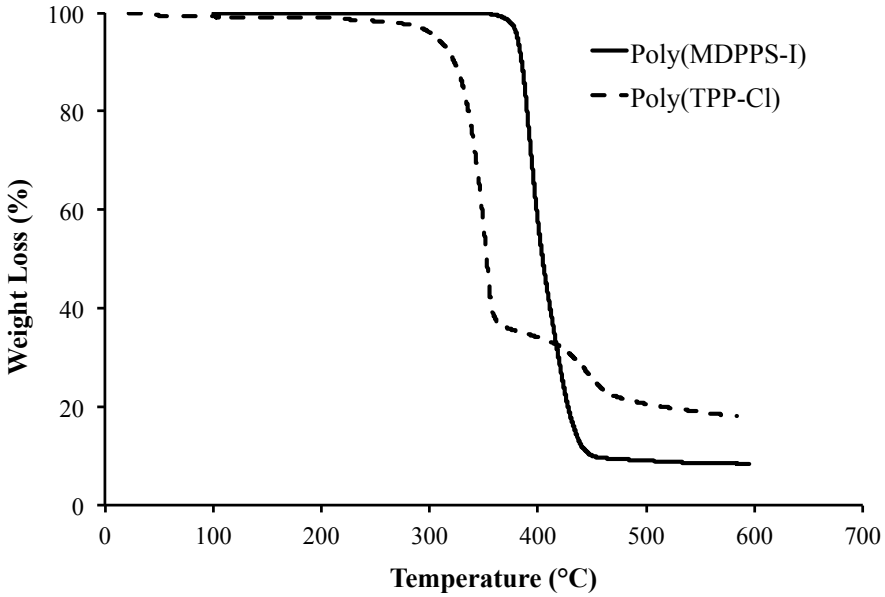

Figure 6.1 Thermogravimetric analysis (TGA) of poly(MDPPS-I) and poly(TPP-Cl) performed at 10 °C/min under N_2 atmosphere. The comparison of charged poly(DPPS) without hydrogen from the β-carbon shows one-step degradation, as compared to poly(triphenyl phosphonium chloride), poly(TPP-Cl) with two-steps degradation because of the presence of β-hydrogen at the benzylic position.

TGA traces shown in Figure 6.2 indicate that thermal stability is dependent upon the basicity of the associated mobile counteranion. Prior reports detail similar results for polymerized ionic liquids (PILs), where a decrease in basicity increases thermal stability.[27]

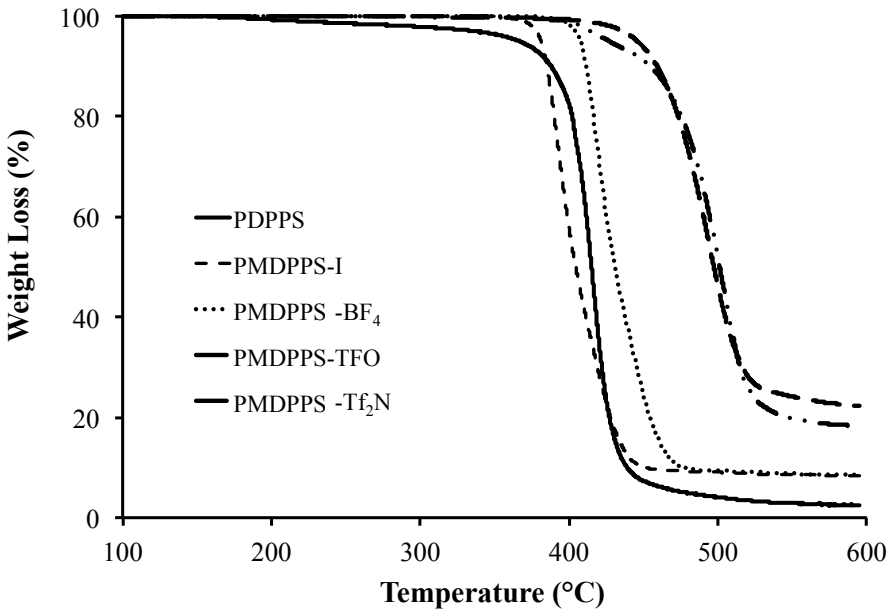

Figure 6.2 Thermogravimetric analysis (TGA) of phosphonium-containing polystyrenes with four different counteranions: $Tf_2N^- > TfO^- > BF_4^- > I^-$. Anion-exchange to bulkier, less basic anions improved the overall thermal stability of phosphine polystyrenes

Figure 6.3 summarizes thermal stability trends with different counterions and alkyl substituent lengths. As the basicity of the counteranion decreased, thermal stability increased in the following order: $Tf_2N^- > TfO^- > BF_4^- > X^-$. As shown in this figure, an increase in alkyl substituent length resulted in decreased thermal stability-presumably due to the degradation of the alkylene substituents. These findings agree with the previously published literature.[4,26,27]

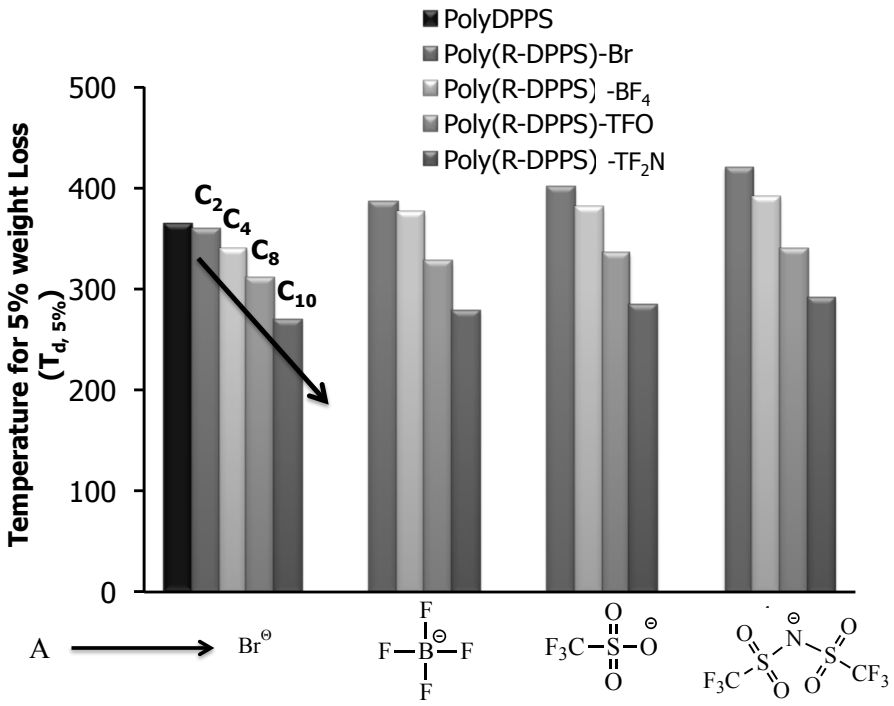

Figure 6.3 Summary of degradation temperature ($T_{d,\,5\%}$) for phosphonium-containing polystyrenes with various alkyl substituent lengths labeled as C_2, C_4, C_8, C_{10} (R= C_2H_5, C_4H_9, C_8H_{17}, and $C_{10}H_{21}$) and counteranions (Br^-, BF_4^-, TfO^-, Tf_2N^-)

It is also important to note that polymer glass transition temperature (T_g) was highly dependent on the size of the associated counteranion, in that it decreased as the size of the counteranion increased. Specifically, these counteranion size effects can be ordered as follows: $Tf_2N^- > TfO^- > BF_4^- > I^-$.Figure 6.4 summarizes T_g values for all homopolymers of DPPS and charged poly(DPPS) with different alkyl chain lengths and various counteranion sizes. These trends are also in agreement with prior literature reports.[4,26,27] Moreover, Long *et al.* showed that the choice of counteranion in phosphonium ionenes had a significant impact on thermal, viscoelastic and conductive properties.[27] In an earlier study, Hunley *et al.* confirmed that the size of the counteranion influenced the T_g of protonated poly(dimethylaminoethyl methacrylate).[32]

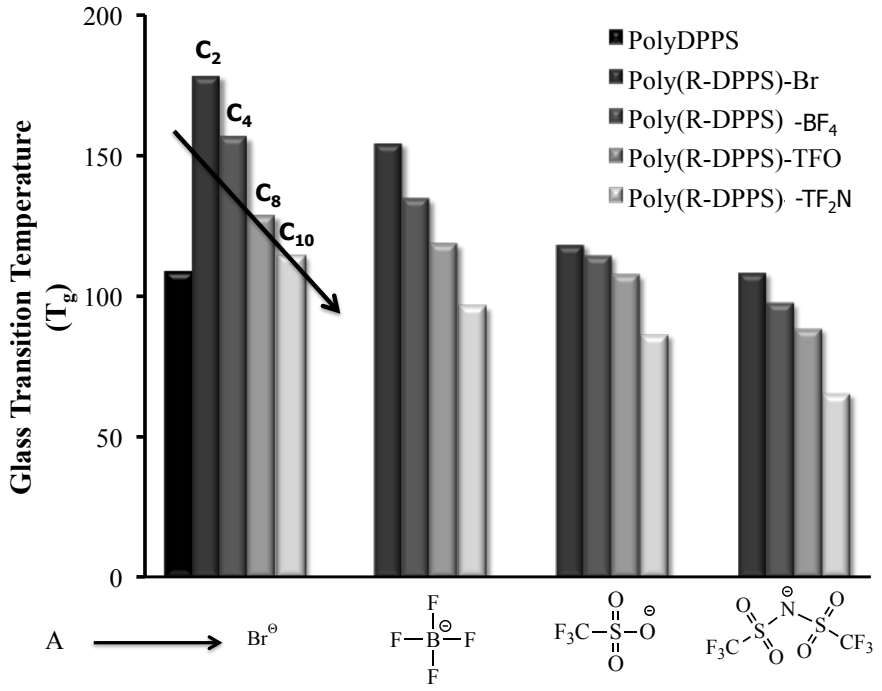

Figure 6.4 Glass transition temperature (T_g) measurements for phosphonium-containing polystyrenes with various alkyl substituent lengths as C_2, C_4, C_8, C_{10} (R= CH_3, C_2H_5, C_4H_9, C_8H_{17}, and $C_{10}H_{21}$) and counteranions (I^-, Br^-, BF_4^-, TfO^-, Tf_2N^-)

The choice of counterion also influenced contact angle measurements; specifically, as the hydrophobicity of the counterion increased, contact angle values increased to a maximum value of 95°. The contact angle and hydrophobicity relationship increased in the following order: Tf_2N^- >TfO^->BF_4^->Br^- as shown in Figure 6.5. The counteranion selection of a substrate influences contact angle measurements and the degree of wetting.

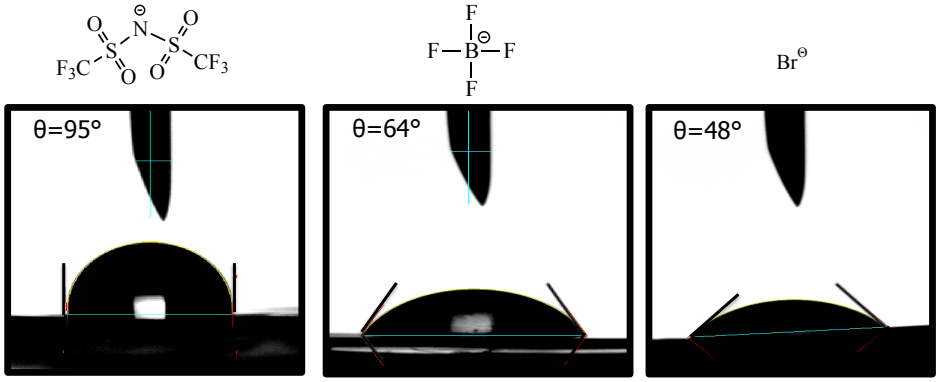

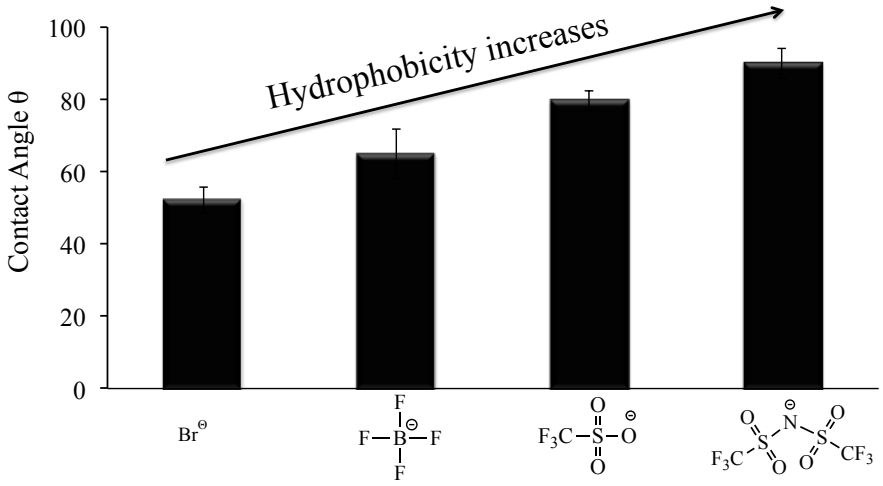

Figure 6.5 Contact angle measurements of poly(DPPS) with ethyl as alkyl substituent and varying counteranion indicates degree of wetting, directly impacted by counteranion selection of substrate

The Long group also explored the influence of the choice of counteranion on the viscoelasticity of phosphonium-containing polystyrenes at constant charge density within the linear viscoelastic region using time-temperature-superposition (TTS). Due to the relatively high T_g or low thermal stability of polyelectrolytes, which impedes the development of a suitable thermal window, it has been difficult to examine their melt characteristics; indeed, literature reports in this area are scare.[26] The high thermal stability (>300 °C) and relatively low T_g values of phosphonium-containing polystyrenes enabled dynamic melt rheological studies to examine the impact of counteranion on flow characteristics. Frequency sweeps carried out at 10 °C temperature steps were employed to examine the broad viscoelastic region for time-temperature-superposition (TTS).Figure 6.6 displays pseudomaster curves for both the storage (G') and loss moduli (G") for all anion-exchange, phosphonium-based polystyrenes. The shift factors obtained from the WLF curve produced TTS master curves using a reference temperature (T_r) of 100 °C. The superimposition of experimental data confirmed acceptable overlap across an angular frequency range of 8-10 decades for both G' and G" master curves for all anion-exchange

phosphonium-containing polystyrenes. The storage and loss moduli pseudomaster curves showed two distinct relaxation phenomena: (a) the onset of long-range segmental motion of polymer chains at shorter time-scales, and (b) a second relaxation mode at higher time scales prior to the onset of terminal flow. As described in published literature from Nakamura and co-workers, as well as Long *et al.*, this relaxation mode corresponds to electrostatic interactions in polyelectrolytes.[4,26,27] In conclusion, our experimental data verified that anion metathesis of phosphonium-based polystyrenes has a profound impact on the viscoelastic behavior of the resulting materials.

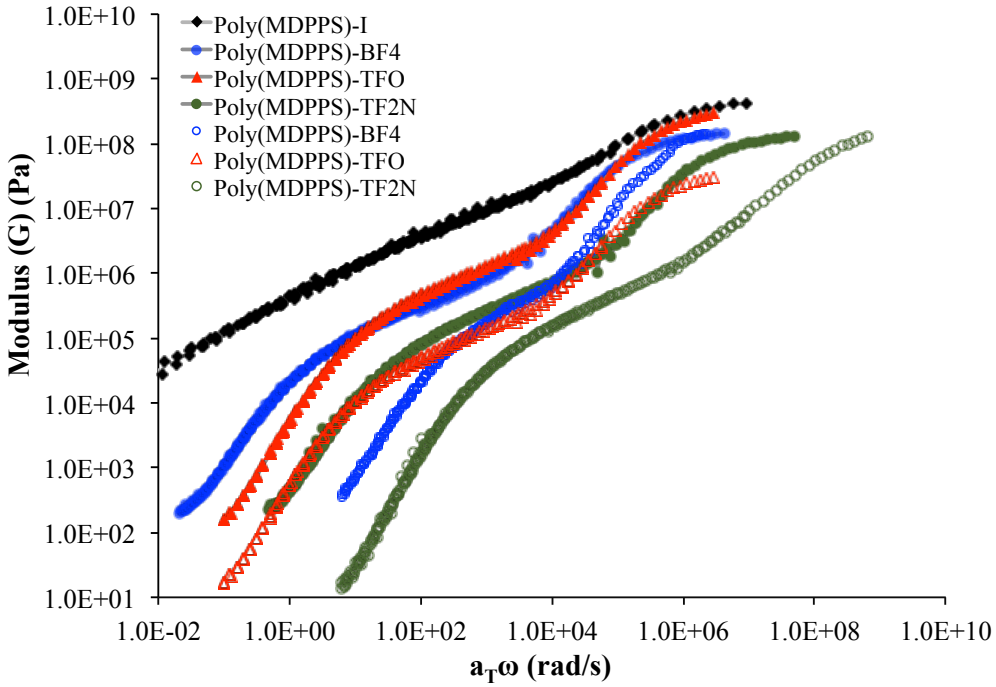

Figure 6.6 Time-temperature superposition (TTS) of phosphonium-containing polystyrenes generated using frequency sweeps at various temperatures. Filled dots correspond to storage modulus (G') and empty dots correspond to loss modulus (G'')

Shift factors (a_T) *versus* temperature for all phosphonium-based polystyrenes obey the Williams-Landel-Ferry equation:

$$log(a_T) = \frac{-C_1(T-T_r)}{C_2+(T-T_r)}$$

C_1 and C_2 are polymer-specific constants and T_r corresponds to the reference temperature chosen. C_1 and C_2 depend on the T_r utilized in the TTS; therefore, they convert to C_1^g and C_2^g values based on T_g according to the following equations to enable direct comparisons to other C_1^g and C_2^g values in the literature:

$$C_1^g = \frac{C_1 C_2}{C_2 + (T_g - T_r)}$$

$$C_2^g = C_2(T_g - T_r)$$

Table 6.1 summarizes C_1^g and C_2^g values for phosphine polystyrenes. WLF constants also provide information regarding polymer fractional free volume at T_g (f_g) and the thermal expansion coefficient (α_f) according to the following equations:

$$f_g = \frac{B}{2.303 C_1^g}$$

$$\alpha_f = \frac{B}{2.303 C_1^g C_2^g}$$

Doolittle and others typically assume a value of unity for the B constant. Interestingly, f_g depended significantly on the size of the counteranion, with larger counteranions Tf_2N^- with higher f_g's.

Table 6.1 WLF fitting parameters for poly(DPPS) with different counteranions

Polymer	**C_1**	**C_2 (K)**	**C_1^g**	**C_2^g (K)**	**f_g**	**E_a (kJ/mol)**
Poly(MDPPS)-I	10.22	68.65	3.08	57.7	0.021	258
Poly(MDPPS)-BF_4	6.7	56.6	8.90	42.6	0.029	167
Poly(MDPPS)-TfO	4.5	34	2.83	54.0	0.028	176
Poly(MPPS)-Tf_2N	5.43	32	2.38	73.0	0.045	165

6.5 *Conclusions*

Homopolymerization of DPPS using conventional free radical polymerization and anion metathesis resulted in interesting variations in thermal and rheological properties. Specifically, anion exchange to bulkier, less basic, anions improved thermal stability and depressed the T_g values of all phosphonium-containing polystyrenes. Rheological characterization facilitated the generation of time-temperature superposition (TTS) pseudomaster curves. TTS of phosphonium polystyrenes generated using frequency sweeps at various temperatures revealed two relaxation modes: long-range segmental motion and electrostatic interactions. The choice of counteranion also dramatically impacted contact angle measurements in that contact angle increased with the increasing hydrophobicity of the counteranion. Ultimately, alkyl substituent length and choice of counteranion strongly influenced the thermal stability and thermal transition temperature of these polymers. Specifically, these phosphonium-containing polystyrenes displayed high thermal stability, as well as tunable viscoelastic properties and wetting behaviors, all of which are essential for high-temperature applications.

Supplementary Information

Table 6.2 Molecular weight analysis of phosphonium polystyrenes with various alkyl substituent lengths (R= CH_3, C_2H_5, C_4H_9, C_8H_{17}, and $C_{10}H_{21}$) and counter anions (I^-, Br^-, BF_4^-, TfO^-, Tf_2N^-)

Polymer	M_w (kg/mol)	PDI
Poly(DPPS)	108	1.75
Poly(MDPPS)-I	115	1.80
Poly(MDPPS)-BF_4	108	1.75
Poly(MDPPS)-TfO	110	1.65
Poly(MDPPS)-Tf_2N	124	1.67
Poly(EDPPS)-Br	125	1.70
Poly(EDPPS)-BF_4	123	1.56
Poly(EDPPS)-TfO	138	1.85
Poly(EDPPS)-Tf_2N	118	1.75
Poly(ODPPS)-Br	144	1.67
Poly(ODPPS)-BF_4	134	1.52
Poly(ODPPS)-TfO	126	1.91
Poly(ODPPS)-Tf_2N	173	1.86
Poly(DDPPS)-Br	145	1.78
Poly(DDPPS)-BF_4	156	1.67
Poly(DDPPS)-TfO	129	1.46
Poly(DDPPS)-Tf_2N	166	1.59

SEC: 35 °C, 1 mL/min, MALLS, 54/23/23 (v/v/v %) $H_2O/CH_3OH/CH_3COOH$, 0.1M NaOAc; Poly(DPPS): 35°C, THF, MALLS

6.6 *References*

(1) Papageorgiou, N.; Athanassov, Y.; Armand, M.; Bonho, P.; Pettersson, H.; Azam, A.; Grätzel, M. *Journal of The Electrochemical Society* **1996**, *143*, 3099.
(2) Jangu, C.; Long, T. E. *Polymer* **2014**.
(3) Cheng, S.; Zhang, M.; Wu, T.; Hemp, S. T.; Mather, B. D.; Moore, R. B.; Long, T. E. *Journal of Polymer Science Part A: Polymer Chemistry* **2012**, *50*, 166.
(4) Hemp, S. T.; Zhang, M.; Allen, M. H.; Cheng, S.; Moore, R. B.; Long, T. E. *Macromolecular Chemistry and Physics* **2013**.
(5) Wasserscheid, P.; Welton, T. *Ionic liquids in synthesis*; Wiley Online Library, 2008; Vol. 1.
(6) Wasserscheid, P.; Keim, W. *Angewandte Chemie* **2000**, *39*, 3772.
(7) Bunyard, W. C.; Long, T. E.; Smith, A. E.; Cheng, S.; Hemp, S. T.; Google Patents: 2013.
(8) Bertin, A. **2013**.
(9) Smith, A. E.; Hemp, S. T.; Allen, M. H.; Bryson, J. M.; Long, T. E. In *MOLECULAR THERAPY*; NATURE PUBLISHING GROUP 75 VARICK ST, 9TH FLR, NEW YORK, NY 10013-1917 USA: 2012; Vol. 20, p S246.
(10) Hemp, S. T.; Smith, A. E.; Bryson, J. M.; Allen Jr, M. H.; Long, T. E. *Biomacromolecules* **2012**, *13*, 2439.
(11) HEMP, S.; ALLEN, M.; SMITH, A.; LONG, T.; WO Patent 2,012,174,543: 2012.
(12) Hemp, S. T.; Allen Jr, M. H.; Green, M. D.; Long, T. E. *Biomacromolecules* **2011**, *13*, 231.

(13) Bradaric, C. J.; Downard, A.; Kennedy, C.; Robertson, A. J.; Zhou, Y. *Green Chemistry* **2003**, *5*, 143.
(14) Frackowiak, E.; Lota, G.; Pernak, J. *Applied physics letters* **2005**, *86*, 164104.
(15) Tsunashima, K.; Yonekawa, F.; Sugiya, M. *Electrochemical and Solid-State Letters* **2009**, *12*, A54.
(16) Tsunashima, K.; Yonekawa, F.; Sugiya, M. *Chemistry letters* **2008**, *37*, 314.
(17) Valade, D.; Boschet, F.; Roualdès, S.; Ameduri, B. *Journal of Polymer Science Part A: Polymer Chemistry* **2009**, *47*, 2043.
(18) van Schalkwijk, W.; Scrosati, B. *Advances in lithium-ion batteries*; Springer, 2002.
(19) Bauer, B.; Strathmann, H.; Effenberger, F. *Desalination* **1990**, *79*, 125.
(20) Dupont, J.; de Souza, R. F.; Suarez, P. A. *Chemical reviews* **2002**, *102*, 3667.
(21) Lu, W.; Fadeev, A. G.; Qi, B.; Smela, E.; Mattes, B. R.; Ding, J.; Spinks, G. M.; Mazurkiewicz, J.; Zhou, D.; Wallace, G. G. *Science* **2002**, *297*, 983.
(22) Wang, P.; Zakeeruddin, S. M.; Exnar, I.; Grätzel, M. *Chemical Communications* **2002**, 2972.
(23) Knifton, J. In *Aspects of Homogeneous Catalysis*; Springer: 1988, p 1.
(24) Sheldon, R. A.; Lau, R. M.; Sorgedrager, M. J.; van Rantwijk, F.; Seddon, K. R. *Green Chemistry* **2002**, *4*, 147.
(25) Ye, Y.; Elabd, Y. A. *Macromolecules* **2011**, *44*, 8494.
(26) Hemp, S. T.; Zhang, M.; Tamami, M.; Long, T. E. *Polym. Chem.* **2013**, *4*, 3582.
(27) Abdulahad, A. I.; Jangu, C.; Hemp, S. T.; Long, T. E. In *Macromolecular Symposia* 2014; Vol. 342, p 56.
(28) Earle, M. J.; Seddon, K. R. *Pure and Applied Chemistry* **2000**, *72*, 1391.
(29) Kenawy, E.-R.; Abdel-Hay, F. I.; El-Magd, A. A.; Mahmoud, Y. *Reactive and Functional Polymers* **2006**, *66*, 419.
(30) Kenawy, E. R.; Mahmoud, Y. A. G. *Macromolecular Bioscience* **2003**, *3*, 107.
(31) Cheng, S.; Beyer, F. L.; Mather, B. D.; Moore, R. B.; Long, T. E. *Macromolecules* **2011**, *44*, 6509.
(32) Hunley, M. T.; England, J. P.; Long, T. E. *Macromolecules* **2010**, *43*, 9998.

Chapter 7: **Switchable Pressure-Sensitive-Adhesives Based on Salt Polyelectrolyte Complexes**

Chainika Jangu[1], Shantanu R. Ranade[2], David A. Dillard[3] and Timothy E. Long[1]

[1]*Department of Chemistry, Macromolecules and Interfaces Institute,*
[2]*Macromolecular Science & Engineering, Macromolecules and Interfaces Institute,*
[3]*Biomedical Engineering and Mechanics, Macromolecules and Interfaces Institute,*
Virginia Tech, Blacksburg, VA 24061-0212

[*]To whom correspondence should be addressed E-mail: telong@vt.edu. TEL: (540) 231-2480

FAX: (540)231-8517

Keywords: Ion-containing polymers, salt-responsive behavior, pressure sensitive adhesive

7.1 *Abstract*

Ion-containing polymers typically display salt-responsive behavior, wherein ionic salts trigger a change in solubility or polymer conformation. In this investigation, conventional free radical polymerization enabled the synthesis of salt-responsive copolymers exhibiting specific rheological characteristics, adhesive properties, cell viability, and DNA binding. The judicious choice of monomers and copolymers facilitated the targeted design of salt-responsive adhesives. An oligo(ethylene glycol) methyl ether methacrylate (OEGMEMA) served as a hydrophilic monomer, while a random copolymer of di(ethylene glycol) methyl ether methacrylate (DEGMEMA) and [2-(methacryloyloxy)ethyl]trimethylammonium chloride (TMAEMA) enabled salt-responsive behavior. Additionally, the rubbery plateaus of storage and loss moduli master curves were tunable such that the copolymers followed the Dahlquist criterion, thus behaving as a tacky polymer system. Adhesive-performance measurements obtained from peel testing and probe tack testing confirmed the suitability of these polymers for incorporation in

pressure-sensitive adhesives. It must also be noted that at less than 5% TMAEMA, the adhesives were soluble in water, but in the presence of salt they remained insoluble.

7.2 *Introduction*

Stimuli-responsive macromolecules represent an evolving field of research wherein the polymer properties change in response to environmental or applied stimuli.[1-3] Such stimuli include temperature, pH, salt incorporation, light, the application of voltage, or analyte concentration level.[4-7] Stimuli-responsive materials find a broad range of applications as drug delivery vehicles, sensors, hydrogels, adhesives, and smart surfaces.[1,8-12] However, there are limited reports on the application of stimuli-responsive materials for underwater bonding applications due to the challenges associated with wettability.[13-17] The numerous potential applications for effective underwater adhesives, i.e., stopping underwater leaks and in medicine in the treatment of wet living tissue, warrants their further investigation.

Stewart and coworkers used complex coacervates for underwater adhesive applications. Coacervates are concentrated, water-immiscible, aqueous fluids formed by the condensation and phase-separation of oppositely charged, water-miscible polyelectrolytes. The chemical and physical properties of coacervates make them ideal candidates for incorporation in waterborne underwater adhesives.[18] Stewart *et al.* also utilized synthetic poly(methacrylate) copolymers in waterborne adhesives, resulting in complex coacervate adhesives that qualitatively replicate many features of the adhesives secreted by aquatic organisms. Bond strength and other material properties also improve with the incorporation of additional polymer networks into adhesive coacervates.[19,18,20-23] Long *et al.* used reversible addition-fragmentation transfer (RAFT) polymerization to prepare stimuli-responsive hydrogels based on ABA block copolymers. The

novel block copolymers displayed tunable salt- and temperature-responsive gel points, making them suitable for use in localized drug delivery systems for adhesives and as hydrogels.[24]

The adhesion performance of soft materials such as hydrogels is dependent upon viscoelastic properties. The efficiency of the bonding step, as well as the separation resistance during the debonding step, are key determinants for adhesive performance. It is well established in the literature that storage modulus G' below 10^5 Pa at 0.01 sec^{-1} favors efficient wetting.[25] The debonding strength is related to the cohesive strength and energy dissipation during debonding, which is typically represented by loss modulus (G'') measured for appropriate debonding factors. With the application of appropriate time scales, higher energy dissipation leads to higher debonding strength. Research has shown that peel testing and probe tack testing are the best routes for measuring adhesion performance.[25-30]

This study investigated the design of a salt-responsive smart adhesive with potential applications in wet conditions. Free radical copolymerization enabled the synthesis of poly(DEGMEMA-*co*-TMAEMA-*co*-OEGMEMA) copolymers for use in adhesives will have a statistical distribution of monomers containing ionic groups and/or permanently hydrophilic groups. Upon exposure to salt, the ionic groups become polyelectrolytes, which trigger a change in solubility or polymer conformation.[31] This work demonstrates the potential of synthetic stimuli-responsive materials for use in switchable pressure sensitive adhesives based on salt-polyelectrolyte coacervates.

7.3 *Experimental*

Materials. Oligo(ethylene glycol) methyl ether methacrylate (OEGMEMA) (485 g/mol) and di(ethylene glycol) methyl ether methacrylate (DEGMEMA) (95%) were obtained from Sigma-Aldrich and the inhibitor was removed using a neutral alumina column prior to the

polymerization. [2-(methacryloyloxy)ethyl]trimethylammonium chloride (80 wt% in water) (TMAEMA) was purchased from Sigma-Aldrich and used as received. α,α′-Azobis-(isobutyronitrile) (AIBN, Fluka, 99%) was recrystallized from ethanol. All solvents were obtained from Fischer Scientific and used as received.

Analytical Methods. ^{1}H Nuclear magnetic resonance (NMR) spectroscopy was performed on a Varian INOVA operating at 400 MHz at 23 °C in deuterated chloroform. Aqueous size-exclusion chromatography (SEC) was performed using a Waters 1515 Isocratic HPLC Pump and Waters 717 plus Autosampler with Waters 2414 Refractive Index and Wyatt MiniDAWN MALLS detectors at a flow rate of 0.8 mL/min. Two Waters Ultrahydrogel Linear columns and one Waters Ultrahydrogel 250 column were utilized. The aqueous solvent was composed of 54/23/23 $H_2O/CH_3OH/CH_3COOH$ with 0.1 M sodium acetate. Prior to SEC analysis, all polymers were analyzed by dynamic light scattering (DLS) to confirm that aggregation did not occur in the aqueous SEC mobile phase. Absolute molecular weights were obtained via a multi-angle laser light scattering (MALLS) detector after offline determination of dn/dc using a Wyatt Opti-lab T-rEX refractometer (λ = 658 nm). Differential scattering calorimetry (DSC) was performed under a nitrogen flush of 50 mL/min at a heating rate of 10 °C/min on a TA instruments Q1000 DSC, which was calibrated using indium (mp =156.60 °C) and zinc (mp = 419.47 °C) standards. Glass transition temperature (T_g) was measured as the midpoint of the transition in the second heating ramp. Thermogravimetric analysis (TGA) was performed using a TA Instruments TGA Q50 at a 10 °C/min heating ramp.

Rheology. Melt rheology using a TA Instruments DHR-2 strain-controlled rheometer with disposable 8 mm diameter aluminum parallel plate geometry directly probed viscoelastic properties of the copolymers and generated time-temperature superposition (TTSP) curves. All

measurements were performed at a constant nominal strain value within the linear viscoelastic regime, determined with strain sweeps (0.004 to 4.0 % oscillatory strain at 1Hz). The samples were subjected to temperature step, frequency sweep experiments at 10 °C/step. The time-temperature superposition (TTSP) method was utilized to investigate frequency dependence over a wide frequency range. The resulting storage and loss moduli for each polymer were shifted using the TA Instruments TRIOS software package and horizontal shift factors (a_T). Master curves based on shifting and overlapping both storage and loss moduli generated horizontal shift factors, which were fitted to the WLF equation using the TRIOS software.

Peel Testing. The samples to be peel testing were prepared from solution casting of the polymer solutions in methanol on a Mylar® backing using a drawdown blade. Coated films were dried at room temperature for 10 mins, and then oven dried at 40 °C for an additional 10 mins. The surface of the stainless steel substrates was carefully cleaned with acetone prior to peel testing. Strips of 2.54 cm width were cut from the polymer coated Mylar®. Upon application of the specimen onto a stainless steel substrate, a 2 kg roller was passed over the sample two times under its own weight before each peel test. After storage under controlled temperature (25 °C) and humidity (50% R.H.) conditions, the specimen was peeled from a stainless steel substrate at an angle of 90 °C and at a speed of 12 in/mm using ChemInstruments Adhesion/Release Tester AR-1000. The peel test and related conditions were performed according to ASTM D3300 standards and each experiment was done in triplicate, where the reported results represent an average of the three samples.

Probe Tack. Probe tack tests were carried out using highly polished precision stainless steel compression plattens in INSTRON 5500R. The copolymer specimen was kept on the bottom probe and the top probe was brought in contact with the specimen at 0.1 mm/s until the

load cell detected a load corresponding to a desired stress. At this point, the probe was kept at a fixed displacement for a desired dwell time. Following the dwell time the probe was pulled away at 0.3 mm/s.

Cell Viability and DNA Binding Assays. Cell viability and polymer cytotoxicity were both determined using the 3-[4,5-dimethylthiazol-2-yl]2,5-diphenyltetrazolium bromide (MTT, Sigma Aldrich) colorimetric assay as previously reported. 100 μL of a 50,000 HeLa cells/mL solution was added to each well of a 96-well plate. The cells were incubated for 24 h at 37 °C with 5 % CO_2. Each well was then aspirated and rinsed with phosphate buffered saline (pH 7.4) prior to application of polymer solutions. The polymer solutions, which were prepared containing varying amounts of polymer and Dulbecco's modified eagle medium (DMEM) to obtain a range of polymer concentrations between 0 and 200 μg/μL, were applied and the cells were incubated for 24 h. After incubation, the polymer solutions were removed and the cells were rinsed with 100 μL of phosphate buffered saline. 100 μL of a 0.5 mg/mL MTT solution in DMEM was added to each well and the cells were incubated for 4 h. The MTT solution was removed using suction, after which 100 μL of DMSO was added to dissolve the formazan product. A BioTek Synergy H1 Hybrid Multi-Mode microplate reader was utilized to measure the resulting solutions absorbance at 570 nm. Cell viabilities were compared to the control wells that contained no polymer to determine the cytotoxicity of the polymers.

For DNA binding assays, each copolymer was initially dissolved at 1 mg/mL in nuclease-free water. Gel shift assays were performed using gWiz-Luc plasmid DNA (0.2 μL, 1 μg/μL in dH_2O, Aldevron). The plasmid DNA was then complexed with each random copolymer by introducing a pre-determined amount of polymer solution into the plasmid DNA solution to obtain appropriate N/P ratios in a total volume of 28 μL of dH_2O. The N/P ratio is defined as the

ratio of total cationic nitrogen groups contributed by the synthetic polymer to the total number of anionic phosphates contributed by the plasmid DNA. The resulting solutions were incubated for 30 min to allow polyelectrolyte complex formation between the plasmid DNA and the cationic copolymer. After incubation, 7 μL of dye-free loading buffer (30 wt% glycerol in 1X tris-acetate-EDTA buffer) was added. 20 μL of each solution was added into a 1 wt% agarose gel stained with SYBR Green I (Sigma Aldrich) and the gel was metered at 70 V for 30 min. A MultiDoc-it Digital Imaging System (UVP) was used to image the gels and examine DNA complexation.

Synthesis of Poly(DEGMEMA-*co*-TMAEMA). All polymers were synthesized via free radical polymerization according to the following procedures. To a 100 mL round-bottomed flask equipped with a stir bar, 1.16 g (0.0056 mol) of TMAEMA and 20.0 g of DEGMEMA (0.1063 mol) were added. To dissolve the monomers, 85 mL of DMF was added. To this reaction mixture, 92.30 mg (0.562 mmol) AIBN was added and dissolved for several minutes. The flask was then sealed and sparged with argon for 30 min to remove oxygen. The free radical polymerization was then conducted at 65 °C for 24 h. The resulting polymer solution was dialyzed against distilled H_2O for 3 d to remove monomer and DMF, lyophilized and stored at room temperature. The composition and removal of solvent was determined using ^{1}H NMR spectroscopy. The synthetic route is shown in Scheme 7.1.

Scheme 7.1 Synthesis of poly(DEGMEMA-*co*-TMAEMA) using free radical copolymerization

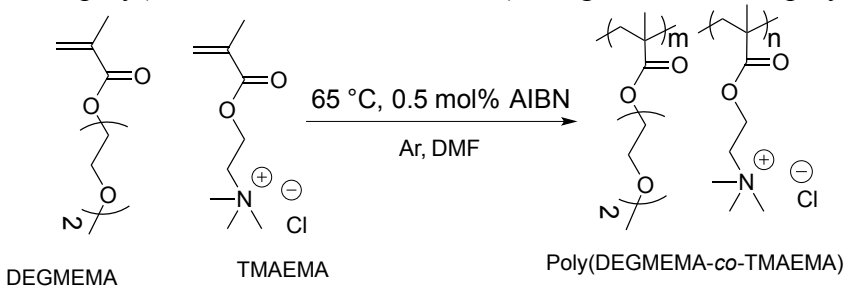

Synthesis of Poly(DEGMEMA-*co*-TMAEMA-*co*-OEGMEMA). DEGMEMA, TMAEMA, and OEGMEMA with different compositions of TMAEMA were prepared using solution free radical copolymerization in DMF with AIBN as the initiator. A round-bottomed flask was charged with DEGMEMA, TMAEMA, OEGMEMA (1 mol%), AIBN (0.5 mol%), DMF (20 wt.%). The reaction mixture was then sparged with argon for 30 min. The reaction mixture was stirred at 65 ºC for 24 h. The solution was dialyzed against methanol for 3 d to remove monomer and DMF and then to rotovaped to obtain a copolymer. ^{1}H NMR confirmed full removal of the solvent. Scheme 7.2 shows the synthetic route for the solution free radical copolymerization.

Scheme 7.2 Synthesis of poly(DEGMEMA-*co*-TMAEMA-*co*-OEGMEMA) using free radical copolymerization

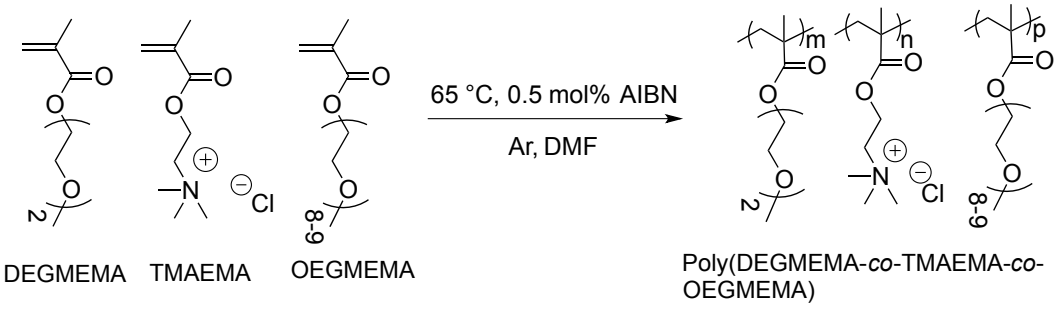

7.4 *Results and Discussions*

By tailoring the properties of copolymers via appropriate monomer choice and varying the monomer composition and charge incorporation, the Long group was able to design salt-responsive copolymers for use in adhesive films. Conventional free radical copolymerization readily enabled the generation of a series of random copolymers using three specific monomers: OEGMEMA, DEGMEMA, and TMAEMA (Scheme 7.1 and Scheme 7.2). OEGMEMA and DEGMEMA are hydrophilic monomers with pendant ethylene-oxide units, which when incorporated into random copolymers, lead to low T_g values and a reduction in modulus.[10]

According to Dobrynin et al., charged polymers display an extended conformation in solution due to electrostatic repulsion in the polymer backbone, which is universally known as the polyelectrolyte effect. The addition of salt to the solution effectively screens the electrostatic repulsion in the polymer backbone, allowing the polymer to adopt a random coil in solution.[31] The charged monomer, TMAEMA, which contains a cationic group, is capable of displaying salt-responsive behavior, wherein salt triggers a change in solubility or polymer conformation.

All of the random copolymers utilized in this study displayed high molecular weights with molecular weight distributions in the range one would anticipate from typical conventional free radical copolymerization (Table 7.1). The molar feed ratios of TMAEMA and DEGMEMA were varied to examine the impact of monomer incorporation. However, accurately determining TMAEMA incorporation using ^{1}H NMR spectroscopy proved difficult due to the low TMAEMA feed in the copolymerization. The composition of all the reported random copolymers corresponded to the monomer feed ratio. As shown in Table 7.1, when we increased the incorporation of TMAEMA, the T_g of the copolymers increased, which can be attributed to enhanced physical crosslinking that results from electrostatic interactions between ionic sites. In contrast, the addition of OEGMEMA to the copolymer of DEGMEMA and TMAEMA reduced T_g by ~ 30℃ due to an increase in free volume from pendant ethylene-oxide units in the OEGMEMA.

Table 7.1 Thermal transitions and molecular weight analysis of salt-responsive copolymers for various compositions

Polymer	M_n (g/mol)[a]	PDI[a]	T_g(℃)[b]	$T_{d,5\%}$(℃)[c]
Poly(DEGMEMA)	131,000	2.2	-30	265
Poly(1%TMAEMA-*co*-DEGMEMA)	145,000	2.1	-25	249
Poly(3%TMAEMA-*co*-DEGMEMA)	95,000	2.2	-20	251
Poly(5%TMAEMA-*co*-DEGMEMA)	141,000	2.1	-17	262
Poly(1%TMAEMA-*co*-DEGMEMA-*co*-OEGMEMA)	368,000	2.7	-62	242
Poly(3%TMAEMA-*co*-DEGMEMA-*co*-OEGMEMA)	262,000	2.3	-58	250
Poly(5%TMAEMA-*co*-DEGMEMA-*co*-OEGMEMA)	328,000	2.4	-52	244

The rheological characterization of each random copolymer generated master curves using time-temperature-superposition (TTS). It is also noteworthy that there were no vertical shifts apparent during the construction of the master curves. Moreover, each random copolymer displayed similar molecular weights; therefore, the rheological properties were comparable. As shown in Figure 7.1 and Figure 7.2, a higher level of TMAEMA increased overall modulus and the breadth of the glass transition, presumably due to physical crosslinks from electrostatic interactions that restricted chain mobility. Dahlquist's criterion empirically correlates the tackiness of a polymer with modulus at 1 Hz frequency. In order for an adhesive to be tacky, the modulus should typically be below 1 MPa to exhibit good tack characteristics. Rheological analysis of the TMAEMA and DEGMEMA random copolymers indicated that storage modulus (G') at 1 Hz followed Dahlquist criterion for tack, as illustrated in Figure 7.2. On the addition of OEGMEMA, the modulus values at 1 Hz dropped further still, but remained within a range to satisfy the Dahlquist criterion (Figure 7.2).

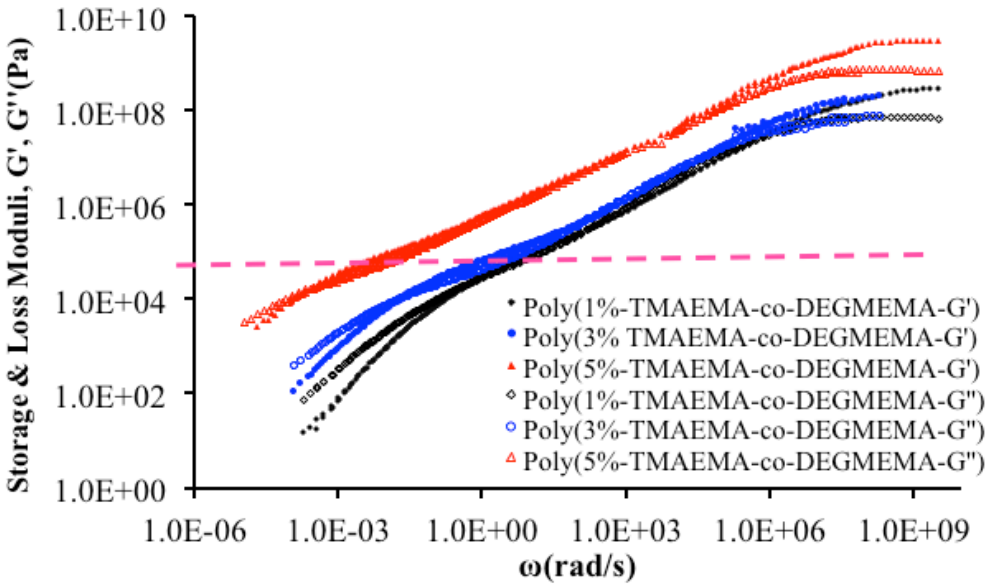

Figure 7.1 Storage and loss moduli (G'& G'') master curves obtained for random copolymers of DEGMEMA and TMAEMA. Poly(DEGMEMA-*co*-TMAEMA) meets Dahlquist criterion (Dotted horizontal line) at 30 °C. G changes with mol% of charged monomer, TMAEMA providing tunable mechanical properties.

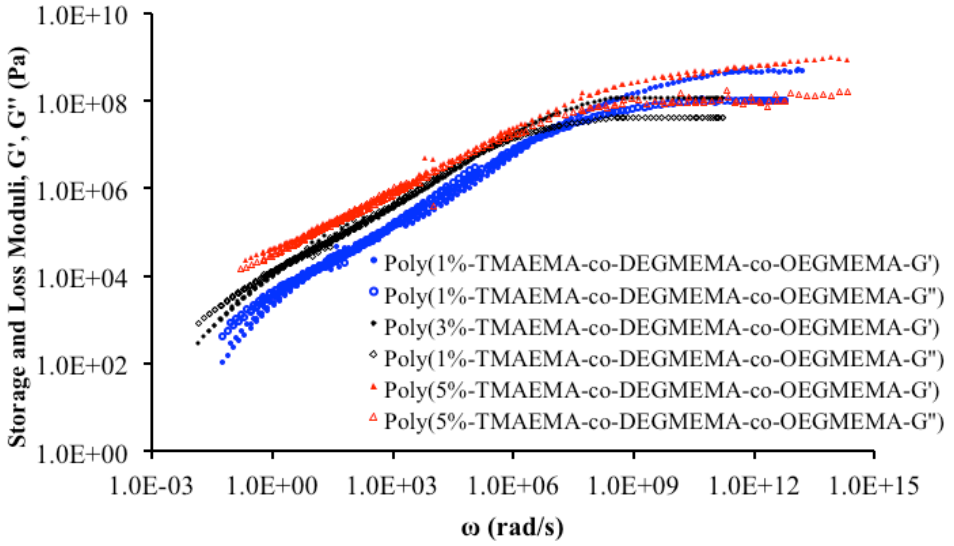

Figure 7.2 Storage and loss moduli (G'& G'') master curves of random copolymers of DEGMEMA, TMAEMA, and OEGMEMA. Dotted horizontal line is where Dahlquist criterion lies.

Even with the addition of salt (NaCl) at a concentration of 0.1 wt.%, the copolymer continued to satisfy the Dahlquist criterion. The random copolymer used for salt incorporation

contained 3 mol% of TMAEMA. Increasing the salt concentration to 1 wt.% increased the overall modulus of the copolymer.

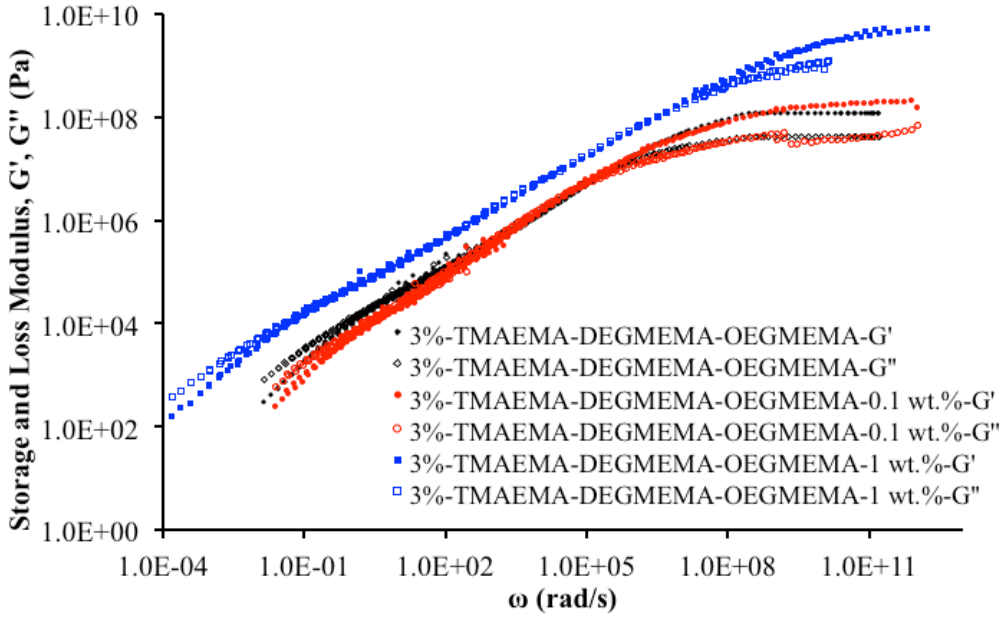

Figure 7.3 Storage and loss moduli master curves of random copolymers of DEGMEMA, TMA and OEGMEMA. These copolymers have different incorporations of TMA at reference temperature of 30 °C.

Shift factors (a_T) *versus* temperature for all copolymers obeyed the Williams-Landel-Ferry (WLF) equation, which follows:

$$log(a_T) = \frac{-C_1(T - T_r)}{C_2 + (T - T_r)} \quad (1)$$

C_1 and C_2 are polymer-specific constants and T_r corresponds to the reference temperature chosen. C_1 and C_2 constants depend on the T_r utilized in the TTS; therefore, they convert to C_1^g and C_2^g values based on T_g using the following equations to enable direct comparisons to other C_1^g and C_2^g values in the literature:

$$C_1^g = \frac{C_1 C_2}{C_2 + (T_g - T_r)} \quad (2)$$

$$C_2^g = C_2 + (T_g - T_r) \quad (3)$$

Table 7.2 summarizes C_1^g and C_2^g values for the copolymers. WLF constants provided information regarding polymer fractional free volume at T_g (f_g) and using the following equation:

$$f_g = \frac{B}{2.303 C_1^g} \quad (4)$$

Doolittle and other researchers typically assume a value of unity for the B constant. In our investigation, there was an increase in free volume with the incorporation of OEGMEMA. This finding provides another important parameter for tuning the modulus of the copolymer at relevant temperatures and frequencies.

Table 7.2 WLF parameters, fractional free volumes, thermal expansion coefficients, and flow activation energies of random copolymers of DEGMEMA and TMAEMA as well as DEGMEMA, TMAEMA and OEGMEMA

Polymer	**T_g (°C)**	**C_1**	**C_2**	**C_{1g}**	**C_{2g}**	**f_g**	**E_a (kJ/mol)**
Poly(1%TMAEMA-*co*-DEGMEMA)	-25	11.3	182.1	16.3	127.1	0.027	91
Poly(3%TMAEMA-*co*-DEGMEMA)	-20	8.5	78.4	23.5	28.4	0.020	98
Poly(5%TMAEMA-*co*-DEGMEMA)	-17	6.7	77.1	17.2	30.1	0.012	122
Poly(1%TMAEMA-*co*-DEGMEMA-*co*-OEGMEMA)	-58	6.3	143.9	16.3	55.9	0.027	71
Poly(3%TMAEMA-*co*-DEGMEMA-*co*-OEGMEMA)	-61	10.4	171.3	22.3	80.3	0.025	69
Poly(5%TMAEMA-*co*-DEGMEMA-*co*-OEGMEMA)	-62	16.8	175.5	35.3	83.5	0.019	100
Poly(3%TMAEMA-*co*-DEGMEMA-*co*-OEGMEMA)-0.1 wt.% NaCl	-	11.5	201.2	13.6	171.2	0.032	73

This study's peel test results are based on ASTM-D3300 standard 90°, as shown in Figure 7.4. For random copolymers without OEGMEMA, the failure mode between the steel substrate

and the copolymer was determined to be interfacial. Upon incorporation of OEGMEMA, the failure mode changed to cohesive failure within the adhesive films, as shown in Figure 7.5. In general, peel strength decreased with increasing concentrations of TMAEMA. It is also important to note that increasing the salt concentration from 0.1 to 1 wt.% did not result in any significant changes in peel strength.

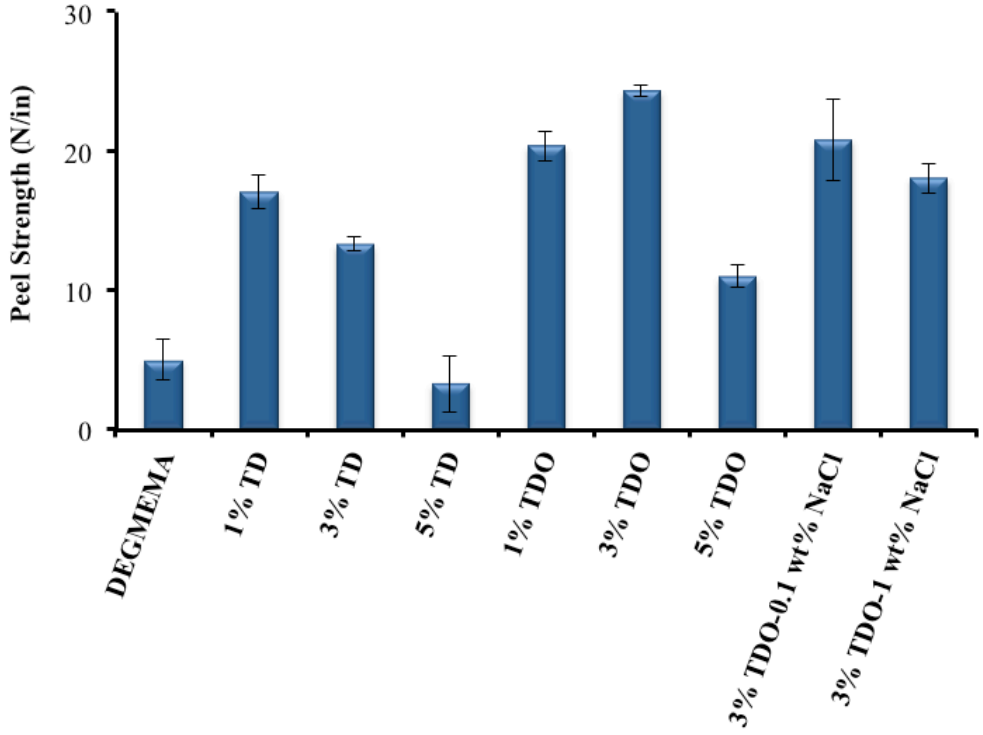

Figure 7.4 Peel strength of random copolymers of TMAEMA and DEGMEMA (TD) and copolymers of TMAEMA, DEGMEMA and OEGMEMA (TDP) with and without salt. An ASTM-D3300 standard 90° peel testing method was adopted

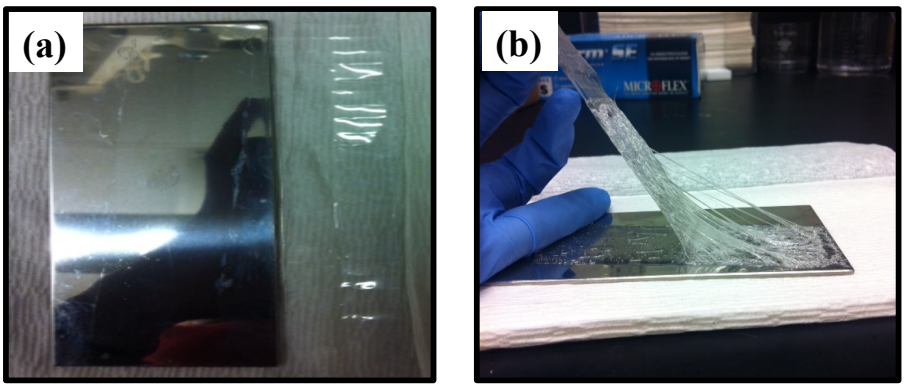

Figure 7.5 Representative failure mode observed in (a) poly(DEGMEMA-*co*-TMAEMA) and (b) poly(DEGMEMA-*co*-TMAEMA-*co*-OEGMEMA)

Figure 7.6 shows probe tack test loads for the copolymers (TMAEMA, DEGMEMA and OEGMEMA (TDO)) and random copolymers (TMAEMA and DEGMEMA (TD)) with and without salt; results were obtained after the probe had moved away from the specimen after a prescribed dwell time of 5 min. In the case of the poly(DEGMEMA-*co*-TMAEMA) copolymers (TD), the peak load increased with increasing salt concentration. This trend corresponds with trends observed during rheological analysis, where the 5% TD copolymer displayed higher modulus values compared to the 1% and 3% TD copolymers. Figure 7.6 also shows that peak load decreased significantly upon incorporation of the OEGMEMA monomer for a given TMAEMA content. Again, this finding parallels rheological data, in that the OEGMEMA-containing copolymers exhibited somewhat smaller modulus values. Amongst OEGMEMA-containing polymers, the 3 mol% TDP showed the highest value for peak load during probe tack tests.

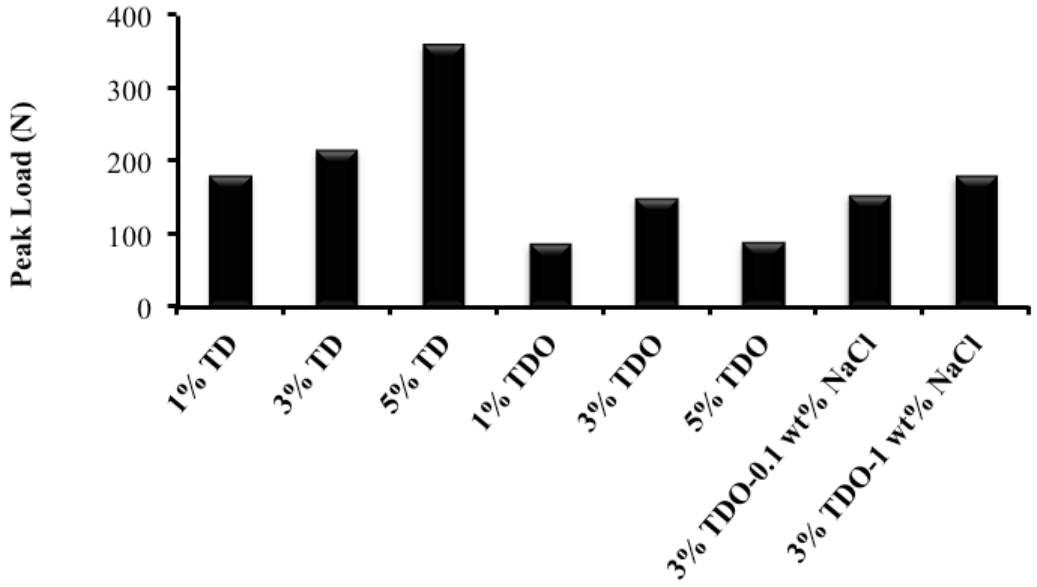

Figure 7.6 Probe tack test of random copolymers of TMAEMA and DEGMEMA (TD) and copolymers of TMAEMA, DEGMEMA and OEGMEMA (TDO) with and without salt. Peak load decreases significantly upon incorporation of the OEGMEMA monomer

It is also important to note the interesting solubility behavior of the copolymers upon incorporation of NaCl. Although these adhesives were soluble in water at less than 5% incorporation of TMAEMA, with addition of NaCl they become water-insoluble. **Figure 7.7** shows a steel panel coated with poly(DEGMEMA-*co*-TMAEMA-*co*-OEGMEMA), which disengaged from the substrate after several minutes in water. In comparison, the copolymer with 0.1 wt.% of NaCl remained intact in water for 5 h.

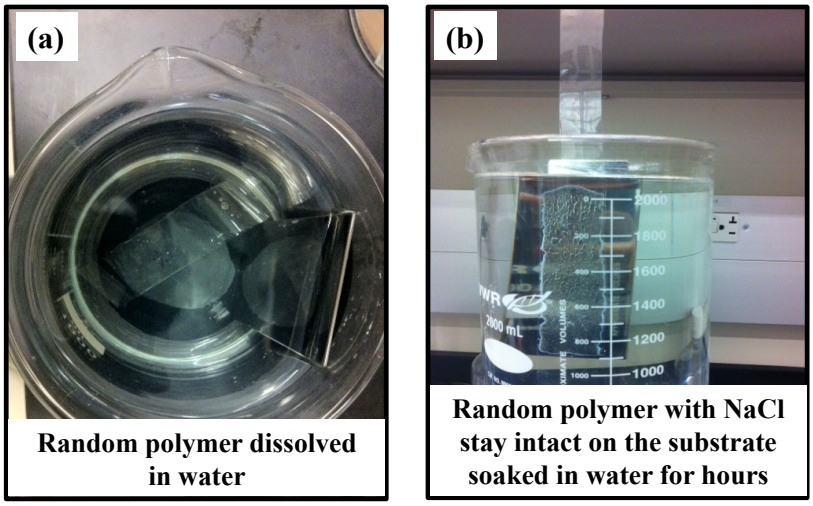

Figure 7.7 (a) Poly((DEGMEMA-*co*-TMAEMA-*co*-OEGMEMA) dissolves in water when left in a beaker filled with water (b) Poly((DEGMEMA-*co*-TMAEMA-*co*-OEGMEMA) with salt is water-insoluble and stays intact for 5 h.

7.5 *Conclusions*

This report details the synthesis of stimuli-responsive random copolymers exhibiting salt-responsive behaviors, wherein the incorporation of salt triggered a change in solubility or polymer conformation. Three different methacrylate monomers were used to tune the composition of the copolymers for application as salt-responsive adhesives. Specifically, an OEGMEMA served as a hydrophilic monomer while a random copolymer of DEGMEMA and TMAEMA imparted the salt-responsive behavior to the copolymer. By varying the composition of copolymers, the rubbery plateaus of the storage and loss moduli master curves were tunable such that copolymers followed the Dahlquist criterion, thus behaving as a tacky polymer system. Peel tests and probe tack measurements confirmed the applicability of these polymers in pressure sensitive adhesives. At less than 5% TMAEMA, the adhesives were soluble in water; in contrast, in the presence of salts, these adhesives showed promise for use in water-insoluble systems.

7.6 *Acknowledgements*

This material is based on work supported by the U.S. Army Research Laboratory and the U.S. Army Research Office under contract/grant number W911NF-07-1-0452 Ionic Liquids in Electro-Active Devices Multidisciplinary University Research Initiative (ILEAD MURI). The authors acknowledge the Laboratory for Research on the Structure of Matter at Penn (MRSEC NSF DMR11-20901) for instrument support.

7.7 *References*

(1) Stuart, M. A. C.; Huck, W. T.; Genzer, J.; Müller, M.; Ober, C.; Stamm, M.; Sukhorukov, G. B.; Szleifer, I.; Tsukruk, V. V.; Urban, M. *Nature materials* **2010**, *9*, 101.
(2) Alexander, C.; Shakesheff, K. M. *Advanced Materials* **2006**, *18*, 3321.
(3) Nath, N.; Chilkoti, A. *Advanced materials* **2002**, *14*, 1243.
(4) Wang, D.; Wu, T.; Wan, X.; Wang, X.; Liu, S. *Langmuir* **2007**, *23*, 11866.
(5) Wang, W.; Ruan, C.; Gu, B. *Analytica chimica acta* **2006**, *567*, 121.
(6) Yao, K.; Chen, Y.; Zhang, J.; Bunyard, C.; Tang, C. *Macromolecular rapid communications* **2013**, *34*, 645.
(7) Yao, K.; Tang, C.; Zhang, J.; Bunyard, C. *Polymer Chemistry* **2013**, *4*, 528.
(8) Kumar, A.; Srivastava, A.; Galaev, I. Y.; Mattiasson, B. *Progress in Polymer Science* **2007**, *32*, 1205.
(9) Liu, X.; Ye, Q.; Yu, B.; Liang, Y.; Liu, W.; Zhou, F. *Langmuir* **2010**, *26*, 12377.
(10) Lutz, J.-F.; Akdemir, Ö.; Hoth, A. *Journal of the American Chemical Society* **2006**, *128*, 13046.
(11) Lutz, J. F. *Journal of Polymer Science Part A: Polymer Chemistry* **2008**, *46*, 3459.
(12) Schmaljohann, D. *Advanced drug delivery reviews* **2006**, *58*, 1655.
(13) Pocius, A. V. *Adhesion and adhesives technology: an introduction*; Carl Hanser Verlag GmbH Co KG, 2012.
(14) Frantzis, P. *Journal of Materials in Civil Engineering* **2008**, *20*, 635.
(15) Cloete, W. E.; Focke, W. W. *International Journal of Adhesion and Adhesives* **2010**, *30*, 208.
(16) Malmsten, M. *Biopolymers at interfaces*; CRC Press, 2010; Vol. 110.
(17) Burkett, J. R.; Wojtas, J. L.; Cloud, J. L.; Wilker, J. J. *The Journal of Adhesion* **2009**, *85*, 601.
(18) Shao, H.; Bachus, K. N.; Stewart, R. J. *Macromolecular bioscience* **2009**, *9*, 464.
(19) Kaur, S.; Weerasekare, G. M.; Stewart, R. J. *ACS applied materials & interfaces* **2011**, *3*, 941.
(20) Shao, H.; Stewart, R. J. *Advanced Materials* **2010**, *22*, 729.
(21) Stewart, R. J.; Ransom, T. C.; Hlady, V. *Journal of Polymer Science Part B: Polymer Physics* **2011**, *49*, 757.

(22) Stewart, R. J.; Wang, C. S.; Shao, H. *Advances in colloid and interface science* **2011**, *167*, 85.
(23) Stewart, R. J.; Weaver, J. C.; Morse, D. E.; Waite, J. H. *Journal of Experimental Biology* **2004**, *207*, 4727.
(24) Hemp, S. T.; Smith, A. E.; Bunyard, W. C.; Rubinstein, M. H.; Long, T. E. *Polymer* **2014**, *55*, 2325.
(25) Chan, H.-K.; Howard, G. *The Journal of Adhesion* **1978**, *9*, 279.
(26) Chang, E. *The Journal of Adhesion* **1991**, *34*, 189.
(27) Chang, E. *The Journal of Adhesion* **1997**, *60*, 233.
(28) Dahlquist, C. *Adhesion fundamentals and practice* **1966**, 143.
(29) Kaelble, D. *The Journal of Adhesion* **1969**, *1*, 102.
(30) Gent, A.; Petrich, R. In *Proceedings of the Royal Society of London A: Mathematical, Physical and Engineering Sciences*; The Royal Society: 1969; Vol. 310, p 433.
(31) Dobrynin, A. V.; Colby, R. H.; Rubinstein, M. *Macromolecules* **1995**, *28*, 1859.

Chapter 8: **Synthesis of Sulfonimide-containing Triblock Copolymers for Enhanced Conductivity and Improved Mechanical Performance**

(*Macromolecules* **2015**)

Chainika Jangu[1], Alice M. Savage[2], Frederick L. Beyer[2], Zhiyang Zhang[2], Alison R. Schultz[1], Louis A. Madsen[1] and Timothy E. Long[1]

[1]*Department of Chemistry & Macromolecules and Interfaces Institute (MII), Virginia Tech., Blacksburg, Virginia 24061, USA*
[2]*U.S Army Research Laboratory Aberdeen Proving Ground, MD 21005-5069*

*To whom correspondence should be addressed E-mail: telong@vt.edu. TEL: (540) 231-2480 FAX: (540) 231-8517

Keywords: RAFT; ABA triblock copolymers; morphology; ionic conductivity

8.1 *Abstract*

Ion-containing block copolymers continue to attract significant interest as conducting membranes in energy storage devices. Reversible addition-fragmentation chain transfer (RAFT) polymerization enables the synthesis of well-defined ionomeric A-BC-A triblock copolymers, featuring a microphase-separated morphology and a combination of excellent mechanical properties and high ion transport. The soft central "BC" block is comprised of poly(4-styrenesulfonyl(trifluoromethylsulfonyl)imide) (poly(Sty-Tf_2N)) with $-SO_2-N^-SO_2-CF_3$ anionic groups associated with a mobile lithium cation and low T_g di(ethylene glycol)methyl ether methacrylate (DEGMEMA) units. External polystyrene A blocks provide mechanical strength with nanoscale morphology even at high ion content. Electrochemical impedance spectroscopy (EIS) and pulse-field-gradient (PFG) NMR spectroscopy have clarified the ion transport properties of these ionomeric A-BC-A triblock copolymers. Results confirmed that well-defined

ionomeric A-BC-A triblock copolymers combine improved ion-transport properties with mechanical stability with significant potential for application in energy storage devices.

8.2 *Introduction*

The demand for safe and economical energy storage devices featuring high energy density and a rapid charge rate continues to grow.[1] As such, the unique properties of ion-containing block copolymers have attracted significant interest due to their potential in energy storage devices.[2-5] Lithium batteries, in particular, have become the preferred technology for powering portable electronic devices (e.g., laptop computers and cell phones) due to several notable features i.e., their high energy density, low self-discharge rate, high open circuit potential, and minimal memory effects.[6-11] A lithium ion battery typically consists of an anode and cathode; the lithium ions travel between the electrodes through an electrolyte system. The most-commonly used liquid electrolyte is a solution of a lithium salt, e.g., lithium hexafluorophosphate ($LiPF_6$) or lithium bis(perfluoroethanesulfonyl)imide ($LiN(SO_2C_2F_5)_2$), dissolved in a polar aprotic organic solvent, such as a carbonate mixture of ethylene carbonate and dimethyl carbonate.[9,12,13] A major drawback of liquid electrolytes is their flammability.[14,15] However, an alternative to liquid electrolytes is a solid polymer electrolyte (SPE), which is comprised of lithium salts bound in a polymer matrix in the absence of organic solvents.[1,15] Balsara et al. published a comprehensive review of different types of polyelectrolytes for energy applications including lithium ion batteries, fuel cells, and water desalination.[16] An efficient SPE should have unique properties, which combines high modulus, environmental resistance, toughness, and high ion conductivity at application temperature. Therefore, SPE act as an ionic conductor as well as separator at the same time.

PEO homopolymers of different molecular weights are extensively studied as dry

polyelectrolytes. For example, Shi *et al.* found that cation mobility decreases as the molecular weight of PEO is increased up to a critical molecular weight of 3200 g/mol.[12] However, an increase in the ionic conductivity of low molecular weight PEO systems is offset by a decrease in mechanical strength.[17] To overcome this limitation, the use of block copolymer architectures enables the incorporation of both ion conducting and mechanically robust blocks. Moreover, the nanoscale phase-separation of block copolymers allows one to achieve an ideal combination of desirable mechanical, chemical, and transport properties for ion-conducting membranes.[6] Giles and Khan groups reported earlier work on triblock copolymers as electrolytes. They reported the synthesis of poly(S-*b*-B-*b*-S) as well as poly(S-*b*-(B-graft-MPEG)-*b*-S) doped with lithium salts to provide ion conductivity of 10^{-6} S/cm at 25 °C, without much information on morphological and mechanical analysis.[18,19] Many studies highlighted the importance of ordered block copolymers over random and homopolymers.[20,21] Monroe and Newmann estimated the shear modulus of ~ 7 GPa inhibit the macroscopic dendritic formation, preventing short-circuiting of the battery.[22] Lodge et al. reported a one-pot synthetic strategy based on polymerization-induced phase separation (PIPS) to generate nanostructured PEMs (polymer electrolyte membranes) exhibiting high modulus with high ionic conductivity. Ion conductivity of 1 mS/cm and elastic modulus of 1 GPa (at 10 Hz frequency) were obtained at room temperature. PEMs also have significantly improved mechanical stability at high temperatures (E' > 0.1 GPa at T < 125 °C).[23]

The use of controlled radical polymerization provides powerful opportunities to expand a wide variety of monomers to form new functional block copolymers with unique transport and mechanical properties.[24-28] Recently, Long *et al.* investigated the synergy of pendent ether and imidazolium sites in A-BC-A triblock copolymers synthesized using RAFT polymerization. This fundamental study of the dependence of ionic conductivity on composition, morphology, and

monomer selection in ionomeric triblock copolymers led to the design of ion-conducting polymers for electroactive devices.[20] Gao *et al.* earlier reported the successful synthesis of PEG-based sulfonated polyurethanes containing sulfonates in either the soft or hard segment. This work confirmed the influence of charge placement on thermomechanical properties, hydrogen bonding interactions, and morphologies of PEG-based sulfonated polyurethanes.[29] The Long group has also synthesized ABA triblock copolymers using nitroxide-mediated polymerization (NMP) with polystyrene external blocks and a charged imidazolium-containing central block. These well-defined triblock copolymers exhibited sufficient moduli and ionic conductivities for later use in electromechanical transducers.[30] RAFT polymerization also facilitated the synthesis of high molecular weight poly[Sty-*b*-(*n*BA-*co*-DMAEMA)-*b*-Sty] triblock copolymers with tunable properties, which demonstrated actuation behavior with applied low voltage (2-4 V).[31]

This manuscript describes the synthesis and subsequent neutralization of novel, well-defined A-BC-A triblock copolymers containing a soft central "BC" block, which consists of Sty-Tf_2N and DEGMEMA with polystyrene external blocks. These ionomeric A-BC-A triblock copolymers allow one to combine and independently tune two opposing properties in a single material i.e., mechanical stability and ion transport. Specifically, external polystyrene blocks provide mechanical stability, while the low T_g, mobile central block facilitates ion transport. In the central block, the Sty-Tf_2N monomer enables an important delocalization of the negative charge.[32] Li^+ ions are not strongly associated to the polymer chain, thus enabling fast transport and high ion conductivity.[33,34] This idea of charge delocalization on perfluorinated sulfonimide group was initially addressed by the Watanabe and DesMarteau groups.[35,36] Armand et al. have demonstrated the synthesis of poly(Sty-Tf_2N) neutralized with lithium ions and blended with PEO to form single-ion polymer electrolytes for lithium batteries. Ion conductivities is about ten

times higher for a membrane with poly(Sty-Tf_2N) (~10^{-6} S/cm at 70 °C) compared to a membrane with lithium poly(styrene sulfonate).[37] It is also demonstrated that adding a neutral monomer with a high dielectric constant to the ion-containing phase without raising T_g improves ion dissociation and, hence, ion transport. In addition, monomers containing ethylene oxide units have a tendency to coordinate with cations, forming crown ether-like complexes to promote solvation and dissociation of ionic aggregates.[38] Furthermore, DEGMEMA lowers the T_g of the charged block copolymers, thereby increasing segmental mobility and ionic conductivity. Feng et al. synthesized copolymers of Li poly(Sty-Tf_2N) and methoxy-polyethylene glycol acrylate, which show ion conductivity ~ 10^{-6} S/cm at 25 C and 10^{-4} S/cm at 60 °C.[33] Forsyth et al. also took advantage of charge delocalization in Sty-Tf_2N as well as low T_g nature of well-known acrylate backbones to obtain new series of Na-ion polymer electrolytes. The highest conductivity measured at 100 °C was found for Na(poly(Sty-Tf_2N-*blend*-ethyle acrylate) around 10^{-9} S/cm.[32,33] This paper will review the relationships among chemical composition, morphology, ionic conductivity, and mechanical properties of triblock copolymers. A-BC-A triblock copolymer architecture enables to tune the composition of central and external blocks to obtain high ion conductivity with mechanical integrity for potential applications in lithium-ion battery technology.

8.3 *Experimental*

8.3.1 Materials

4-Styrenesulfonic acid, sodium salt (Sigma-Aldrich), sulfonyl chloride (Alfa-Aesar), trifluoromethylsulfonamide (Rhodia), triethylamine (Sigma Aldrich),. N, N'-dicyclohexylcarbodiimide (DCC, 99%), 4-(dimethylamino)pyridine (DMAP, Sigma >99.0%),

1,6-hexanediamine (98%), 1,6-hexanediol (99%) were used as received. 4-Cyano-4-(ethylsulfanylthiocarbonylsulfanyl)pentanoic acid (CEP) and Sty-Tf_2N were synthesized according to the previous literature. Di(ethylene glycol) methyl ether methacrylate (DEGMEMA, 95%) and styrene (99%) were purchased from Sigma-Aldrich and passed through an alumina packed column prior to use. 4,4'-azobis(4-cyanovaleric acid) (V-501, Aldrich, 98%) and 2,2'-azobisisobutyronitrile (AIBN, Aldrich) were recrystallized from ethanol. All solvents were obtained from Spectrum and used as received.

8.3.2 Synthesis and neutralization of poly(Sty-Tf_2N) using free radical polymerization

The synthesis of this monomer was adopted from previous literature.[26,27] Sty-Tf_2N (2.0 g, 6.3 mmol) and AIBN (1.04 mg, 0.1 mol%) were dissolved in DMF (7.5 mL) in a round-bottomed flask, which was sealed and sparged with argon for 30 min to remove oxygen. Conventional free radical polymerization was then conducted at 65 °C for 24 h. The resulting polymer was neutralized using excess LiOH, KOH, and $Ca(OH)_2$ in a water/ethanol (50/50 v/v) mixture, after which the reaction was allowed to proceed for an additional 24 h. The resulting polymer solution was dialyzed against water for 2 d, and the polymerization was confirmed using ^1H NMR spectroscopy. A ~65% yield of poly(Sty-Tf_2N) was obtained. Scheme 8.1 summarizes the overall synthetic strategy to obtain charged poly(Sty-Tf_2N). XPS spectroscopy and flame color tests confirmed the neutralization with cations.

Scheme 8.1 Free radical polymerization generated poly(Sty-Tf_2N) and subsequent neutralization with different cations

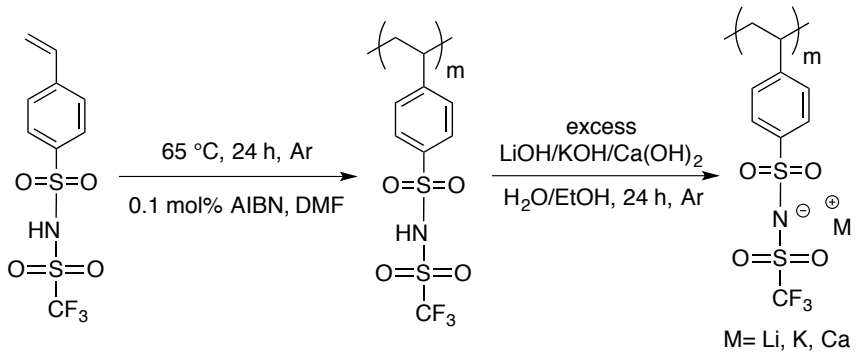

8.3.3 Synthesis of charged A-BC-A triblock copolymer poly[Sty-*b*-(Sty-Tf_2N-Li-*co*-DEGMEMA)-*b*-Sty]

In a representative copolymerization, Sty-Tf_2N (4 g, 12.7 mmol), DEGMEMA (2.4 g, 12.7 mmol), V-501 (9.5 mg, 33.8 μmol) and *d*CEP-NH_2 (51.3 mg, 169 μmol) were dissolved in DMF (25 mL) added to 100 mL round-bottomed flask equipped with a stir bar. The reaction was sparged with argon for 30 min and placed in a oil bath at 70 °C. Different compositions of Sty-Tf_2N and DEGMEMA were targeted to obtain poly(Sty-Tf_2N-Li-*co*-DEGMEMA) copolymers. The resulting polymers were dialyzed (MWCO=3500 g/mol) for 2 d against methanol while changing the solvent every 24 h. SEC using a THF solvent was utilized to determine the absolute molecular weights of random copolymers of Sty-Tf_2N and DEGMEMA, and the resulting polydispersity indices (PDI < 1.2). The synthetic scheme is presented in Scheme 8.2.

The purified macroCTA (280 mg, 12.2 μmol) was redissolved in DMF (23.1 mL) in a round-bottomed flask with a magnetic stir bar. Styrene (0.8 g) and V-501 (1.97 mg) were added to the flask and the reaction was sparged with argon for 30 min at room temperature. The reaction was carried out at 70 °C to obtain desired compositions in the central blocks. Poly[Sty-*b*-(Sty-Tf_2N-*co*-DEGMEMA)-*b*-Sty] dissolved in a THF/CH_3OH (80/20 v/v) solvent mixture

and excess LiOH in a THF/CH_3OH (80/20 v/v) solvent were mixed and purged for 30 min. The reaction was heated at 40 °C for 48 h to obtain poly[Sty-*b*-(Sty-Tf_2N-Li-*co*-DEGMEMA)-*b*-Sty]. The synthetic strategy is demonstrated in Scheme 8.3.

Scheme 8.2 RAFT polymerization yielded a central BC block

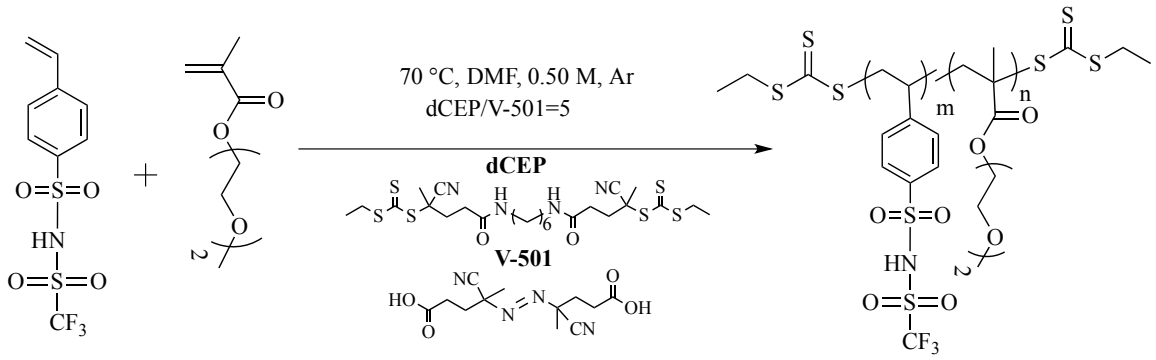

The purified macroCTA was redissolved in DMF in a round-bottomed flask with magnetic stir bar. Styrene and V-501 were added to the flask and the reaction was sparged with argon for 30 min at room temperature. The reaction was carried out at 70 °C to obtain desired compositions in the central blocks. Poly[Sty-*b*-(Sty-Tf_2N-*co*-DEGMEMA)-*b*-Sty] dissolved in THF/CH_3OH solvent mixture and LiOH in THF/CH_3OH solvent were mixed and purged for 30 min. The reaction was heated at 40 °C for 48 h to obtain Poly[Sty-*b*-(Sty-Tf_2N-Li-*co*-DEGMEMA)-*b*-Sty].The synthetic strategy is demonstrated in Scheme 8.3.

Scheme 8.3 RAFT polymerization yielded A-(BC)-A triblock copolymers for subsequent neutralization with LiOH

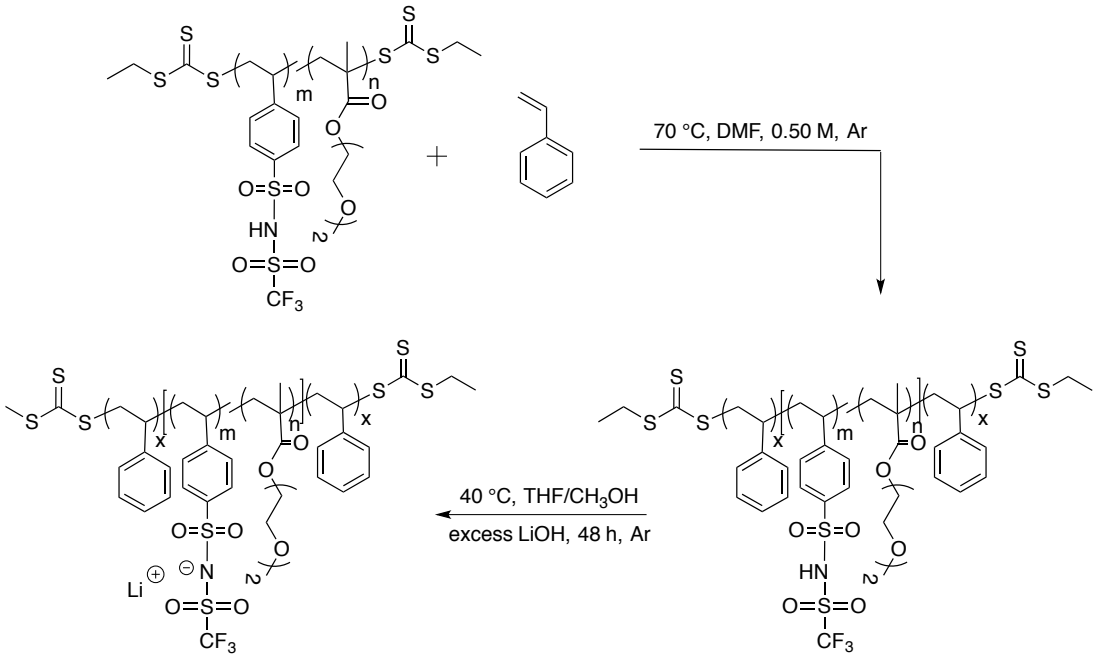

8.3.4 Analytical methods

^{1}H NMR spectroscopy (Varian Inova, 400 MHz) determined CTA, monomer, and polymer composition. Thermogravimetric analysis (TGA) of the triblock copolymers was carried out on a TA Instruments thermogravimetric analyzer (TGA Q50) with a heating rate of 10 °C/min to 600 °C under a nitrogen atmosphere after holding the sample at 100 °C for 60 min. A TA Instruments Q5000 sorption analyzer (TGA-SA) was used to measure the water uptake of triblock copolymer and random copolymer samples (relative humidity (RH) 0-95%, 5% increments) at 25 °C. A TA Instruments Q1000 differential scanning calorimeter (DSC) at a heating rate of 10 °C/min) utilizing a heat/cool/heat cycle was used to determine thermal transitions.. T_g was determined from the second heat cycle of the DSC thermogram. Dynamic mechanical analysis (DMA) (TA Instruments Q800, 3 °C/min heating rate, -50 °C to 150 °C) was performed on the triblock copolymer films in the tension mode of 1 Hz, oscillatory

amplitude of 10 μm, and a static force of 0.01 N. Polymer molecular weight was measured using aqueous size exclusion chromatography (SEC) through two Waters ultrahydrogel linear columns with one Waters ultrahydrogel 250 column in a solvent consisting of 54/23/23 water/methanol/acetic acid (v/v/v%) with 0.1 M sodium acetate. The instrumentation consisted of a Waters 1515 isocratic HPLC pump operating at a flow rate of 0.8 mL/min, 35 °C, a Waters 717plus Autosampler, a Wyatt miniDAWN multiangle light scattering detector operating at a wavelength of 690 nm. A Waters 2414 differential refractive index detector was used to determine the refractive index increment (dn/dc), and thus absolute molecular weight. A Wyatt Optilab refractive index detector operating at 658 nm and 35 °C determined the offline specific refractive index increment values. Wyatt ASTRA SEC/LS software was used to calculate the absolute molecular weight and PDI of the A-BC-A triblock copolymers. Dynamic light scattering (DLS) (Malvern Zetasizer NanoZS) indicated the absence of polymer aggregation in the aqueous mobile phase prior to injection onto the SEC columns. All triblock copolymers were dissolved in 80:20 v:v $CHCl_3$: CH_3OH solvent mixture and cast from a 30 wt.% solution. Films were slowly dried at ambient conditions for 2 d under reduced pressure. The films were annealed at 120 °C for 3 d. The films were then stored in a dry box until analyzed.

8.3.5 Atomic Force Microscopy (AFM)

A Veeco MultiMode scanning microscope in tapping mode provided atomic force microscopy (AFM) images of the A-BC-A triblock copolymers. Samples were imaged with a set-point ratio of 0.6 at (3x3) μm and (1x1) μm magnifications using a nanosensor silicon tip with a spring constant of 42 N/m.

8.3.6 Transmission Electron Microscopy (TEM)

Transmission electron microscopy (TEM) was performed on sections prepared by cryoultramicrotomy. Each material was sectioned at -80 °C using a Leica UC7 ultramicrotome equipped with a Leica FC7 cryochamber, generating sections ranging in thickness between 50 and 70 nm. A JEOL JEM-2100F TEM and a Gatan 806 high-angle annular dark field scanning TEM (HAADF STEM) detector were used to collect dark field data from each sample. The TEM was operated at 200 kV, with a 40 μm condenser aperture, a HAADF STEM collection angle of 48 to 168 mrad, and spot size of 0.2 nm. Gatan Digital Micrograph was used to collect and analyze the data.

8.3.7 Small-Angle X-Ray Scattering

Small-angle X-ray scattering (SAXS) data were collected using a 2D multiwire area detector manufactured by Molecular Metrology, with a 1.5 μm pinhole-collimated camera. Photons with a wavelength of 1.54 Å were generated using an Ultrax18 rotating copper anode X-ray generator, manufactured by Rigaku Americas, Inc. The generator was operated at 4.5 kW and was equipped with a Ni filter. Two-dimensional data were collected at sample-to-detector distances of 1.5 m and 0.5 m, then azimuthally averaged to yield intensity, I, as a function of scattering vector magnitude, q, where $q = 4\pi\sin(\theta)/\lambda$, 2θ is the scattering angle, and λ is wavelength. Distance calibrations were performed using silver behenate.[29] Averaged data were corrected for background noise and scaled to absolute intensity using glassy carbon as a secondary standard, previously calibrated at the Advanced Photon Source, Argonne National Laboratory.[29] All data manipulation and analysis were performed using Igor Pro v. 6.22A (Wavemetrics, Inc.).[30]

8.3.8 Electrochemical Impedance Spectroscopy (EIS)

Electrochemical impedance spectroscopy (EIS) was performed using an Autolab PGSTAT 302N potentiostat and a through plane, as well as a four-point electrode sample cell purchased from BekkTeck, Inc. An applied alternating sine-wave potential was applied at 0.2 V with frequencies ranging from 0.1 Hz to 1 MHz. An ESPEC BTL- 433 environmental chamber was used to control the temperature to ±0.1 °C and 10% RH to ±0.1%. An alternating current was applied to the outer electrodes and the real impedance or resistance, R, was measured between the two inner reference electrodes. A high x-intercept of the semicircle regression of the Nyquist plot determined the resistance. Ionic conductivity was determined by $\sigma = L/AR$, where L is distance between the two inner electrodes and A is the cross-sectional area of the polymer film. The cross-sectional area is defined as $A = Wl$, where W is the film width and l is the film thickness. Samples equilibrated for 1-2 h under each measurement condition, followed by at least five measurements at that condition. The values reported are an average of these steady-state measurements.

8.3.9 ^{7}Li Diffusion Measurements using PFG-NMR Spectroscopy

In order to obtain ^{7}Li self-diffusion measurements, membranes were deposited into 5 mm NMR tubes after equilibrating in an ESPEC BTL-433 environmental chamber at 60 °C and 10% RH for 24 h. ^{7}Li self-diffusion measurements were performed using the pulsed-gradient stimulated echo sequence (PGSTE) on a Bruker Avance III 9.4 T widebore spectrometer equipped with a Diff60 diffusion probe and a 5 mm ^{7}Li coil (155.45 MHz) and optimized according to previous studies.[31,32] The NMR signal attenuation due to diffusion is described by the Stejskal-Tanner equation:

$$I = I_0 e^{-D\gamma^2 g^2 \delta^2 (\Delta - \delta/3)} \qquad \text{Equation 1}$$

where I is the spin-echo signal intensity, I_0 is the signal intensity at zero gradient, γ is the gyromagnetic ratio of ^{7}Li nucleus (rad s^{-1} T^{-1}), g is the magnitude of the gradient pulse (T m^{-1}), and D is the self-diffusion coefficient of lithium ions in the membranes derived by fitting Equation 1. Δ is the duration between the leading edges of the two gradient pulses (100-300 ms in this work), and δ is the duration of the gradient pulse (1 ms in this work), depending on the corresponding relaxation times of the membranes. 16-step variation in gradient strength (*g)* with 64 scans taken at each step yielded sufficient signal-to-noise ratio (SNR) for accurate diffusion coefficient quantification. Errors in D are < +/- 10%. All diffusion experiments were conducted at various temperatures ranging from 20 to 80 °C.

8.4 *Results and Discussions*

The Sty-Tf_2N monomer was synthesized according to previously published procedures.[26,27] The Sty-Tf_2N repeat unit enabled delocalization of the negative charge upon neutralization. After neutralizing with MOH (M = Li, K, or Ca), M^+ displayed weak interactions with the anionic site, thus enabling a high dissociation level to improve ion transport. To gain a better understanding of reaction conditions and neutralization procedures, conventional free radical polymerization yielded poly(Sty-Tf_2N), followed by neutralization using excess LiOH, KOH, and $Ca(OH)_2$. The overall synthetic route is described in Scheme 8.1.

Table 8.1 summarizes the thermal and molecular weight properties of poly(Sty-Tf_2N) and the charged poly(Sty-Tf_2N) polymers with different cations. All polymers displayed high molecular weights with PDIs in the range one would expect from conventional free radical polymerization. The T_g of the homopolymer poly(Sty-Tf_2N) was 110 °C. After neutralization

with monovalent and divalent cations, T_g values increased due to electrostatic interactions. It should be noted, however, that T_g varied significantly depending on the choice of counterion, as shown in Table 8.1. In particular, the network featuring divalent calcium cation proved to be stronger in comparison to those incorporating monovalent cations. All polymers displayed two-step degradation behavior with increasing temperature. The thermal weight loss behavior was similar to results described in the literature for sodium poly(styrene sulfonate).[33] Specifically, thermal decomposition likely occurs as follows. First, a cleavage of the C-S bonds takes place to produce styryl radicals, SO_2, and trifluoromethylsulfonamide. Then, the styryl radical reacts with hydrogen from the polymer chain, which is accompanied by polystyrene degradation and the subsequent formation of benzene, toluene, and methyl styrene. The suggested thermal decomposition mechanistic pathway of poly(Sty-Tf_2N) is shown in Figure 8.1.

Table 8.1 Molecular weight and thermal analysis of poly(Sty-Tf_2N) and charged poly(Sty-Tf_2N) with different cations

Polymer	M_n (g/mol)[a]	PDI [a]	T_g (°C) [b]	T_d (°C) [c]
Poly(Sty-Tf_2N)	136,000	1.65	110	245, 395
Poly(Sty-Tf_2N)-Li	125,000	1.96	153	220, 345
Poly(Sty-Tf_2N)-K	133,000	1.87	167	236, 368
Poly(Sty-Tf_2N)-Ca	141,000	1.78	197	245, 400

[a] SEC: 35 ˚C, THF, MALLS detector
[b] DSC: 10 ˚C/min, N_2 atm., heat/cool/heat cycle, second heat
[c] TGA: 10 ˚C/min, N_2 atm., first column is temperature at which C-S bond cleavage occurs in poly(Sty-Tf_2N) degradation, second is the backbone decomposition temperature

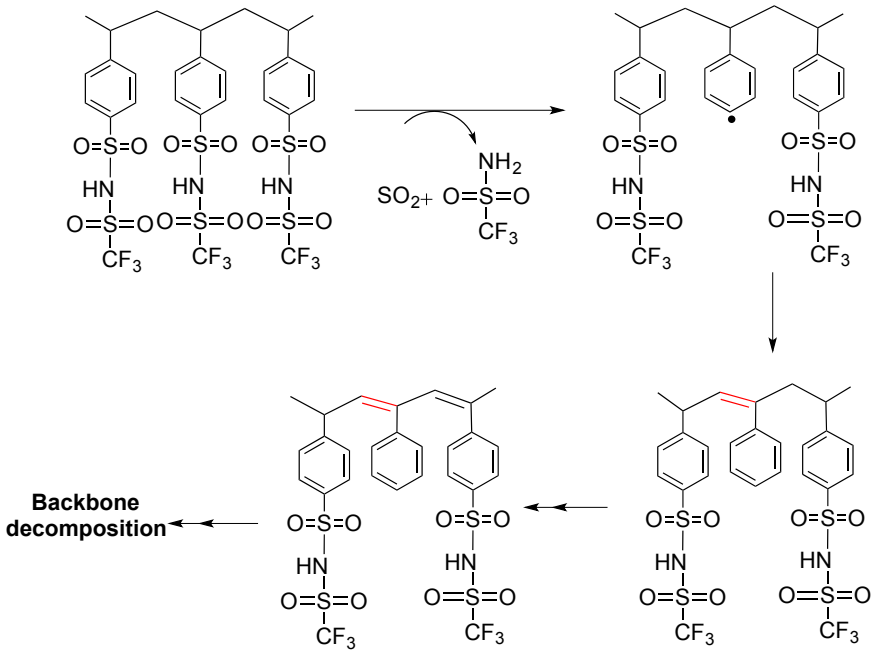

Figure 8.1 Proposed mechanistic pathway for thermal decomposition of poly(Sty-Tf_2N)

RAFT polymerization is a controlled radical polymerization method used to synthesize triblock copolymers. For this investigation, a difunctional trithiocarbonate chain transfer agent (CTA), facilitated divergent chain growth, to design A-BC-A triblock copolymers. This process involved the synthesis of poly(DEGMEMA-*co*-Sty-Tf_2N) copolymers with a difunctional CTA (*d*CEP), a V-501 azo initiator, and DMF as the solvent to generate the "BC" central blocks (see Scheme 8.3). ^{1}H NMR spectroscopy was utilized to analyze copolymer composition, with resulting spectra confirming that the polymerization proceeded at conversions of 70-80%.

RAFT polymerization facilitated the synthesis of a series of low-T_g central blocks with varying molar ratios of Sty-Tf_2N and DEGMEMA. Table 8.2 summarizes the molecular weights and thermal properties of these various poly(Sty-Tf_2N-*co*-DEGMEMA) copolymers . Subsequent SEC analysis revealed unimodal symmetric chromatograms, and all copolymers exhibited narrow molecular weight distributions (PDIs). It should be noted that the T_g values of the copolymer central blocks decreased with increasing DEGMEMA. For example, as the

concentration of the low T_g monomer DEGMEMA increased to 90 mol%, the T_g of the copolymer decreased to 2 °C, as shown in Table 2. The predicted T_g values using the Fox equation fitted well with experimentally obtained T_g values, confirming the random incorporation of monomers (Figure 8.2).

Table 8.2 Molecular weight and thermal properties of poly(Sty-Tf_2N-*co*-DEGMEMA) central "BC" blocks with various compositions using RAFT copolymerization

Polymer	M_n (g/mol) [a]	PDI [a]	T_g (°C) [b]	$T_{d,5\%}$ (°C) [c]
Poly(Sty-Tf_2N_{10}-*co*-DEGMEMA$_{90}$)	39,000	1.05	2	190, 280
Poly(Sty-Tf_2N_{23}-*co*-DEGMEMA$_{77}$)	42,000	1.08	22	184, 271
Poly(Sty-Tf_2N_{46}-*co*-DEGMEMA$_{54}$)	49,000	1.15	47	198, 265
Poly(Sty-Tf_2N_{64}-*co*-DEGMEMA$_{36}$)	38,000	1.09	64	178, 265

[a]SEC: 35 ˚C, 1 mL/min, MALLS, 54/23/23 (v/v/v %) $H_2O/CH_3OH/CH_3COOH$, NaOAc
[b]DSC: 10 ˚C/min, N_2 atm., heat/cool/heat cycle, second heat
[c]TGA: 10 ˚C/min, N_2 atm., first column is temperature at which C-S bond cleavage occurs in poly(Sty-Tf_2N) degradation, second is the backbone decomposition temperature

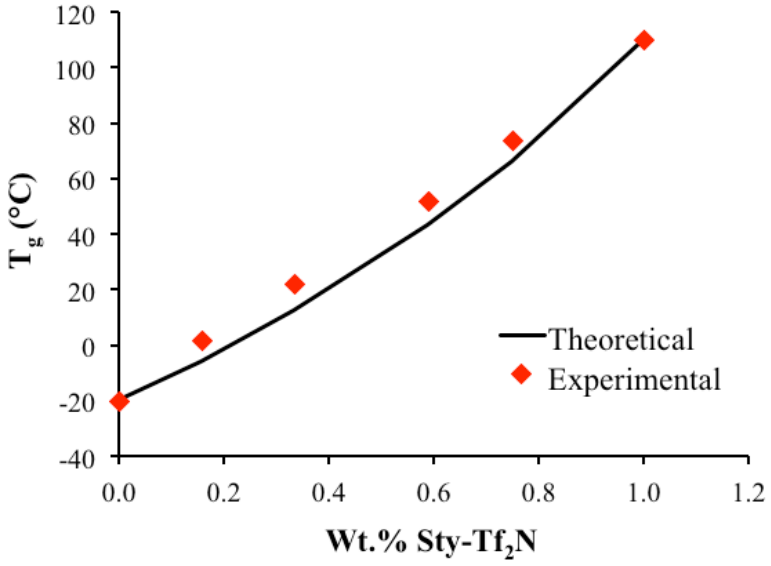

Figure 8.2 Central "BC" block follows Fox equation indicating random incorporation of monomers, Sty-Tf_2N and DEGMEMA

RAFT polymerization controlled the reaction kinetics for the block copolymerization of styrene onto both ends of the poly(DEGMEMA-*co*-Sty-Tf_2N) macroCTA. Adjusting the

polymerization reaction time facilitated the synthesis of optimally designed triblock copolymers with desired molecular weights. As depicted in Scheme 8.3, subsequent neutralization of the triblock copolymers with an excess of LiOH yielded A-BC-A triblock copolymers with Li^+ as the counterion, where polystyrene served as the mechanical reinforcing external blocks and the central blocks provide pathways for counterion transport. The composition of these charged A-BC-A triblock copolymers could be tuned to obtain enhanced properties, wherein the compositions are tunable to obtain enhanced properties. The detailed synthetic procedure to obtain charged A-BC-A triblock copolymers is shown in Scheme 8.3. The quantitative neutralization of the sulfonimides with an excess of LiOH was achieved, after which dialysis was employed to remove the excess base. ^{1}H NMR spectra confirmed the composition of the triblock copolymers after neutralization.

Triblock copolymers of varying central block composition and with similar external and central block molecular weights were synthesized. As listed in **Table 8.3**, the wt.% of the external blocks was approximately 50%. The resulting unimodal SEC chromatograms and narrow molecular weight distributions (< 1.30) of these triblock copolymers synthesized using RAFT polymerization confirmed the controlled nature of the polymerization. After neutralization with LiOH, the molecular weights of the triblock copolymers remained similar, thereby verifying the stability of these polymers under the described reaction conditions. However, the choice of chain extension and countercation, resulting in a change in composition, influenced the thermal properties of the triblock copolymers. As confirmed with DSC, two transitions occurred in the poly[Sty-*b*-(Sty-Tf_2N_{64}-*co*-$DEGMEMA_{36}$)-*b*-Sty] block copolymers: (a) the low temperature transition resulting from the soft ionic blocks, and (b) the high temperature transition caused by the polystyrene blocks. Increasing DEGMEMA content decreased the central block T_g of the

block copolymers. The T_g of the central blocks and in the triblocks remained similar, which suggested the absence of appreciable phase mixing in the poly[Sty-*b*-(Sty-Tf_2N_{64}-*co*-$DEGMEMA_{36}$)-*b*-Sty] triblock copolymers. After neutralization, the T_g of the central blocks increased due to strong electrostatic interactions. Additionally, conventional free radical polymerization enabled the synthesis of the poly[Sty-*co*-(Sty-Tf_2N_{64}-Li-*co*-$DEGMEMA_{36}$)] random copolymer with a similar composition with a T_g of 85 °C, indicative of a phase-mixed morphology.

Table 8.3 Molecular weight and thermal properties of all A-BC-A triblock copolymers with varying compositions

Polymer	T_g (°C)[b]	$T_{d,\,5\%}$ (°C)[c]	M_n (g/mol)[a]	PDI[a]
Poly[Sty-*b*-(Sty-Tf_2N_{10}-*co*-$DEGMEMA_{90}$)-*b*-Sty]	2	190, 280	47k-36k-47k	1.20
Poly[Sty-*b*-(Sty-Tf_2N_{23}-*co*-$DEGMEMA_{77}$)-*b*-Sty]	32	221, 300	51k-41k-51k	1.29
Poly[Sty-*b*-(Sty-Tf_2N_{46}-*co*-$DEGMEMA_{54}$))-*b*-Sty]	52	243, 305	49k-47k-49k	1.27
Poly[Sty-*b*-(Sty-Tf_2N_{64}-*co*-$DEGMEMA_{36}$) -*b*-Sty]	74, 120	201, 323	47k-36k-47k	1.20
Poly[Sty-*b*-(Sty-Tf_2N_{10}-Li-*co*-$DEGMEMA_{90}$)-*b*-Sty]	6	201, 296	51k-38k-51k	1.28
Poly[Sty-*b*-(Sty-Tf_2N_{23}-Li-*co*-$DEGMEMA_{77}$)-*b*-Sty]	36	214, 290	51k-42k-51k	1.35
Poly[Sty-*b*-(Sty-Tf_2N_{46}-Li-*co*-$DEGMEMA_{54}$)-*b*-Sty]	62	219, 295	49k-49k-49k	1.38
Poly[Sty-*b*-(Sty-Tf_2N_{64}-Li-*co*-$DEGMEMA_{36}$)-*b*-Sty]	78, 120	198, 305	47k-38k-47k	1.32
Poly[Sty-*co*-Sty-Tf_2N_{64}-Li-*co*-$DEGMEMA_{36}$]	85	196, 350	ND	ND

[a]SEC: 35 ˚C, THF, MALLS detector
[b]DSC: 10 ˚C/min, N_2 atm., heat/cool/heat cycle, second heat
[c]TGA: 10 ˚C/min, N_2 atm., first column is temperature at which C-S bond cleavage occurs in poly(Sty-Tf_2N) degradation, second is the backbone decomposition temperature

Earlier literature reports have described the use of small-angle x-ray scattering (SAXS) to elucidate the multiphase morphology of block copolymers.[22,24] Similarly, SAXS revealed the microphase-separation of the poly[Sty-*b*-(Sty-Tf_2N_{64}-Li-*co*-$DEGMEMA_{36}$)-*b*-Sty] and poly[Sty-*b*-(Sty-Tf_2N_{23}-Li-*co*-$DEGMEMA_{77}$)-*b*-Sty] triblock copolymers, which are illustrated in Figure 8.3. The scattering peaks at *1q**, *2q**, and *3q** indicated lamellar structures, as compared to a homogeneous morphology for the random copolymer. By fitting Lorentzian distributions to the Bragg scattering maxima, the lamellar periods for poly[Sty-*b*-(Sty-Tf_2N_{64}-Li-*co*-$DEGMEMA_{36}$)-

b-Sty] and poly[Sty-*b*-(Sty-Tf_2N_{23}-Li-*co*-$DEGMEMA_{77}$)-*b*-Sty] were determined to be 24.2 nm and 24.5 nm respectively. The similarity in the lamellar period is attributed to the similarity in molecular weight of the individual blocks of the triblock copolymers.

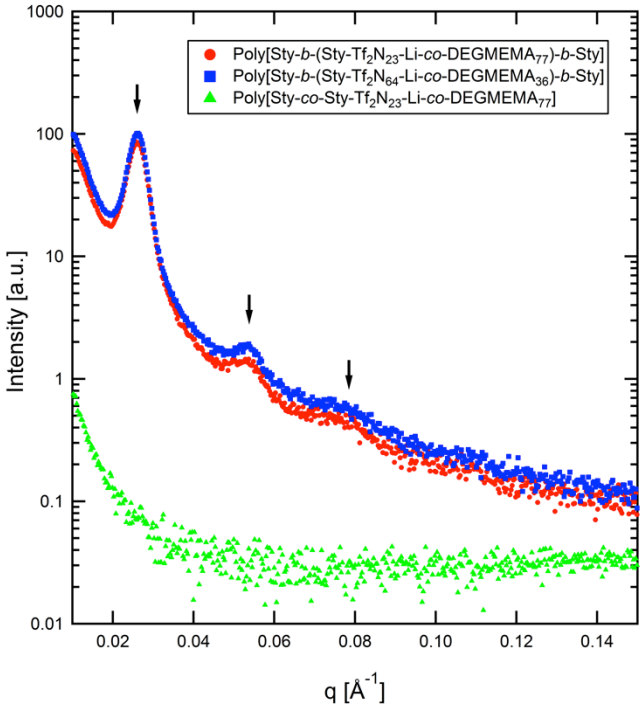

Figure 8.3 SAXS analysis of A-BC-A triblock copolymers confirming microphase-separation as compared to no morphology observed in random copolymer

Morphological investigations using AFM and TEM also confirmed a microphase-separated morphology. Specifically, AFM and TEM micrographs showed the presence of phase-separated morphologies with orientation for the poly[Sty-*b*-(Sty-Tf_2N_{64}-Li-*co*-$DEGMEMA_{36}$)-*b*-Sty] block copolymer with the highest ion content (Figure 8.4 left and Figure 8.5). It should be noted, however, that AFM results also verified a phase-separated surface structure for the poly[Sty-*b*-(Sty-Tf_2N_{23}-Li-*co*-$DEGMEMA_{77}$)-*b*-Sty] block copolymer as well, even with its low ion content (Figure 8.4 right).

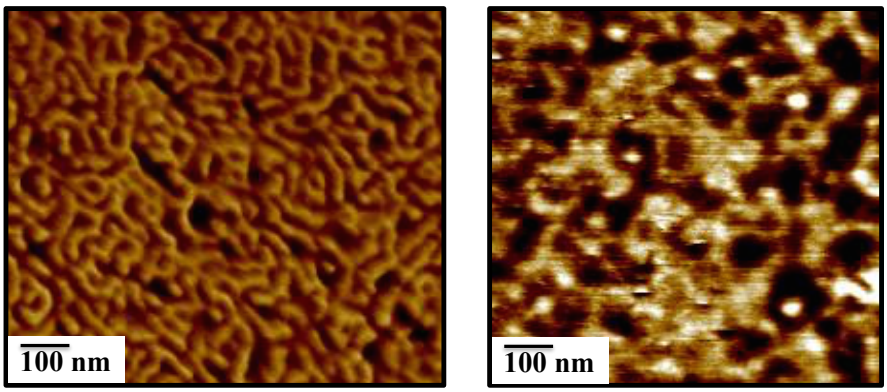

Figure 8.4 Atomic force microscopy (AFM) indicates microphase-separation in charged A-(BC)-A triblock copolymers. (a) Poly[Sty-*b*-(Sty-Tf_2N_{64}-Li-*co*-$DEGMEMA_{36}$)-*b*-Sty] (b) Poly[Sty-*b*-(Sty-Tf_2N_{23}-Li-*co*-$DEGMEMA_{77}$)-*b*-Sty]

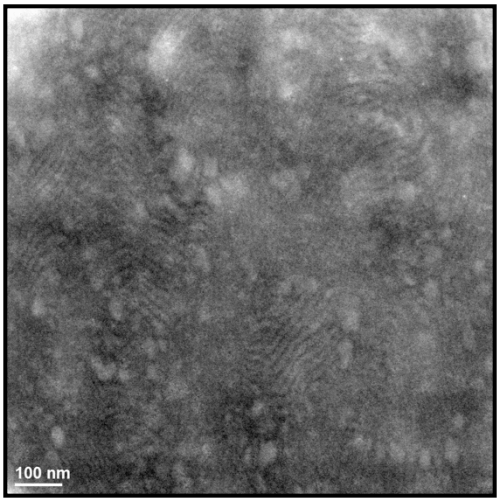

Figure 8.5 Transmission electron microscopy (TEM) indicates the microphase-separation in charged A-(BC)-A triblock copolymer poly[Sty-*b*-(Sty-Tf_2N_{64}-Li-*co*-$DEGMEMA_{36}$)-*b*-Sty]

Storage moduli (G') *vs.* temperature results for the charged triblock copolymers with varying ion content are shown in Figure 8.6. DMA confirmed the mechanical robustness of the charged A-BC-A triblock copolymers at room temperature. The poly[Sty-*b*-(Sty-Tf_2N-*co*-DEGMEMA)-*b*-Sty] triblock copolymers with the lowest and highest ion content exhibited two distinct transitions-the T_g of the soft central block, and the second transition at ~100 °C; which was consistent with the T_g of a polystyrene hard phase. For the highest ion-content copolymer, the T_g of the central block increased in comparison to the analogous low ion-content copolymer,

which was consistent with DSC results. This corresponded to strong electrostatic interactions with increasing ion content. In contrast, the T_g of the polystyrene external block remained constant with varying compositions of the central blocks. DMA confirmed the mechanical robustness of the charged A-BC-A triblock copolymers at room temperature with G'> 10^8 Pa. Even at 90 °C, triblock copolymer with low ion-content have G'~ 10^7-10^8 Pa at 1 Hz frequency.

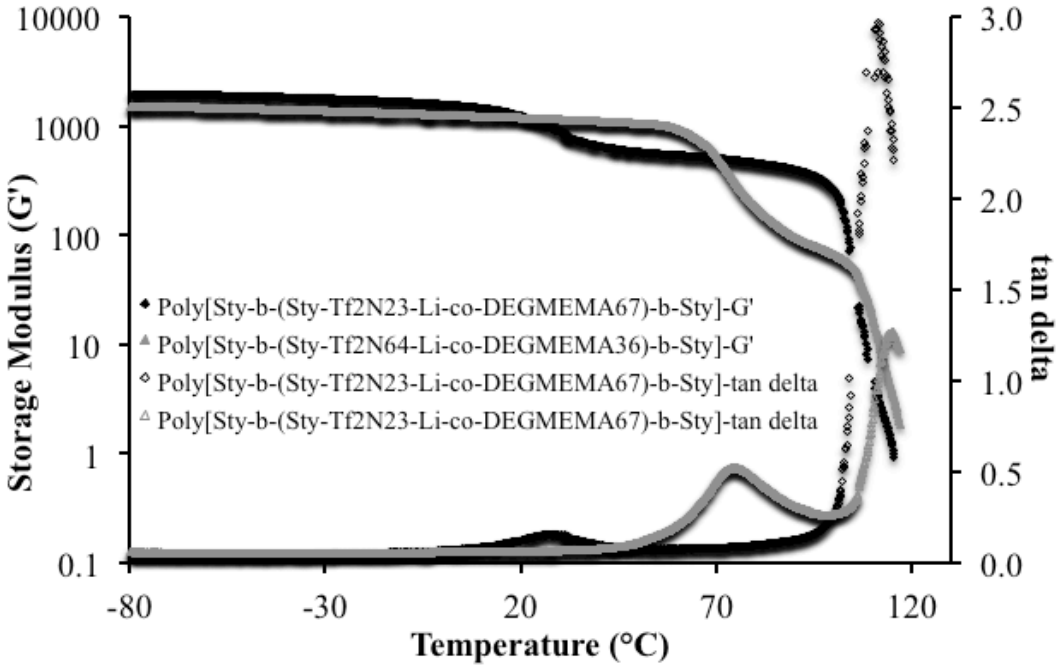

Figure 8.6 Dynamic mechanical analysis (DMA) of A-BC-A triblock copolymers poly[Sty-*b*-(Sty-Tf_2N-Li-*co*-DEGMEMA)-*b*-Sty] with varying compositions

Achieving morphological and compositional control in these triblock copolymers translates into the ability to carefully tune ion transport properties. The ion conductivity of the triblock copolymers was investigated using AC electrochemical impedance spectroscopy, and pulse-field-gradient (PFG) NMR diffusometry afforded Li^+ diffusion coefficient measurements. Figure 8.7 shows the temperature-dependent through-plane ion conductivities of neutralized A-BC-A triblock copolymers using EIS spectroscopy, plotted along with conductivities calculated from PFG NMR. EIS determined the resistance, R from a high x-intercept of the semi-circle

regression of the Nyquist plot, while ionic conductivity was defined using $\sigma = L/AR$, where L represents the distance between the two inner electrodes, and A represents the cross-sectional area of the polymer film. Accordingly, the cross-sectional area can be defined as $A = Wl$, where W is the film width and l is the film thickness.

Since the Li^+ ions serve as the only mobile charge carriers in these triblock copolymers, Li^+ dominates the ionic conductivity. Ion conductivity, σ_{NMR} from the ^7Li PFG NMR measurements, is based on the following equation:

$$\sigma_{NMR} = \rho \frac{Z^2 eFD_{Li}}{k_B T}$$

where ρ is ion density, e is fundamental electric charge on each ion, Z is the valence charge number of the moving ion (+1 in this case), F is Faraday's constant, k_B is Boltzmann's constant, T is temperature, and D_{Li} is the measured ^7Li self-diffusion coefficient from PFG NMR. Since the exchange rate for the chemical equilibrium between the dissociated and associated Li^+ species in triblock copolymers tends to be faster than the time scale of PFG NMR measurements (~10 ms),[31] NMR diffusion measurements cannot separately distinguish the transport properties of the dissociated and associated Li^+ species in the equilibrium state. σ_{NMR} from above equation is based on the assumption that all of the diffusing Li^+ species detected with NMR diffusometry contribute to the ion conductivity and that the ions are decoupled from each other and from the polymer-fixed ions. Thus, the ion conductivities σ_{NMR} are higher than the ion conductivities σ_{EIS} from EIS, as shown in Figure 8. The Haven ratio, the ratio $\sigma_{NMR}/\sigma_{EIS}$, provides an evaluation of the ion dissociation degree in an ion conductor. When $\sigma_{NMR}/\sigma_{EIS} = 1$, all ions contribute to conduction on all time scales and are fully decoupled from each other, whereas ratios > 1 indicate associations among ions. In this case, Li^+ associates with the polymer-fixed anions. For the present materials, the calculated Haven ratio is in the range of 4 to 10, indicating that the Li^+

ions have only moderate associations with the anionic polymer backbone. Scharfenberger et al. calculated the Haven ratio for proton conduction in imidazole-functionalized polysiloxane, and their values are significantly higher ($\sigma_{NMR}/\sigma_{EIS}$ = 7 to 11), and they attributed this ratio to correlated proton transfers that dominate proton diffusion.[34] Kataoka et al. used Haven ratio to evaluate the dissociation degree of a lithium electrolyte liquid solution dispersed with 10-15 wt.% polyvinylidene fluoride-type polymer (PVDF-HFP copolymer). Even for this predominantly liquid solution, $\sigma_{NMR}/\sigma_{EIS}$ was in the range of 1.4 to 2. We note that the definition of the Haven ratio is inverted ($\sigma_{EIS}/\sigma_{NMR}$) in this last reference, and in other literature describing many liquid electrolytes including salt solutions and ionic liquids.[35] Conductivity values were then normalized with T_g (Figure 8.7). Results confirmed that ion conductivity increased with temperature with respect to T_g for all the copolymers. Since the wt.% of external and central blocks was similar for all the block copolymers, one cannot attribute this behavior to block length. Indeed, ion conductivity also increased with increasing ion content in the central block. This observed trend was similar using either EIS or NMR diffusometry. As ion density in the central block increased from 23 to 64 mol%, the ion conductivity increased almost 3 orders of magnitude. This effect was attributed to a combination of an increase in the number of charge carriers in the conducting phase, accompanied by a substantial improvement in morphological phase-separation and channel connectivity for the higher ion content polymers.

(A)

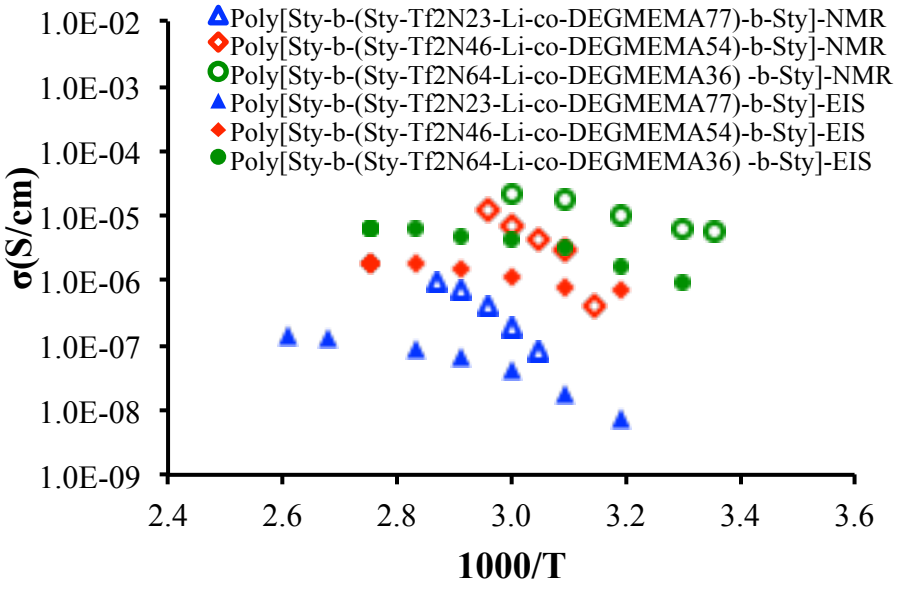

(B)

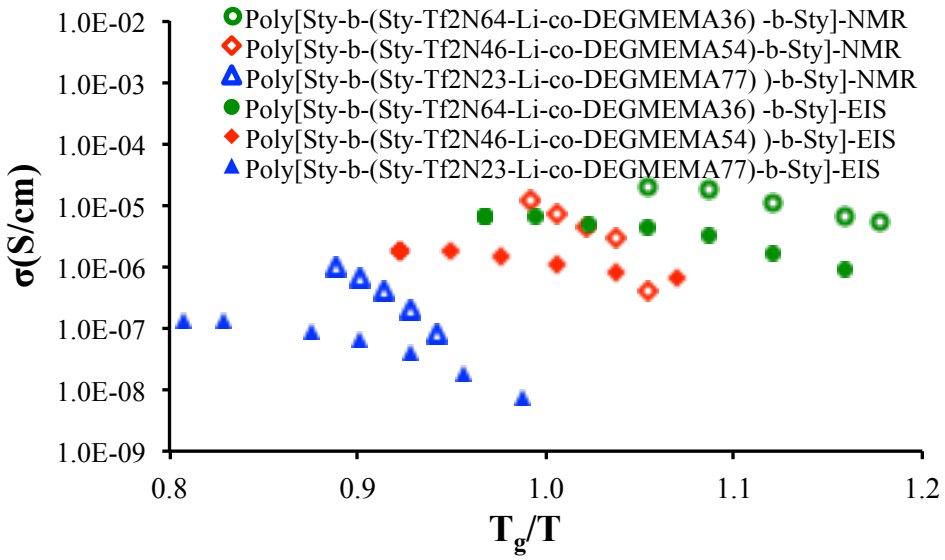

Figure 8.7 (A) Temperature-dependent ionic conductivity (σ) of triblock copolymers with varying compositions obtained using NMR (open symbols) and electrochemical impedance spectroscopy (EIS) (closed symbols) **(B)** Temperature-dependent ionic conductivity normalized with T_g of the central block

8.5 *Conclusions*

RAFT copolymerization enabled the synthesis of well-defined ionomeric A-BC-A triblock copolymers, poly[Sty-*b*-(Sty-Tf_2N-Li-*co*-DEGMEMA)-*b*-Sty] with microphase-separated morphology. The soft central "BC" block were comprised of poly(Sty-Tf_2N) containing -SO_2-N^--SO_2-CF_3 anionic groups and low T_g DEGMEMA. External polystyrene A blocks provided mechanical reinforcement with nanoscale morphology even at high ion content. EIS and PFG NMR spectroscopy clarified the ion transport properties of the triblock copolymers. Specifically, ion conductivity drastically increased with increasing ion content in the central blocks up to high values (~ 10^{-1} S/cm), likely due to an improvement in ionic phase-separation and phase percolation. These well-defined ionomeric A-BC-A triblock copolymers displayed excellent ion-transport properties, as well mechanical robustness, making them well suited for application in energy storage devices.

8.6 Acknowledgements

The PFG NMR diffusometry work was supported in part by the US National Science Foundation under award number DMR 1507764. We acknowledge Solvay for providing Tf_2N-based ionic liquids used in the research. A.M.S. was supported by the Postgraduate Research Participation Program at the US Army Research Laboratory, administered by the Oak Ridge Institute of Science and Education through an interagency agreement between the US Department of Energy and Army Research Laboratory (Contract ORISE1120-1120-99). We would also like to acknowledge Dr. Ken Sakaushi at National Institute of Materials Science, Japan for insightful discussions on this research.

8.7 *References*

(1) Bouchet, R.; Maria, S.; Meziane, R.; Aboulaich, A.; Lienafa, L.; Bonnet, J.-P.; Phan, T. N.; Bertin, D.; Gigmes, D.; Devaux, D. *Nature materials* **2013**, *12*, 452.
(2) Yuan, J.; Mecerreyes, D.; Antonietti, M. *Progress in Polymer Science* **2013**.
(3) Jangu, C.; Long, T. E. *Polymer* **2014**, *55*, 3298-3304.
(4) Hemp, S. T.; Zhang, M.; Allen, M. H.; Cheng, S.; Moore, R. B.; Long, T. E. *Macromolecular Chemistry and Physics* **2013**.
(5) Tsunashima, K.; Yonekawa, F.; Sugiya, M. *Electrochemical and Solid-State Letters* **2009**, *12*, A54.
(6) Young, W. S.; Kuan, W. F.; Epps, T. H. *Journal of Polymer Science Part B: Polymer Physics* **2014**, *52*, 1.
(7) Yanilmaz, M.; Chen, C.; Zhang, X. *Journal of Polymer Science Part B: Polymer Physics* **2013**, *51*, 1719.
(8) Tsunashima, K.; Yonekawa, F.; Sugiya, M. *Chemistry letters* **2008**, *37*, 314.
(9) van Schalkwijk, W.; Scrosati, B. *Advances in lithium-ion batteries*; Springer, 2002.
(10) Goodenough, J. B.; Kim, Y. *Chemistry of Materials* **2009**, *22*, 587.
(11) Tarascon, J.-M.; Armand, M. *Nature* **2001**, *414*, 359.
(12) Bouchet, R.; Lascaud, S.; Rosso, M. *Journal of the electrochemical society* **2003**, *150*, A1385.
(13) Wilkes, J. S.; Zaworotko, M. J. *Journal of the Chemical Society, Chemical Communications* **1992**, *0*, 965.
(14) Thackeray, M. M.; Wolverton, C.; Isaacs, E. D. *Energy & Environmental Science* **2012**, *5*, 7854.
(15) Meyer, W. H. *Advanced materials* **1998**, *10*, 439.
(16) Shi, J.; Vincent, C. A. *Solid State Ionics* **1993**, *60*, 11.
(17) Lowe, A. B.; McCormick, C. L. *Progress in Polymer Science* **2007**, *32*, 283.
(18) Smith, A. E.; Xu, X.; McCormick, C. L. *Progress in Polymer Science* **2010**, *35*, 45.
(19) Bates, F. S.; Hillmyer, M. A.; Lodge, T. P.; Bates, C. M.; Delaney, K. T.; Fredrickson, G. H. *Science* **2012**, *336*, 434.
(20) Grubbs, R. B. *Polymer Reviews* **2011**, *51*, 104.
(21) Destarac, M. *Macromolecular Reaction Engineering* **2010**, *4*, 165.
(22) Jangu, C.; Wang, J.-H. H.; Wang, D.; Fahs, G.; Heflin, J. R.; Moore, R. B.; Colby, R. H.; Long, T. E. *Journal of Materials Chemistry C* **2015**, *3*, 3891-3301.
(23) Gao, R.; Wang, D.; Heflin, J. R.; Long, T. E. *Journal of Materials Chemistry* **2012**, *22*, 13473.
(24) Jangu, C.; Wang, J. H. H.; Wang, D.; Sharick, S.; Heflin, J. R.; Winey, K. I.; Colby, R. H.; Long, T. E. *Macromolecular Chemistry and Physics* **2014**, *215*, 1319-1331.
(25) Wu, T.; Wang, D.; Zhang, M.; Heflin, J. R.; Moore, R. B.; Long, T. E. *ACS applied materials & interfaces* **2012**, *4*, 6552.
(26) Feng, S.; Shi, D.; Liu, F.; Zheng, L.; Nie, J.; Feng, W.; Huang, X.; Armand, M.; Zhou, Z. *Electrochimica Acta* **2013**, *93*, 254.
(27) Meziane, R.; Bonnet, J.-P.; Courty, M.; Djellab, K.; Armand, M. *Electrochimica Acta* **2011**, *57*, 14.
(28) Luo, S.; Zhang, S.; Wang, Y.; Xia, A.; Zhang, G.; Du, X.; Xu, D. *The Journal of organic chemistry* **2010**, *75*, 1888.

(29) Huang, T.; Toraya, H.; Blanton, T.; Wu, Y. *Journal of applied crystallography* **1993**, *26*, 180.
(30) Ilavsky, J.; Jemian, P. R. *Journal of Applied Crystallography* **2009**, *42*, 347.
(31) Hou, J.; Zhang, Z.; Madsen, L. A. *The Journal of Physical Chemistry B* **2011**, *115*, 4576.
(32) Hou, J.; Li, J.; Madsen, L. A. *Macromolecules* **2009**, *43*, 347.
(33) Jiang, D. D.; Yao, Q.; McKinney, M. A.; Wilkie, C. A. *Polymer degradation and stability* **1999**, *63*, 423.
(34) Scharfenberger, G.; Meyer, W. H.; Wegner, G.; Schuster, M.; Kreuer, K. D.; Maier, J. *Fuel Cells* **2006**, *6*, 237.
(35) Kataoka, H.; Saito, Y. *The Journal of Physical Chemistry B* **2002**, *106*, 13064.

Chapter 9: **Overall Conclusions**

The work focused on the synthesis of novel styrenic monomers, VBIm, DPPS, and Sty-Tf_2N and styrenic-macromolecules. We also studied the effect of incorporating ethylene oxide units containing monomers to tune the solubility, thermomechanical properties, and ion transport properties in homopolymers, random copolymers, and block copolymers. Following are the major conclusions from this work:

1. Nitroxide-mediated polymerization enabled the synthesis of well-defined imidazole-containing ABA triblock copolymers with charged imidazolium-containing central blocks (VBIm) and polystyrene external blocks. These are microphase-separated triblock copolymers, exhibiting good mechanical stability and well-defined structure as observed using DMA and SAXS, respectively. For the first time, a detailed study of ion transport in these triblock copolymers was performed using DRS to understand the contributions of mobile ion concentration, static dielectric constant, and ionic mobility. When cast with 32 wt.% ionic liquid, these triblock copolymers showed actuation for the first time in the literature.
2. We were also able to understand the synergy between T_g and electrostatic solvation of ethylene-oxide containing units, which is crucial to observe the influence on ionic conductivity in triblock copolymers. RAFT polymerization enabled the synthesis of well-defined A-BC-A triblock copolymers containing a low T_g monomer DEGMEMA in the central block to increase segmental motion and improve ion transport. Controlling the composition of the polystyrene

external blocks and ion content enabled the tuning of thermomechanical properties. SAXS and AFM confirmed the microphase separation and showed that the morphology can be tuned with change in ion content in the triblock copolymer system. DRS demonstrated the importance of triblock copolymer architecture as compared to random copolymers. Ionic conductivity of the copolymers was dependent on morphology, composition and ion-content. The data suggested that these triblock copolymers provide more efficient ion transport channels for electrolytes resulting in faster and greater accumulation of the cations on the anode side of the CNC. The development of these new A-BC-A triblock copolymer systems enables the design of future electroactive devices by changing morphology, ion-content and composition to tune the macromolecular properties.

3. Conventional free radical copolymerizations enabled the synthesis of poly(VBIm-*co*-EG_9MA). *In situ* FTIR was used to confirm random incorporation of the two monomers and also to investigate thermal polymerization behavior of acrylates and their methacrylates analogues. The acrylates were found to have lower activation energies than methacrylates suggesting relatively less control in the polymerizations. NMP copolymerizations of EG_9MA with VBIm as comonomer exhibited controlled polymerization behavior confirmed by kinetic plots coupled with narrow molecular weight distributions observed from SEC chromatograms. The control behavior of the copolymerization is likely attributed to the observed decrease in calculated apparent rate constants for the copolymerizations with addition of VBIm as comonomer.
4. Phosphonium polystyrene synthesized using conventional free radical

polymerization and anion metathesis displayed significantly different thermal and rheological properties. Anion exchange to bulkier, less basic anions improved the thermal stability and depressed the T_g's of all phosphine polystyrenes. TTS of phosphonium polystyrenes generated using frequency sweeps at various temperatures revealed two relaxation modes attributed to long-range segmental motion and electrostatic interactions. Contact angle measurements were also dramatically impacted by the choice of the counterion. It was observed contact angle increases with the hydrophobicity of counterion. Ultimately, the absence of β-hydrogen in DPPS, alkyl substituent length, and counteranion structural changes influenced the thermal stability and thermal transitions. These phosphine polystyrenes displayed high thermal stability and tunable viscoelastic and wetting behavior for high temperature applications.

5. We reported stimuli-responsive random copolymers that exhibit salt-responsive behavior wherein a salt triggers a change in solubility or polymer conformation. Three different methacrylate monomers were used to tune the composition of the copolymer for their application as salt-responsive adhesives. An oligo(ethylene glycol methyl ether methacrylate (OEGMEMA) acted as a hydrophilic monomer while a random copolymer of di(ethylene glycol methyl ether methacrylate) (DEGMEMA) and [2-(methacryloyloxy)ethyl]trimethylammonium chloride (TMA) gave the copolymer the salt-responsive behavior. By varying the composition of a copolymer, rubbery plateau of storage and loss moduli master curves was tuned such that copolymers followed the Dahlquist criterion, thus behaving as a tacky polymer system. Peel tests and probe tack measurements

confirmed the application of these polymers as pressure sensitive adhesives. At less than 5% of TMA the adhesives were soluble in water while in presence of salts, these adhesives behave as water insoluble system.

6. Well-defined ionomeric A-BC-A triblock copolymers, poly[Sty-*b*-(Sty-Tf_2N-Li-*co*-DEGMEMA)-*b*-Sty], with microphase-separated morphology were synthesized using RAFT polymerization. The soft central "BC" block comprised of poly(4-styrenesulfonyl(trifluoromethylsulfonyl)imide) (poly(Sty-Tf_2N)) contained $–SO_2\text{-}N^-\text{-}SO_2\text{-}CF_3$ anionic groups and low T_g DEGMEMA. External polystyrene A blocks provided mechanical reinforcement with nanoscale morphology even at high ion contents. EIS and PFG NMR spectroscopy probed ion transport properties of the triblock copolymers. The ion conductivities increased with increasing ion content in the central blocks up to high values ($\sim 10^{-1}$ S/cm). These well-defined ionomeric A-BC-A triblock copolymers had excellent ion-transport properties combined with mechanical stability for potential application in energy storage devices.

Chapter 10: **Suggested Future Work**

1. The sulfonimide-containing A-BC-A triblock copolymers synthesized using RAFT polymerization. As described in Chapter 8, these ionomeric A-BC-A triblock copolymers allow one to combine two opposing properties: mechanical stability and ion transport. Sty-Tf_2N monomer enables delocalization of the negative charge, consequently enabling high ion transport. We explored the relationships among chemical composition, morphology, ionic conductivity, and mechanical properties of these triblock copolymers. However, potential applications for these sulfonimide-containing triblock copolymers as lithium-ion batteries are lacking. Future investigations on fabricating these block copolymers into coin cells and understanding the effect of morphology on battery performance will shed some light on the current understanding of new materials used for Li-ion battery applications.
2. The nature of the labile C-S bond facilitating RAFT polymerization is well-understood concern for many commercial applications. Therefore, initial reasons for removal of end groups from polymers synthesized from RAFT polymerization include inherent reactivity and possibility of decomposition into sulfur-containing materials giving color and odor to polymers. There are number of methods

described in the literature to cleave thiocarbonylthio groups as shown in Figure 10.1.

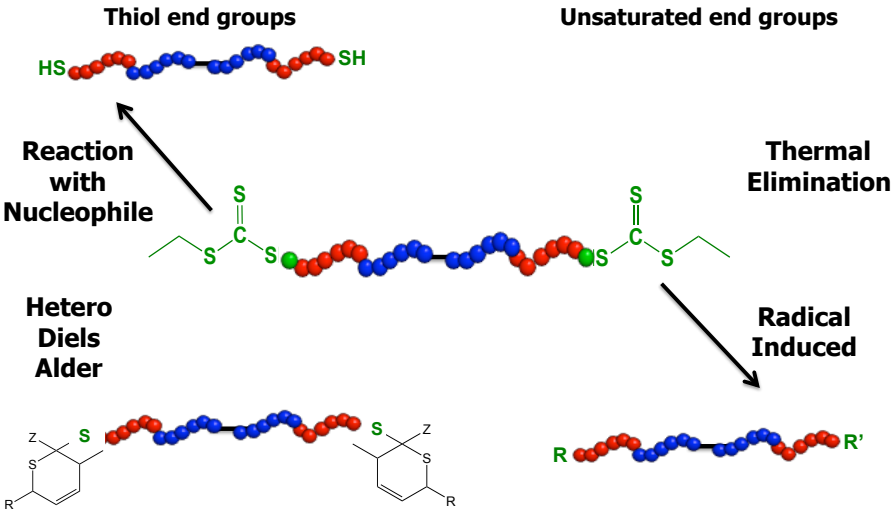

Figure 10.1 Main methods to modify end groups yielding different functionalization of RAFT synthesized polymers

Preliminary results show that the reaction with nucleophile reducing agents for example primary or secondary amines resulted in almost 100% polymer end group modification. Aminolysis and Michael addition sequence in transforms RAFT end groups to more stable functional groups. Figure 10.2 shows the synthetic route of above-mentioned one-pot-transformation. UV-vis spectroscopy, SEC, and NMR spectroscopy results show that it is possible to remove thiocarbonylthio end groups. The thiol end group results in a multitude of reactions, from the introduction of fluorescently labeled groups using the thiol-ene reaction to conjugation to biomolecules with disulfide coupling.

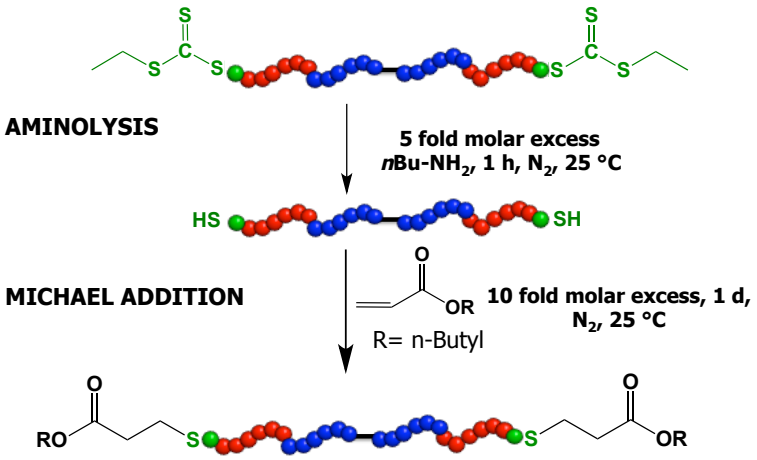

Figure 10.2 One-pot-transformation of RAFT end groups using aminolysis and Michael addition sequence

3. Homopolymerization of DPPS using conventional free radical polymerization and anion metathesis leads to interesting variations in thermal and rheological properties as shown in Chapter 6. Alkylation with subsequent anion exchange to BF_4^-, TfO^-, and Tf_2N^- improves the thermal stability due to decreased basicity of the mobile counteranion. Bulkier anions also depress the T_g of homopolymers, with the counteranion Tf_2N^- displaying the lowest T_g at 100 °C. Longer alkyl chain lengths lead to decreased thermal stability and lower T_g values. Investigation of these novel polymers provided fundamental understanding of the counteranion effects on thermal, viscoelastic, and wetting properties of phosphonium-containing polystyrenes. Tuning the architecture using block copolymers and also investigating copolymers with DEGMEMA, OEGMEMA, isoprene, and PMMA will widen the scope of these copolymers for variety of applications for example hot melt adhesives, ion-conducting membranes etc. Electrochemical impedance, ^1H NMR spectroscopies, dynamic measurements,

SEC can be utilized to understand the ion transport in phosphonium polystyrenes containing block copolymers.